Development of Sulfonated Chitosan Membranes Modified with Inorganic Nanofillers and Organic Materials for Fuel Cell Applications

Nondumiso Petunia Zungu

208075763

A dissertation submitted in fulfilment of the requirements for the degree of

Master of Engineering

in

Chemical Engineering

Department: Chemical Engineering

Faculty of Engineering and Technology

Vaal University of Technology

Vanderbijlpark

Supervisor: Prof PO Osifo

Co-supervisor: Prof A Ofomaja

Date: 06/07/2021

DECLARATION

I, Nondumiso Petunia Zungu, declare that this dissertation, entitled: Development of sulfonated chitosan membranes modified with inorganic nanofillers and organic materials for fuel cell applications, is my own work. This dissertation is submitted in fulfilment of the requirements for the degree of Master of Engineering: Chemical Engineering at the Vaal University of Technology.

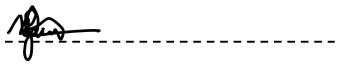

Nondumiso Petunia Zungu

Date: 06/07/2021

DEDICATION

I wish to dedicate this thesis to my family, especially to my mother, Sizakele Ngema. Mostly, I am thankful to God for the opportunity to further my education.

ACKNOWLEDGEMENTS

I wish to acknowledge my supervisor, Prof PO Osifo for his guidance and support throughout this research work, and my Co-supervisor, the late Prof A Ofomaja for his valuable contribution to the project. I also wish to express great gratitude to Prof HCvZ Pienaar for the support and the invitation to be part of the excellent team at the Telkom Centre of Excellence.

I wish to acknowledge CHIETA for the financial sponsorship of this project and express sincere appreciation to the people mentioned below for their contribution to this research work, some through their kindness and some through their technical expertise.

- Mr WJvZ Pienaar (VUT)
- Prof J Bekker (VUT)
- Dr L Shoko (VUT)
- Mrs JE Van Zyl (VUT)
- Mrs R Visage (VUT)
- Prof H Krieg (NWU)
- Dr J Jordaan (NWU)
- Dr A Jordaan (NWU)
- Mrs B Venter (NWU)
- Mr P Mwai (VUT)
- Mr FM Ogunniyi (VUT)
- Mr O Alo (VUT)
- Mr O Oluokun (VUT)
- Mr T Sebekedi (VUT)
- Mr LJ Matlatle (VUT)
- Mr S Khumalo (VUT)
- Mr A Coetzee (Pert Industrials (Pty) Ltd)
- Mr M Van Dyk (Pert Industrials (Pty) Ltd)

ABSTRACT

Fuel cell technology is a promising clean energy source compared to internal combustion engines and electricity generating plants which are associated with high emissions of greenhouse gases. The aim of this study was to modify chitosan into polymer electrolyte membranes suitable for use in PEMFC and DMFC fuel cells. Chitosan modification was done with 2-aminoethanesulfonic acid (2-AESA), dimethylformamide (DMF) and silica nanoparticles. The effect of the modification on the properties of the developed chitosan membranes was studied using FTIR, XRD, SEM-EDS and TGA. The performance of the membrane electrode assemblies was investigated.

The formation of electrostatic interactions in the developed sulfonated chitosan membranes was confirmed via the Fourier transform infrared (FTIR) analysis, indicating a shift in the wavenumber of the N-H bonds from 1581 cm^{-1} on the chitosan spectrum to a lower wavenumber of 1532 cm^{-1} in the FTIR spectra of the membranes and by the new peak at the wavenumber of ~1260 cm^{-1} attributed to the asymmetric O=S=O stretching vibrations of the sulphate groups and sulfonic acid groups from the cross-linking sulphuric acid solution and 2-aminoethanesulfonic acid incorporated on the chitosan polymer chain during the modification. Notably, the FTIR spectra of the developed sulfonated chitosan membranes lacked the peak at the wavenumber of ~1153 cm^{-1} attributed to the stretching of C-O-C bonds of the polysaccharide ring of chitosan. A reaction mechanism was proposed in this study illustrating the possible conversion of the polysaccharide rings of chitosan into a poly (cyclohexene-oxide) thermoplastic rings in the developed membranes.

The TGA/DTGA results of the developed sulfonated chitosan membranes showed three degradation stages. The initial weight loss occurred at temperatures <100 °C due to the evaporation of volatile components and water molecules inside the membranes. The second degradation phase of the membranes occurred at 208 °C with a loss in weight of >30% resulting from the decomposition of cross-linking networks. The third degradation stage was associated with the decomposition of the main polymer backbone of the membranes and occurred at 263°C for the chitosan membranes modified with 2-aminoethanesulfonic acid and at 266 °C for the chitosan membrane modified with silica nanofiller.

The TGA/DTGA curves of Nafion 117 showed a small loss in weight of ~ 5% before a sharp decomposition that occurred between 346–505 °C.

The XRD diffractograms of the developed sulfonated chitosan membranes showed amorphous phases, the crystal peaks of chitosan at 2theta of 10° and 20° were flattened on the membranes.

The SEM images showed a homogenous surface morphology for the sulfonated chitosan membrane with a higher weight percentage of 2-aminoethanesulfonic acid (13,6 wt.%).

The SEM images performed on the surface of the sulfonated chitosan membrane modified silica nanoparticles showed a slight agglomeration associated with the migration of the unbonded silica to the surface.

The methanol permeability coefficient of the developed sulfonated chitosan membrane modified with 2-aminoethanesulfonic acid was calculated to be 2.29×10^{-6} cm^2/s. This value was close to the methanol permeability coefficient of 2.33×10^{-6} cm^2/s associated with unfavourable depolarisation at the cathode in direct methanol fuel cells when using Nafion 117.

The proton diffusion coefficient of Nafion 117 was calculated to be 1.64×10^{-5} cm^2/s and that of the developed sulfonated chitosan membrane modified with 2-aminoethanesulfonic acid was found to be 6.56×10^{-6} cm^2/s, respectively.

The fuel cell performance of the developed sulfonated chitosan membrane modified with 2AESA was investigated in a hydrogen fuel cell (PEMFC) supplied with H_2 and O_2 directly from the electrolyser. The sulfonated chitosan membrane modified with 2-aminoethanesulfonic acid (13.6 wt.%) achieved an open-circuit voltage of ~0.9 V and a maximum power output of 64.7 mW/cm^2 at a maximum current of 70 mA. The current produced by the developed chitosan membrane was applied into the load and was able to turn (power) the electric fan.

The sulfonated chitosan membrane modified with silica nanoparticles (2 wt.%) yielded an open-circuit voltage of ~0.9 V and attained a maximum power output of 58 mW/cm^2 at a maximum current output of 60 mA/cm^2. The current generated by the membrane was also able to turn the electric fan. The Nafion 117 membrane was also investigated under similar conditions and obtained an open-circuit voltage of 0.6 V and a maximum power output of 130 mW/cm^2 at the maximum current output of 308 mA. The current produced by Nafion 117 was supplied into the load and was able to turn the electric fan.

CONFERENCE AND PUBLICATION

A research paper titled “Development of Chitosan Membrane Modified with 2-Aminoethanesulfonic Acid and Silica for Fuel Cell Applications” detailed the preliminary findings of this work and was accepted for presentation at the Southern Africa Telecommunication Networks and Applications Conference (SATNAC) held between 1–4 September 2019 at Fairmont Zimbali Resort, Kwa-Zulu Natal, South Africa.

TABLE OF CONTENTS

LIST OF FIGURES

CHAPTER 2

CHAPTER 3

CHAPTER 4

APPENDIX A

APPENDIX C

APPENDIX D

APPENDIX E

LIST OF TABLES

CHAPTER 4

APPENDIX

NOMENCLATURE

Symbol	Definition	Unit
A	Membrane area	cm^2
C_A	Methanol concentration compartment A	mol/L
C_B	Methanol concentration compartment B	mol/L
C_x	Hydronium ion concentration compartment B	mol/L
C_y	Hydronium ion concentration compartment A	mol/L
D	Diffusion coefficient	cm^2/s
I	Current	A
K	Mass transfer coefficient	cm/s
l	Thickness of the membrane	cm
P	Methanol permeability coefficient	cm^2/s
t	Time	seconds
V	Voltage	V
V_B	Solution volume in compartment B	cm^3

ABBREVIATIONS

Abbreviation	Definition
cm	Centimeter
cm^2	Square centimetre
cm^3	Cubic centimeter
°C	Degree Celsius
g	Gram
m	Meter
mL	Milliliter
Mol/L	Moles of solute per liter of solution
µm	Micrometer
s	Second
S/cm	Siemens per centimeter
Ɵ	Theta
W	Watt
W/cm^2	Watts per square centimeter
W/m^2	Watts per square meter

ABBREVIATIONS

Abbreviation	Definition
2AESA	2-aminoethanesulfonic acid
CS	Sulfonated chitosan membrane
DDA	Degree of deacetylation
DMF	Dimethylformamide
DMFC	Direct methanol fuel cell
DSC	Differential scanning calorimetry
DTG	Differential thermogravimetric
FE-SEM	field emission scanning electron microscopy
FTIR	Fourier transform infrared spectroscopy
GDE	Gas diffusion electrode
MEA	Membrane electrode assembly
NASA	National Aeronautics and Space Administration
OCV	Open-circuit voltage
PEM	Proton exchange membrane/polymer electrolyte membrane
PEMFC	Proton exchange membrane fuel cell
PTFE	Polytetrafluoroethylene
SEM-EDS	Scanning electron microscopy- Energy-dispersive X-ray
TGA	Thermogravimetric analysis
VUT	Vaal University of Technology
XRD	X-ray diffraction

CHAPTER 1: INTRODUCTION

1.1 BACKGROUND

The growth in the population and industrial developments, especially in the transportation sector raises a need for further research on renewable energy. In the quest for alternative sources of energy to meet the socio-economical demands, pollution remains a global threat to the current energy conversion technologies. Fuel cell technology is a promising clean alternative power source compared to internal combustion engines associated with high emissions of greenhouse gases. The overall emission of greenhouse gases from automotive engines is a significant contributor to global warming; a phenomenon related to radical climate change and its impact on the environment. The greenhouse gas emissions from the combustion of diesel and gasoline fuels in vehicle engines rank as a secondary source of all global emissions of carbon dioxide (Geng *et al.* 2016). Fuel cell technology is an electrochemical process that generates electricity through the direct conversion of chemical energy to electrical energy. The simplified infrastructure and high-power densities have made direct methanol fuel cells favourable as an alternative power source, however, direct methanol fuel cells have slow oxidation kinetics and low cell efficiency compared to hydrogen fuel cells, also known as the proton exchange membrane fuel cell (Zakil *et al.* 2016b).

Direct methanol fuel cells (DMFCs) and the proton exchange membrane fuel cells (PEMFCs) are two types of fuel cells that consist of a polymer electrolyte membrane inserted between the two electrodes. Nafion 117 is a polymer electrolyte membrane used in commercial fuel cell applications due to its ability to permeate protons from the anode towards the cathode. However, Nafion 117 is expensive and presents another challenge when used in DMFCs due to the affinity of this membrane to methanol, which in turn yields a reduction in fuel cell efficiency due to depolarisation occurring at the cathode. The fabrication of polymer electrolyte membranes for use in solid polymer fuel cell applications was a trial and error attempt for decades until the development of a per-fluorinated sulfonic acid membrane called Nafion 117 by Du Pont (Smitha *et al.* 2005, Mališ *et al.* 2018).

The thermal strength and chemical stability of Nafion 117 is attributed to its polytetrafluoroethylene hydrophobic backbone. The high proton-conducting ability of Nafion

117 is credited to its sulfonic acid groups (-SO_3H) attached to the per-fluoroalkyl ether side chain (Mališ *et al.* 2018, Stenina *et al.* 2004)

The high cost of Nafion 117 and its permeability to methanol have prompted much research interest on the low-cost biodegradable polymer called chitosan (Ying *et al.* 2018, Vijayalekshmi & Khastgir 2018, Shirdast *et al.* 2016). Chitosan is obtained from the alkaline de-acetylation of chitin, a waste product from the exoskeletons of crustaceans such as lobsters, crabs and shrimps (Zhu *et al.* 2019a). Chitosan is a polysaccharide consisting of poly β-1,4-linked 2-amino-2-deoxy-D-glucopyranose and 2-acetamido-2-deoxy-D-glucopyranose repeating units (Ma & Sahai 2013). Chitosan membranes are reported to have high methanol barrier properties compared to Nafion-117 membranes (Bai *et al.* 2015). However, chitosan polymer electrolytes membranes have low proton conductivity compared to Nafion 117 and present poor mechanical stability such as brittleness (Liu *et al.* 2014, Chen *et al.* 2018).

The hydroxyl groups (-OH) and amino groups (-NH_2) in the chemical structure of chitosan enable its modification with compatible chemical agents - a promising feature in the efforts to improve properties such as proton conductivity, chemical and mechanical stability, water absorption capacity, thermal properties, power density (voltage and current outputs) of developed chitosan membranes for fuel cell applications (Zhang *et al.* 2016).

In this study, chitosan was modified with dimethylformamide, 2-aminoethanesulfonic acid and silica nanoparticles as inorganic nanofiller. The developed chitosan membranes were sulfonated by cross-linking in a sulphuric acid solution. A study was carried out using various analytical methods to investigate properties of the developed proton exchange membranes for fuel cell applications.

1.2 PROBLEM STATEMENT

The combustion of fossil fuels in internal combustion engines of vehicles is the secondary source of carbon dioxide emissions; a major contributor to global warming. Thus far, fuel cell technology is a promising cleaner alternative energy source with the capacity to power vehicles. Currently, Nafion 117 is a proton exchange membrane used in direct methanol fuel cells (DMFCs) and proton exchange membrane fuel cells (PEMFCs), also known as the hydrogen fuel cell. However, Nafion 117 is expensive and is highly permeable to methanol, resulting in reduced fuel cell efficiency of DMFC.

A research gap exists in fuel cell technology to develop low-cost polymer electrolyte membranes with high proton exchange capacity, low methanol permeation, high voltage and current density outputs. Chitosan is a low-cost biopolymer with good methanol barrier properties, however, membranes developed using chitosan are reported to have low proton conductivity and are susceptible to brittleness. Chitosan requires an intense modification to produce membranes with good properties to be deemed a reasonable alternative to Nafion 117.

1.3 RESEARCH QUESTIONS

- What will be the outcome of incorporating 2-aminoethanesulfonic acid, dimethylformamide and silica nanofillers on the chemical structure of the developed chitosan membranes?
- What will be the water uptake percentage, proton diffusion coefficient and methanol permeability coefficient of the developed chitosan polymer electrolyte membranes?
- What will be the thermal profile of the developed chitosan membranes?
- What will be the fuel cell performance of the developed chitosan membrane electrode assemblies (MEAs)?
- How does the modified chitosan performance compare with Nafion 117?

1.4 AIM

The main aim of this study is to modify chitosan biopolymer into polymer electrolyte membranes suitable for use in PEMFC and DMFC applications.

1.5 SPECIFIC OBJECTIVES

The specific objectives of this research study are:

- To modify chitosan into sulfonated chitosan membranes using 2-aminoethanesulfonic acid, dimethylformamide and silica nanoparticles as modifying agents
- To characterise the developed chitosan membranes with FTIR, TGA, SEM-EDS and XRD
- To determine water uptake percentages and proton diffusion coefficient of the membranes
- To determine the methanol permeability coefficient of developed chitosan membranes

- To fabricate chitosan membrane electrode assemblies (MEAs) and compare fuel cell performances (voltage and current output) with the Nafion 117 MEA

1.6 PROJECT SCOPE: OVERVIEW

Chapter 1 covers the introduction, the problem statement, research questions and the objectives.
Chapter 2 covers the literature review on chitosan, proton exchange membranes and fuel cells.
Chapter 3 covers the research methodology and experimental procedures.
Chapter 4 covers the results and discussion.
Chapter 5 covers the conclusion and recommendations.

CHAPTER 2: LITERATURE REVIEW

2.0 INTRODUCTION

This section begins with a brief introduction to chitosan, its synthesis, chemical structure and the related studies performed by other authors to modify chitosan into membranes for fuel cell application. The section advances with a background history of polymer electrolyte membranes to the current commercial Nafion 117 membranes used in direct methanol fuel cell (DMFC) and the hydrogen fuel cell, also known as the proton exchange membrane fuel cell (PEMFC).

Lastly, an introduction to fuel cell technology and to the different types of fuel cells is presented in this section, with the primary focus on the DMFC and PEMFC fuel cells.

2.1 CHITOSAN BIOPOLYMER

Chitosan is a linear polysaccharide obtained from the de-acetylation of chitin, a secondary abundant polysaccharide on earth (Zhu *et al.* 2019b). Chitin is a polysaccharide mainly obtained from the shells of crustaceans such crabs, lobsters and shrimps and is also attainable from fungal sources (Zhu *et al.* 2019b, Yuan *et al.* 2021).

The chemical structure of chitin consists of a 2-acetylamino-2-deoxy-D-glucose repeating unit. Chitin undergoes a process of de-acetylation to chitosan, a non-toxic biodegradable polymer with good film-forming properties (Takara *et al.* 2015). Chitosan consists of β (1- 4) linked glucosamine units and N-acetyl glucosamine units in its polymer chain units (Gabriele *et al.* 2021). Chitosan is insoluble in water but soluble in organic acids when the degree of de-acetylated units is greater than 50%. The solubility of chitosan in organic acids is due to the protonation of amine groups in its polymer chain units (Wang *et al.* 2021). Chitosan is a low cost biopolymer; this property makes chitosan an attractive polymer in the current quest to develop cheaper proton exchange membranes that can serve as alternatives to the expensive Nafion membranes used in DMFC and PEMFC fuel cells (Ma & Sahai 2013). Furthermore, chitosan shows high selectivity to methanol compared to Nafion 117 and has earned favourability in the fabrication of polymeric membranes that can be used in DMFC (Mukoma *et al.* 2004, Wang *et al.* 2008).

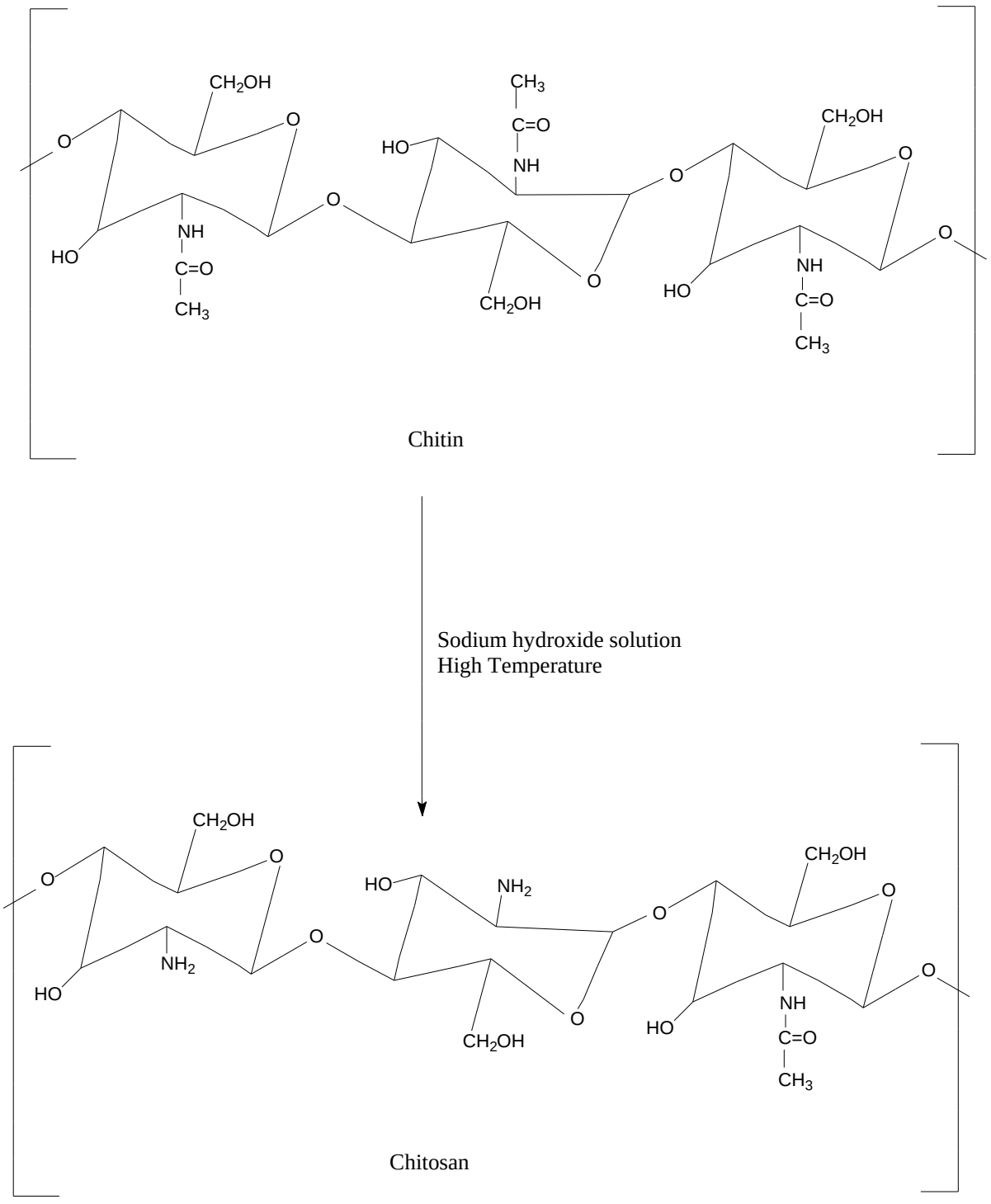

Figure 2. 1: Chemical structure of chitosan (Bocchetta 2020)

Figure 2.1 shows a typical diagram of the synthesis of chitosan from chitin. The chemical structure of chitosan consists of hydrophilic functional groups; the ether groups (C-O-C), hydroxyl groups (OH) and the amino groups (NH_2). Hydrophilicity is an attractive property in the development of proton exchange membranes that can retain chemical and mechanical stability inside the fuel cell when used at high temperatures and relatively low humidity

conditions. The current Nafion 117 membranes are limited to fuel cell operations of not more than 80 °C in PEMFC, this is due to its susceptibility at high temperatures and low hydration conditions (Ma & Sahai 2013, Mališ *et al.* 2018).

The hydroxyl groups (OH) and amino groups (-NH_2) of chitosan enables incorporation of compatible modifying agents in the chitosan polymer matrix. Zhang *et al.* (2016) investigated the interaction between different functionalised graphene sheets and chitosan through density functional theory. The interaction energy (E_{ads}) of OH– modified graphene and COOH–modified graphene with the amino groups (-NH_2) of the chitosan was -0.93 eV and -1.34 eV, respectively. A more negative E_{ads} of -1.34 eV indicated the formation of a stable structure via amide bonding formed between the carboxyl group of COOH–modified graphene and the amino group of chitosan. A lowest interaction with an E_{ads} of 1.10 eV was reported between the NH_2-modified graphene and the amino groups (NH_2) of chitosan (Ma & Sahai 2013, Zhang *et al.* 2016).

However, the membranes developed using chitosan have been reported to present brittleness, have low proton conductivity, low power densities and low current densities compared to Nafion 117 membranes (Chen *et al.* 2018, Shirdast *et al.* 2016).

2.2 MODIFICATION OF CHITOSAN TO MEMBRANES FOR FUEL CELL

The performance of polymer electrolyte membranes is dependent on the nature of the hydrophobic backbone, the extent of sulfonated regions and the distance between the backbone and ion conducting domains. The Nafion 117 membrane has a high proton conducting ability and is thus a preferred membrane in fuel cell applications. However, a strong quest now exist in the research community to modify low-cost polymers to membranes with high power densities and high selectivity to methanol (Chakrabarty *et al.* 2010). Researchers have adopted several strategic methods in the quest to improve the proton-conducting ability of chitosan membranes; these methods include quaternisation phosphorylation and sulfonation of chitosan (Bai *et al.* 2015, Li *et al.* 2016, Ma & Sahai 2013).

2.2.1 Modification of chitosan with quaternised polyvinyl alcohol and glutaraldehyde

Li *et al.* (2016) investigated the modification of chitosan into polymer electrolyte membranes through functionalisation with quaternised polyvinyl alcohol (QPVA) and cross-linking with glutaraldehyde (GL). The functional groups present in the resulting membranes were confirmed via FTIR analysis. The incorporation of glutaraldehyde in the chitosan matrix was confirmed with a C=N peak at the wavenumber of 1640 cm^{-1} resulting from the reaction between the carbonyl groups (O=C) of glutaraldehyde and the amino groups ($–NH_2$) of chitosan. Notably, the chitosan-QPVAGL membrane had a low methanol permeability of $4.5x10^{-8}$ cm/s compared to the chitosan membrane synthesis with quaternised polyvinyl alcohol in the absence of glutaraldehyde. However, the chitosan-QPVAGL membrane yielded a proton conductivity of $1.8x10^{-2}$ S/cm. The proton conductivity of the chitosan-QPVAGL membrane was low when compared to a proton conductivity of $3x10^{-2}$ S/cm obtained with the chitosan membrane consisting only QPVA (Li *et al.* 2016).

The chitosan-QPVA membrane delivered a low power density compared to chitosan-QPVAGL under similar conditions at 60 °C in a direct methanol fuel cell doped with potassium hydroxide solution. The maximum power obtained for the chitosan-QPVA membrane was 51 mW/cm^2 at the open-circuit voltage of 0.73 V; this was lower compared to the maximum power density of 58 mW/cm^2 at the open-circuit voltage of 0.78 V obtained for the chitosan-QPVAGL membrane. The improved fuel cell performance in the chitosan-QPVAGL membrane was attributed to the effect of glutaraldehyde as the cross-linking agent in lowering methanol permeation and depolarisation at the cathode (Li *et al.* 2016).

2.2.2 Modification of chitosan with sulfonated-graphene oxide

Shirdast *et al.* (2016) reported that chitosan membranes modified with sulfonated graphene oxide yielded a low methanol permeability coefficient and exhibited a high proton conducting ability contrary to the un-sulfonated chitosan membranes. The proton conductivity of the chitosan membrane significantly increased from 0.0013 S/cm to 0.0072 S/cm after incorporating sulfonated-graphene oxide. The methanol permeability coefficient was significantly reduced from $6.03x10^{-8}$ cm^2s^{-1} obtained using 5 wt% graphene oxide to $4.75x10^{-8}$ cm^2s^{-1} with the incorporation of 5 wt% sulfonated graphene oxide (Shirdast *et al.* 2016).

Shirdast *et al.* (2016) utilised 2-aminoethanesulfonic acid to sulfonate graphene oxide. Figure 2.2 shows the chemical structure of 2-aminoethanesulfonic acid.

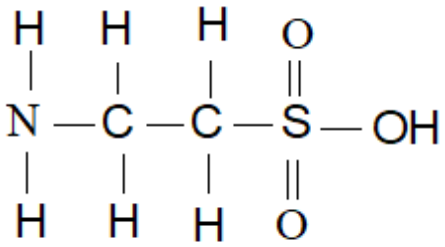

Figure 2. 2: Chemical structure of 2-aminoethanesulfonic acid (Wu *et al.* 2017)

2.2.3 Modification of chitosan with phosphotungstic acid

Bocchetta (2020) investigated the modification of chitosan with an inorganic acid phosphotungstic acid for use in a PEMFC. Phosphotungstic acid is high proton conducting heteropoly acid with a proton conductivity value of 0.17 S/cm. However, the challenge with the use of phosphotungstic acid is its solubility inside a fuel cell. The focal point of the study was to develop insoluble phosphotungstic acid functionalised chitosan membranes with good proton conducting channels. The phosphotungstic anions were introduced in the chitosan matrix through the ionotropic gelation method. The optimum results were obtained using the chitosan membrane cross-linked for 2.5 days in phosphotungstic acid solution, the membrane achieved a power density of 505 mW/cm^2 in a H_2/O_2 fuel cell at 25 °C (Bocchetta 2020).

The thermogravimetric analysis of the membranes cross-linked in phosphotungstic acid between 60-120 hrs showed minimal weight % loss at the second degradation stage, which occurred between 180 °C – 350 °C. This good thermal stability was ascribed to the formation of strong bonds between the poly- anions and poly-cations of phosphotungstic acid in the chitosan matrix. The electrostatic interactions were further confirmed via the FTIR analysis of the membranes (Bocchetta 2020).

2.2.4 Modification of chitosan with polyacrylamide and phosphoric acid

The susceptibility of Nafion 117 membrane to mechanical degradation at high temperatures is amongst factors resulting in research studies on other polymers such as chitosan. Yuan *et al.* (2014) investigated the modification of chitosan with polyacrylamide and phosphoric acid (H_3PO_4) for use as a polymer electrolyte membrane in a PEMFC operated at 150 °C (Haile 2003, Mališ *et al.* 2018, Yuan *et al.* 2014). The incorporation of polyacrylamide in the chitosan matrix provided binding sites for the incorporation of phosphoric acid. The membranes were loaded at different weight percentages of phosphoric acid. Optimum results were obtained using the chitosan membrane consisting of ~92 wt.% loading of H_3PO_4. The performance of the membrane was investigated in a PEMFC fuel cell operated at 150 °C. The maximum power density of 405 mW/cm^2 was achieved at a current density of 0.8 A/cm^2 and a voltage of 0.5 V using a phosphoric acid- polyacrylamide- chitosan membrane with a thickness of 500 µm (Yuan *et al.* 2014).

2.2.5 Modification of chitosan with inorganic fillers

Vijayalekshmi & Khastgir (2018) investigated the development of chitosan membranes modified with silica-supported silicotungstic acid. The incorporation of a tungstic-based heteropoly acid (HPA) on the chitosan matrix was also reported by Bocchetta (2020). Heteropoly acids are reported to improve proton exchange channels and water retention when incorporated into the chitosan chain (Bocchetta 2020, Vijayalekshmi & Khastgir 2018).

The enhancement of thermal properties is also reported for the chitosan membranes modified with HPA due to the formation of strong hydrogen bonding between the chitosan matrix and the heteropoly acids. However, unsupported HPA has high solubility in water formed as a by-product inside the fuel cell from the reduction reaction at the cathode electrode (Bocchetta 2020, Vijayalekshmi & Khastgir 2018).

Vijayalekshmi & Khastgir (2018) investigated the incorporation of inorganic nanosilica and silicotungstic acid on the chitosan polymer matrix. The interaction between chitosan and the nanosilica-silicotungstic nanofiller was investigated via the FTIR analysis. The integration of the nanofiller on the chitosan matrix was associated with the formation of a hydrogen bond between the carbonyl of chitosan and silanol group of the incorporated nanosilica-silicotungstic acid nanoparticles. The improvements in the proton conductivity were noted from 2.9×10^{-3}

S/cm in the pristine chitosan membrane to $3.9x10^{-3}$ S/cm after the incorporation of 3 wt.% silica-silicotungstic acid on the chitosan matrix (Vijayalekshmi & Khastgir 2018)

A uniform distribution of the nanofiller without agglomeration is essential to attain good proton channels inside the membrane. The FESEM images of the chitosan membrane without the silica-silicotungstic acid showed a uniform structure. In contrast, agglomeration was observed on the chitosan membrane with silica-silicotungstic acid when the loading of the nanofiller was 7 wt.%. The unbonded silica nano-particles have been reported to move towards the surface when the maximum loading is exceeded due to the low surface energy of silica (Su *et al.* 2007, Vijayalekshmi & Khastgir 2018).

The thermal properties of the chitosan membranes modified with nanosilica-silicotungstic acid were investigated and three degradation stages were observed on the TGA/DTG curve. The first loss in weight was recorded between 50 – 180 °C and was attributed to the loss of water and solvent molecules. The second degradation was observed at 180 – 260 °C and was linked to the degradation of the cross-linked networks. The third weight loss occurred between 260 – 400 °C and was associated with the degradation of the main polymer of the membrane. The chitosan membrane modified with 3 wt.% nanosilica-silicotungstic acid gave the highest fuel cell performance with the open-circuit voltage of 0.73 V and maximum power density of 54 mW/cm^{-1} at a current density of 154 mA/cm^{-1} (Vijayalekshmi & Khastgir 2018). The developed membranes were deemed potential membranes for application in DMFC usually operated at ~80 °C (Alias *et al.* 2020, Khuhro *et al.* 2018).

2.2.6 Modification of chitosan with glycerol

Chen *et al.* (2018) elucidated the plasticising effect of glycerol on chitosan in the quest to combat the brittle nature of chitosan membranes. The modification of chitosan with glycerol was reported to improve the flexibility of chitosan membranes, which was attributed to the ability of glycerol to integrate itself and initiate a disruption of the intermolecular hydrogen bonding networks present in chitosan polymer chain units.

Theoretically, plasticisers are known as chemical agents that increase the amorphous content of a plasticised material. Polymer electrolyte membranes with a high degree of crystallinity have low proton conductivity values. In contrast, a high degree of the amorphous phase in the membrane increases its proton conductivity. A study conducted by Kumar *et al.* (2017) using

triflouromethane sulfonic acid, polyethylene oxide and an amide plasticiser called dimethylacetamide reported a significant increase in proton conductivity from $3.74x10^{-5}$ S/cm to $4.26x10^{-3}$ S/cm when 50 wt.% dimethylacetamide was added to the polymer. The X-ray diffraction analyses of the polymer electrolyte obtained from 8wt % triflouromethane sulfonic acid and polyethylene oxide showed broader amorphous peaks when dimethylacetamide was incorporated into the polymer (Kumar *et al.* 2017).

Dimethylformamide is another amide plasticiser investigated in polymer electrolyte research. Nithya *et al.* (2012) report a high proton conductivity value of $5.8x10^{-4}$ S/cm^{-1} after plasticising poly(epichlorohydrin-ethyleneoxide) with dimethylformamide compared to the un-plasticised membrane (Nithya *et al.* 2012). The chemical structure of dimethylformamide is shown in Figure 2.3.

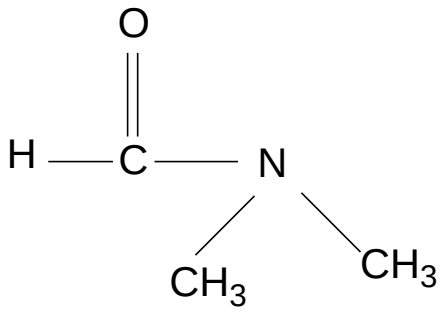

Figure 2. 3: Chemical structure of dimethylformamide (Umadevi & Poornima 2009)

Umadevi & Poornima (2009) investigated the molecular-interaction of dimethylformamide (DMF) and propanoic acid (PA) using FTIR analysis. The stretching vibration of the carbonyl group (C=O) of pure dimethylformamide was reported to appear at a wavenumber of 1660 cm^{-1} and was shifted to a lower wavenumber of 1648 cm^{-1} after the dilution with propanoic acid. The shift of the carbonyl groups observed on the FTIR spectrum was associated with the formation of strong hydrogen bonding between the C=O group of DMF and the hydroxyl group of propanoic acid. The bond stretch of the C-O group of propanoic acid was reported to shift from 1075 cm^{-1} to a lower wavenumber of 1062 cm^{-1} due to the formation of strong hydrogen bonding with DMF (Umadevi & Poornima 2009). In summary, Umadevi & Poornima (2009) report the interaction of DMF and propanoic acid to occur via intermolecular hydrogen bonding between:

- The carbonyl group (C=O) of dimethylformamide and the hydrogen atom of the hydroxyl group (-OH) of propanoic acid.
- The carbonyl group (C=O) of propanoic acid and hydrogen atom of dimethylformamide.
- The nitrogen lone pair of dimethylformamide and the –OH group of propanoic acid.

2.3 HISTORY OF POLYMER ELECTROLYTE MEMBRANES

The development of polymer electrolyte membranes (PEM) for fuel cell technology dates back to 1959 from the phenolic membranes and the partially sulfonated polystyrene sulfonic acid membranes synthesised by General Electric (GE). The sulfonated polystyrene sulfonic acid membranes yielded power outputs in a range of 0.4-0.6 kW/m^{2,} which secured the application of these membranes in NASA Gemini flights (Smitha *et al.* 2005).

However, the sulfonated polystyrene sulfonic acid membranes presented a problem of brittleness and this prompted General Electric to develop cross-linked polystyrene-divinylbenzene sulfonic acid membranes. The polystyrene-divinylbenzene sulfonic acid membranes exhibited higher power densities ~0.75-0.8 kW/m^2, however, the legacy of polystyrene membranes was short-lived due to instabilities and power density outputs of less than the design specification of 1 kW/m^2 for commercial fuel cells. The polystyrene membranes manufactured by GE were superseded by the Nafion membranes that were developed in the 1970s by Du Pont. Nowadays, Nafion 117 is thus far the preferred polymer electrolyte membrane in DMFCs and PEMFCs due to its high proton exchange ability and high power densities in fuel cell operations (Brandon *et al.* 2003, Haile 2003, Smitha *et al.* 2005) .

2.4 NAFION 117 POLYMER ELECTROLYTE MEMBRANE

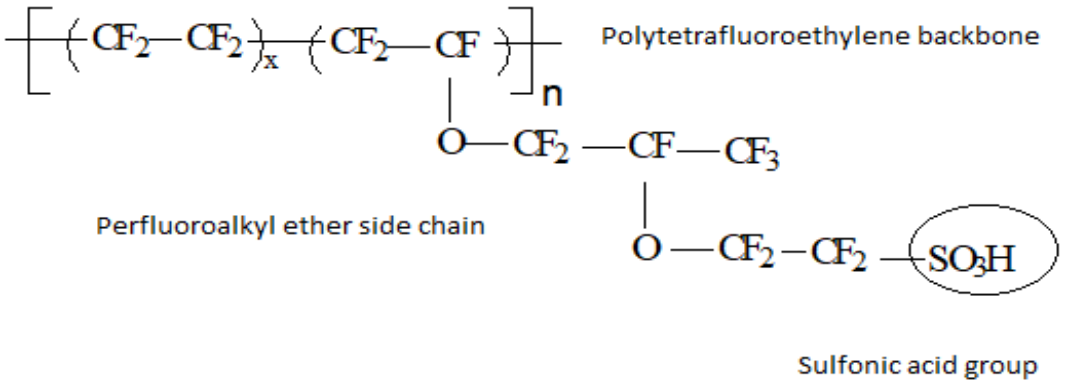

Figure 2. 4: Chemical structure of Nafion 117 ionomer (Zakil *et al.* 2016a)

Figure 2.4 shows the chemical structure of the repeating unit present in the polymer chain of Nafion 117. The Nafion membrane consist of a hydrophobic polytetrafluoroethylene (PTFE) backbone, which accounts for its good chemical and mechanical stability. The high proton conducting ability of Nafion 117 is attributed to the presence of sulfonic acid groups attached to the hydrophilic perfluoroethylether side chains (Huang *et al.* 2008, Smitha *et al.* 2005).

Nafion 117 is reported to have proton conductivity values in the range of 10^{-2} S/cm depending on the experimental conditions; Smitha *et al.* (2005) reported a proton conductivity of 8.56 $x10^{-2}$ S/cm for Nafion 117 at 100% relative humidity and Huang *et al.* (2008) reported Nafion 117 to have a proton conductivity of $2.3x10^{-2}$ S/cm. However, the use of Nafion 117 in fuel cells is met with several challenges such as its low selectivity to methanol in DMFC and low fuel cell performances at high temperatures due to membrane dehydration. The high cost of Nafion 117 is estimated at 1700 \$ /m^2 and is another contributory factor that limits the wider application of fuel cell technology (Huang *et al.* 2008, Neethu *et al.* 2019, Smitha *et al.* 2005). The mechanical stability and ion exchange capacity of Nafion 117 is susceptible to high temperatures. Currently, DMFCs and PEMFCs are limited to operating temperatures of ~80 °C. The development of polymer electrolyte membrane that can withstand high temperature fuel cell operations of ~150 – 200 °C is desirable to combat the carbon monoxide poisoning of the platinum catalyst used in fuel cell technology. The carbon monoxide poisoning is a result of the incomplete oxidation of methanol in DMFCs and the usage of reformed hydrogen which

consist of trace amounts of carbon monoxide in PEMFCs (Alias *et al.* 2020, Brandon *et al.* 2003, Mališ *et al.* 2018).

Zakil *et al.* (2016a) presented several research findings on modifications conducted on the Nafion 117 membrane to improve its fuel cell performances at high temperature conditions. The modification of Nafion 117 with silica and phosphotungstic acid was reported to yield enhanced thermal properties and optimum power density of 250 mW/cm^2 in a DMFC operated at a high temperature of 145 °C. The Nafion 117 membrane modified with zeolite attained a maximum power density of 390 mW/cm^2 in a DMFC operated at 140 °C (Zakil *et al.* 2016a). The enhanced fuel cell performances seen with the modified Nafion 117 were attributed to the improvements in water retention properties initiated by the incorporation of zeolite on the Nafion 117 matrix during the modification (Zakil *et al.* 2016a).

The high permeation of methanol across the Nafion 117 membrane is another challenge experienced in DMFCs. The high methanol cross-over associated with the use of Nafion 117 in DMFC results in depolarisation at the cathode which reduces fuel cell efficiency due to the unwanted oxidation of the fuel at the cathode. Huang *et al.* (2008) modified Nafion 117 polymer matrices with polyaniline and investigated the permeability of methanol across the modified membrane using methanol solution at a concentration of IM. The methanol permeability coefficient of Nafion 117 was found to be $1.09x10^{-6}$ cm^2/s before and after the modification of Nafion 117 with polyaniline the methanol permeability coefficient was reduced to $1.8x10^{-7}$ cm^2/s (Huang *et al.* 2008). Mukoma *et al.* (2004), reported a methanol permeability coefficient of $2.33x10^{-6}$ cm^2/s for the Nafion 117 membrane in an investigation conducted using 12 M concentrated methanol solution (Huang *et al.* 2008, Mukoma *et al.* 2004).

In a review conducted by Hickner & Pivovar (2005), Nafion 117 is reported to have the methanol permeability coefficient of $2.3x10^{-6}$ cm^2/s , which is higher in comparison to the methanol permeability coefficient of $2.7x10^{-7}$ cm^2/s obtained using a polystyrene sulfonic acid membrane. The high methanol permeation in Nafion 117 membrane was attributed its higher electro-osmotic drag coefficient compared to the value of ~2 for the polystyrene sulfonic acid membrane. The electro-osmotic drag coefficient measures the number of water molecules transported per proton conducted through the membrane. However, Nafion 117 achieved a higher proton conductivity value of 0.085 S/cm compared to 0.012 S/cm obtained for the polystyrene sulfonic acid membrane. Furthermore, Nafion 117 was reported to have a high methanol permeability of ~$1.7x10^{-6}$ cm^2/s compared to the low methanol permeability

coefficient obtained using the poly-arylene ether sulfone membranes with a lower electro-osmotic drag coefficient. However, the proton conductivity value of the Nafion 117 membrane was still higher at ~0.1 S/cm compared to a value of ~0.04 S/cm obtained using the poly-arylene ether sulfone membranes under similar conditions (Hickner & Pivovar 2005, Sahu *et al.* 2009).

The fuel cell performances of Nafion 117 membrane and two sulfonated poly-arylene ether sulfone membranes were investigated in a DMFC using IM methanol solution at 60 °C. The Nafion 117 membrane yielded a maximum current density of ~350 mA/cm^2 and lowest open-circuit voltages of below 0.3 V compared to the two poly-arylene ether sulfone membrane. The low open-circuit voltages seen with the Nafion 117 membrane were attributed to its high methanol permeability coefficient of $1.67x10^{-6}$ cm^2/s compared to the methanol permeability coefficient of $3.6x10^{-7}$ cm^2/s and $8.1x10^{-7}$ cm^2/s attained for the two sulfonated poly-arylene ether sulfone membranes (Hickner & Pivovar 2005). Clearly, there is a correlation between the high electro-osmotic drag coefficient of Nafion 117 and its low selectivity to methanol. However, Nafion 117 is still the high proton conducting polymer electrolyte membrane despite the challenges associated with the depolarisation at the cathode due to methanol permeation. The high conducting ability of Nafion 117 have been attributed to a well-defined phase separation between the hydrophobic polytetrafluoroethylene backbone and the sulfonic acid groups attached to its per-fluorinated ethyl ether side chain. The proton diffusion coefficient and water diffusion coefficient of Nafion 117 are reported to be similar at a lower content of water molecules inside the membrane. However, at high water levels the trend is disrupted creating a huge gap between the proton diffusion coefficient and the water diffusion coefficient. The proton conductivity of Nafion 117 and its water diffusion coefficient increase with the hydration number of the membrane. The hydration number denotes the number of water molecules per sulfonic group site in the membrane and is reported to be 22 for Nafion 117 at its complete hydration state and corresponds to the electro-osmotic force of ~3 (Bai *et al.* 2015, Hickner & Pivovar 2005).

The proton diffusion coefficient and water diffusion coefficient of a fully hydrated Nafion 117 membrane were found to be ~$5x10^{-6}$ cm^2/s and ~$2x10^{-5}$ cm^2/s, respectively (Hickner & Pivovar 2005). Furthermore, Stenina *et al.* (2004) reported the Nafion 117 membrane exhibited a proton diffusion coefficient of $5.3x10^{-6}$ cm^2/s when using the hydrochloric acid solution (1N) as the electrolyte solution.

2.5 FUEL CELL TECHNOLOGY

Fuel cell technology is an electrochemical process that generates electricity through the direct conversion of chemical energy to electrical energy. A fuel cell is an electrochemical device that converts chemical energy into electrical energy (Brandon *et al.* 2003, Haile 2003, Ogungbemi *et al.* 2019).

Nowadays, fuel cell technology is gaining much recognition in the quest to find renewable sources of energy to combat green-house gas emissions and reduce its impact on global warming and climate change. The high emission of green-house gases has been associated with the current energy conversion systems, which involve the combustion of fossil fuels in the internal combustions engines, diesel engines in ships and power generating plants (Geng *et al.* 2016, Inal & Deniz 2020, Khan *et al.* 2021).

The combustion of diesel in internal combustion engines and in maritime ship engines is linked to high emissions of greenhouse gases such as carbon dioxide (CO_2) and sulphur oxides (SOx). The study conducted by the International Maritime Organisation highlighted that the shipping industry was responsible for ~800 $x10^6$ tons of CO_2 emitted in 2012 and this has put both land and maritime transportation sectors as major contributors to the global greenhouse gas emissions (Geng *et al.* 2016, Inal & Deniz 2020).

The hydrogen fuel cell (PEMFC) is gaining favourable attention in the transportation sector due to the possible generation of electricity without the emission of greenhouse gases, with only water and heat released as by-products of the redox reaction. Japan projected at least 40 000 hydrogen fuel cell vehicles to be operational on its roads by 2020, however, the projected figure was down to 4 000 in 2020. Japan is showing a progressive commitment to eradicate greenhouse gas emissions associated with the automotive sector by rolling out the hydrogen fuel cell electric vehicles, the construction of the world's largest hydrogen production facility called Fukushima Hydrogen Energy Research field and the distribution of over 100 hydrogen re-fuelling stations (Brandon *et al.* 2003, Khan *et al.* 2021).

The shipping industry has been imposed with strict regulations to limits the emission of greenhouse gases resulting from the use of diesel engines. Different types of fuel cells are being investigated using different criteria in the search for the most compatible fuel cell option to replace the diesel engines used in the shipping industry (Inal & Deniz 2020).

There are different types of fuel cells and these devices can be applied through a broader spectrum such as to cater for the domestic needs of electricity, to power portable devices and for use of fuel cells in automobiles (Alias *et al.* 2020, Brandon *et al.* 2003, Haile 2003).

Fuel cells can be categorised according to high temperature fuel cells and low temperature fuel cells. High temperature fuel cells such as the SOFC, MCFC and PAFC utilises both pure hydrogen and reformed hydrogen from hydrocarbon sources such as diesel and liquefied natural gas (LNG). Reformed hydrogen is obtained from the conversion of hydrocarbon sources to hydrogen through passing fuel through complex steam reforming unit and water-gas shift reactors (Brandon *et al.* 2003, Haile 2003, Ogungbemi *et al.* 2019).

Steam reforming reaction:

$$CH_4 + H_2O \rightarrow CO + 3H_2 \quad (2.1)$$

Water-gas shift reaction

$$CO + H_2O \rightarrow CO_2 + H_2 \quad (2.2)$$

The hydrogen is oxidised at the anode electrode of the fuel cell to liberate protons that are used in the electrochemical process to generate electricity. The process of producing hydrogen using reformed hydrogen sources is associated with the emission of greenhouse gases. However, the emissions resulting from the use of reformed hydrogen are minimal compared to greenhouse gases emitted from the combustion of fuels by internal combustion engines (Inal & Deniz 2020, Khan *et al.* 2021).

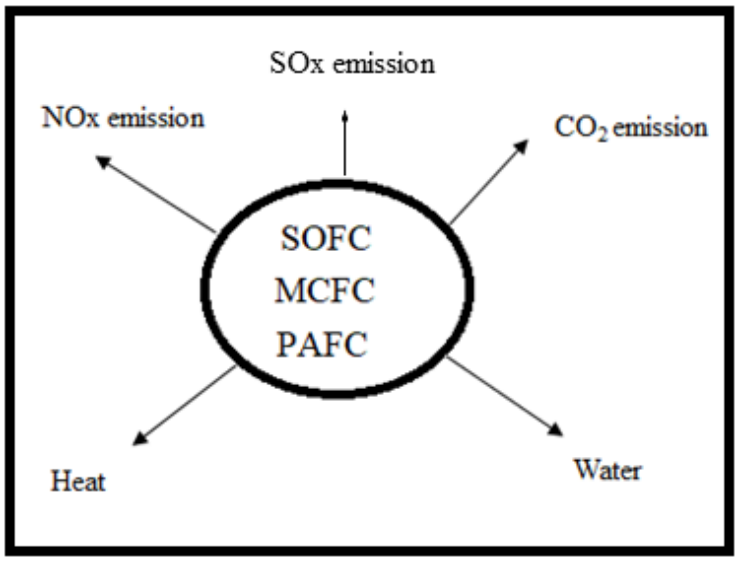

Figure 2. 5: Reformed hydrogen and GHG emissions in fuel cells

Figure 2.5 shows greenhouse gases (GHG) emitted by the solid oxide fuel cell, molten carbonate fuel cell and the phosphoric acid fuel cell where water and heat are released as by-products of the redox reaction (Inal & Deniz 2020, Khan *et al.* 2021).

2.5.1 Solid oxide fuel cells (SOFC)

The SOFC is a high temperature fuel cell operated at temperatures up to 1000 °C. Zirconium is used as the electrolyte in the solid oxide fuel cells, however, calcium oxide is also used. Zirconium serve to conduct the O^{2-} oxide from the cathode towards the anode. Oxygen is fed from the cathode and interacts with electrons liberated from the oxidation reaction of hydrogen. The SOFC have the electricity efficiency ~60% and utilises hydrogen as the oxidant for the oxidation reaction at the anode (Brandon *et al.* 2003, Inal & Deniz 2020). The metal electrolyte used in SOFC does not require the aid of a catalyst such as platinum. The disadvantages associated with the use of SOFC are the high cost and the thermal challenges on the material due to high temperature operation (Haile 2003, Ogungbemi *et al.* 2019).

The redox reactions occuring in a solid oxide fuel cell are shown below:

Anode reaction:

$$H_2 + O^{2-} \rightarrow H_2O + 2\ e^- \quad (2.3)$$

$$CO + O^{2--} \rightarrow CO_2 + 2\ e^-$$

Cathode reaction:

$$O_2 + 4\ e^- \rightarrow 2O^{2-} \quad (2.4)$$

Overall reaction:

$$H_2 + \frac{1}{2}O_2 \rightarrow H_2O \quad (2.5)$$

2.5.2 Molten carbonate fuel cell (MCFC)

Molten carbonate fuel cells are operated at high temperatures of ~650 °C. The MCFC consist of a liquid electrolyte made up of the carbonate salts such as potassium carbonate. The salt is melted inside the fuel cell and releases the carbonate anion (CO_3^{2-}) at the cathode, which then combines with the oxidised hydrogen from the anode to form water and carbon dioxide. Nickel is used as the anode and nickel oxide is used as the cathode electrode, respectively. MCFCs

have high reaction kinetics and high intolerance to sulfur impurities of ~ above 5 ppm in the fuel gas at the anode. High sulfur content at the anode results in reduced cell efficiencies. The electrical efficiency of MCFC is in the range of 50 – 60% (Brandon *et al.* 2003, Haile 2003, Inal & Deniz 2020, Ogungbemi *et al.* 2019).

The redox reactions occurring in the MCFC are shown below:

Anode reaction:

$$H_2 + CO_3^{2-} \rightarrow H_2O + CO_2 + 2e^- \quad (2.6)$$

Cathode reaction:

$$O_2 + 2CO_2 + 4e^- \rightarrow 2CO_3^{2-} \quad (2.7)$$

Overall reaction:

$$H_2 + \frac{1}{2}O_2 + CO_2 \rightarrow H_2O + CO_2 \quad (2.8)$$

2.5.3 Phosphoric acid fuel cell (PAFC)

A phosphoric acid fuel cell utilises concentrated phosphoric acid solution as liquid electrolyte. The protons diffuse through the liquid electrolyte towards the cathode whereby water is produced through the interaction of oxygen with the diffused protons and electrons from the external circuit. PAFC are operated at the temperature range of ~150 – 210 °C and have a fuel cell efficiency of ~40 – 50% (Haile 2003, Inal & Deniz 2020).

The redox reactions are shown below:

Anode reaction:

$$H_2 \rightarrow 2H^+ + 2e- \quad (2.9)$$

Cathode reaction:

$$O_2 + 4H^+ + 4e- \rightarrow 2H_2O \quad (2.10)$$

Overall cell reaction:

$$\frac{1}{2}O_2 + H_2 \rightarrow H_2O \quad (2.11)$$

2.5.4 Alkaline fuel cell (AFC)

Alkaline fuel cells were first developed in 1939 and were used by NASA to generate electricity during the space initiative. The AFC offer an advantage of high fuel cell efficiency, less corrosion and operate at relatively low temperaures ~70 ℃. The alkaline fuel cells utilise a solution of potassium hydroxide (KOH) as the alkaline electrolyte. The AFC fuel cells utilise hydrogen as fuel and are intolarence to carbon dioxide due to the undesired reaction between the electrolyte and carbon dioxide to form potassium carbonate. The AFC can generate power in the range of 1 – 5 kWatts and have a fuel cell efficiency of ~50 – 60 % (Brandon *et al.* 2003, Haile 2003, Inal & Deniz 2020).

The redox reactions occuring in the AFC cell are listed below:

Anode reaction:

$$H_2 + 2K^+ + 2OH^- \rightarrow 2K + 2H_2O \quad (2.12)$$

$$2K \rightarrow 2K^+ + 2e^- \quad (2.13)$$

Cathode reaction:

$$\frac{1}{2}O_2 + H_2O \rightarrow 2OH \quad (2.14)$$

$$2OH + 2e^- \rightarrow 2OH^- \quad (2.15)$$

Overall reaction:

$$H_2 + 2OH^- \rightarrow 2H_2O + 2e^- \quad (2.16)$$

$$\frac{1}{2}O_2 + H_2O + 2e^- \rightarrow 2OH^- \quad (2.17)$$

2.5.5 DMFC and PEMFC fuel cells

The proton exchange membrane also referred to as polymer electrolyte membrane serves to transport protons from the anode electrode towards the cathode electrode of the PEMFC and DMFC fuel cells. The diffused protons and electrons from the external circuit interact with oxygen at the cathode to produce water and heat as the by-products of the electrochemical reaction. Notably, there is zero emission of greenhouse gases when a hydrogen fuel cell (PEMFC) is used, however, when the direct methanol fuel cell (DMFC) is used there is minimal

release of carbon dioxide from the oxidation reaction of methanol at the anode (Alias *et al.* 2020, Haile 2003, Mourya & Inamdar 2008).

DMFC and PEMFC fuel cells utilise Nafion 117 as a standard polymer electrolyte membrane in most fuel cell applications. Nafion 117 is a per-fluorinated sulfonic acid membrane developed by Du Pont and is favoured amongst other membranes due to its high proton conducting ability (Ogungbemi *et al.* 2019, Sahu *et al.* 2009, Smitha *et al.* 2005).

Hydrogen fuel cells (PEMFC) are gaining much attention as an energy source in the transportation sector in the initiative to replace traditional internal combustion engines associated with high emissions of green-house gases. The DMFC has achieved research interest as an electrical source for portable appliances such as chargers and sensors and other low-power appliances (Alias *et al.* 2020, Khan *et al.* 2021).

The automotive industry in Japan and California (United States) have now implemented the use of hydrogen fuel cell (PEMFC) electrical vehicles. Hydrogen fuel cell electrical vehicles offer the advantage of zero emission of green-house gases such as carbon dioxide (CO_2) and nitrogen oxides (NOx). However, the high capital cost and operational cost associated with fuel cell technology limits its global spread compared to the cost of internal combustion engines. The cost of a PEMFC fuel cell stack was estimated by Brandon *et al.* (2003) to be in the range of 40 – 200 US$/kW based on the production of 30 000 units. However, the United State Department of Energy has projected a reduction in the cost of PEMFC stack to ~45 US$/kW by 2025 by mass production of $5x10^5$ units (Brandon *et al.* 2003, Haile 2003, Inal & Deniz 2020, Khan *et al.* 2021).

The other challenges limiting the wider application of PEMFC and DMFC are the high cost of Nafion membranes and the low selectivity of Nafion 117 to methanol when used in a direct methanol fuel cells. There is a growing research interest in the development of new membranes using cheaper polymers. Another strategy suggested to reduce the cost of Nafion 117 entails reducing the current thickness of the Nafion membranes from ~175 µm to 25 µm (Brandon *et al.* 2003, Haile 2003, Mukoma *et al.* 2004, Zakil *et al.* 2016a)

The polymer electrolyte membrane most suitable for fuel cell applications comprises of the properties listed below (Brandon *et al.* 2003, Ogungbemi *et al.* 2019):

- Good proton transport
- No affinity to electrons

- Inexpensive to fabricate
- Good chemical and mechanical properties
- Good thermal properties
- Good water uptake properties and less swelling
- Restrict methanol permeation.

The Nafion 117 membrane is susceptible to mechanical degradation at high temperatures, which has limited the operation of DMFC and PEMFC fuel cells to temperatures of <90 °C. However, the low temperature operation of DMFC and PEMFC fuel cells favours carbon monoxide (CO) poisoning of the platinum catalysts from trace amounts of carbon monoxide when using reformed hydrogen gas in PEMFC and CO-poisoning of the platinum catalyst from the incomplete oxidation reaction of methanol in DMFC (Alias *et al.* 2020, Kamarudin *et al.* 2013, Lin *et al.* 2008, Ogungbemi *et al.* 2019).

The CO-poisoning of the platinum catalyst results from the ability of carbon monoxide to occupy the active sites originally intended for the binding of hydrogen at the anode (Brandon *et al.* 2003, Haile 2003, Wang & Jiang 2017).

Below is the list of strategies that have been put forward to combat carbon monoxide poisoning of the platinum catalyst in PEMFC and DMFC operations (Brandon *et al.* 2003):

- To develop tolerant CO- platinum catalyst through a modification with metals such as ruthenium, for example, Pt-Ru catalyst for use in DMFC fuel cells
- To introduce a low dose of oxygen as an oxidising agent to react with carbon monoxide to produce carbon dioxide
- To suppress CO poisoning by operating DMFC and PEMFC at high temperatures in a range of ~150 – 200 °C. However, this strategy requires the development of new membranes or a modification of Nafion 117 to withstand high temperature conditions.

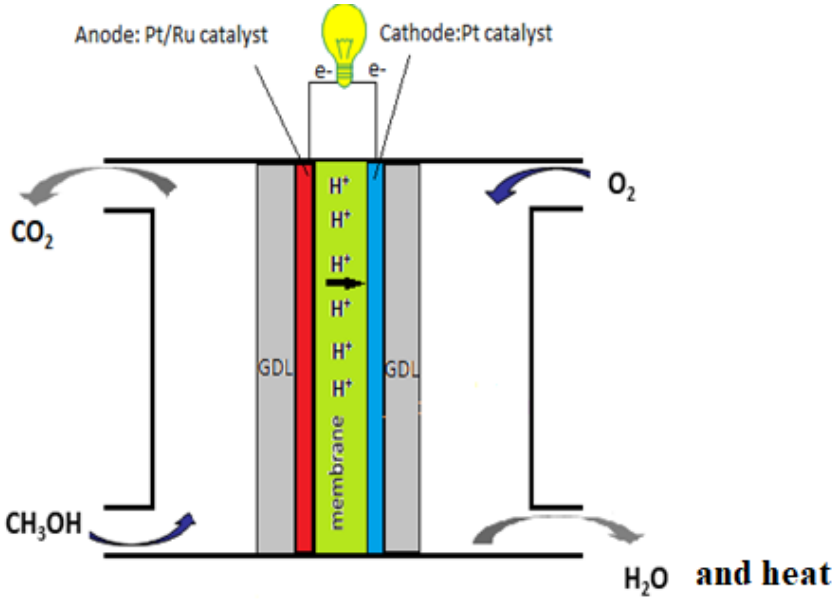

Figure 2. 6: A simplified diagram of a direct methanol fuel cell (DMFC)

Figure 2.6 shows a simplified diagram of the direct methanol fuel cell. The oxidation reaction of methanol occurs at the anode usually with the platinum-ruthenium catalyst. The fuel cell performance in a DMFC is dependent on several parameters such as the concentration of the fuel, the operating temperature, the thickness of the PEM and the quality of the MEA. Equations 2.18 – 2.20 illustrate the oxidation and reduction reactions in a direct methanol fuel cell. The oxidation of methanol liberates protons that diffuse through the polymer electrolyte membrane and electrons that migrate to the external circuit; there is also a minimal release of carbon dioxide. The reduction reaction occurs at the cathode when oxygen accept diffused protons to produce water molecules as the by-product (Alias *et al.* 2020, Khuhro *et al.* 2018).

Oxidation reaction:

$$CH_3OH + H_2O \rightarrow CO_2 + 6H^+ + 6e^- \quad (2.18)$$

Reduction reaction:

$$\frac{3}{2}O_2 + 6\,H^+ + 6e^- \rightarrow 3H_2O \quad (2.19)$$

The overall reaction:

$$CH_3OH + \frac{3}{2}O_2 \rightarrow CO_2 + 2H_2O \quad (2.20)$$

The liquid state of methanol used as fuel in direct methanol fuel cell is advantageous compared to the intensive storage requirements for hydrogen fuel used in PEMFC. The economic aspects in fuel cell technology take into consideration both the capital cost and the operational cost. The capital cost is mainly influenced by the cost of fuel cell components and the storage cost. The cost associated with the storage in hydrogen fuel cells (PEMFC) is high due to a series of comprehensive storage processes which are due to low-storage density of fuel in the gaseous form (Alias *et al.* 2020, Brandon *et al.* 2003, Inal & Deniz 2020).

The major challenge in direct methanol fuel cells is the high permeability of methanol across the Nafion 117 membrane. The permeation of methanol across the membrane towards the cathode electrode leads to low power densities due to the mixed potential. There is a significant research interest on the modification of Nafion 117 to a membrane with a high selectivity to methanol and the development of alternative cheaper membranes with high selectivity to methanol and high proton exchange ability (Alias *et al.* 2020, Chakrabarty *et al.* 2010, Khuhro *et al.* 2018, Mukoma *et al.* 2004, Sahu *et al.* 2009)

Notably, the oxidation kinetics of methanol in the DMFC are slower compared to the oxidation reaction of hydrogen in the PEMFC (Li *et al.* 2016, Ogungbemi *et al.* 2019). Figure 2.7 shows a typical diagram of a hydrogen fuel cell, also known as the PEMFC.

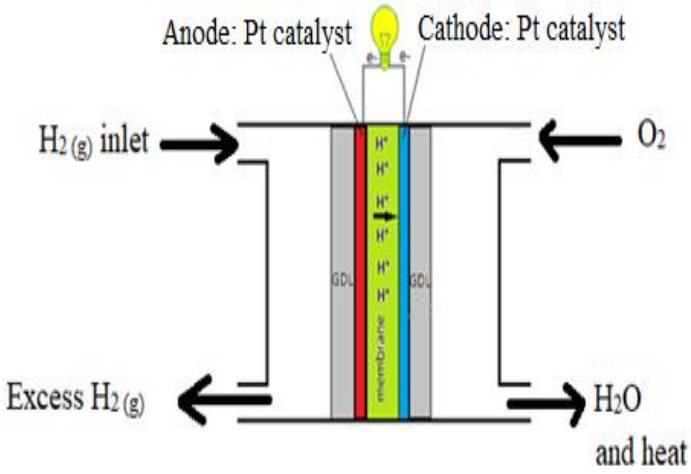

Figure 2. 7: Diagram showing hydrogen fuel cell (PEMFC)

The operating temperature in a PEMFC is limited to ~80 °C due to the susceptibility of the Nafion 117 membrane to degradation at high temperatures and low relative humidity.

Hydrogen is used as fuel and is oxidised at the anode to liberate protons that diffuses through the proton exchange membranes, the electrons migrate to the external circuit. The reduction reaction occurs at the cathode when the protons and electrons interacts with oxygen. Electricity is produced as the product of the electrochemical process, whilst water and heat are produced as by-products of the redox reaction (Brandon *et al.* 2003, Mališ *et al.* 2018).

The redox reactions of the hydrogen fuel cell are shown below (Ogungbemi *et al.* 2019):

Anode reaction:

$$2H_2 \rightarrow 4H^+ + 4e^- \quad (2.21)$$

Cathode reaction:

$$O_2 + 4e^- + 4H^+ \rightarrow 2H_2O \quad (2.22)$$

Overall reaction:

$$2H_2 + O_2 \rightarrow 2H_2O \quad (2.23)$$

Theoretically, PEMFC can achieve fuel cell efficiencies of around 80 percent at room temperatures compared to the internal combustion engines, which burn the fuel. However, this is unattainable practically due to irreversible resistive losses and polarisation losses, which limit the fuel cell efficiency to ~60% (Inal & Deniz 2020, Mališ *et al.* 2018, Wang *et al.* 2008). Developments in PEMFC shows a significant growth between 1984 – 2002 with improvement in power density outputs from ~100 mW/cm^2 to ~1000 mW/cm^2 (Haile 2003). The high power densities of 1W/ cm^2 achieved in laboratories were, however, limited to the maximum power density of 500mW/cm^2 for the fuel cell stacks due to demands for a heat management system. For a fuel cell with the open-circuit of 1 V and a current density of 0.7 A/cm^2, the voltage losses of not more than 0.3 V would be necessary to achieve the power density of 0.5 W/cm^2 (Brandon *et al.* 2003, Haile 2003, Ogungbemi *et al.* 2019).

The challenges associated with PEMFCs include the high cost of hydrogen due to its complex production process from hydrocarbon sources such as natural gas, which require equipment such as reformers and high temperature water-gas shift reactors. The cost of processing fuel to hydrogen accounts for ~29 percent of the total cost of operating the hydrogen fuel cell. The operating cost is escalated by the complex fuel processing system consisting of a fuel reformer operating at temperatures >1000 °C with a Pt/Ni catalyst and two high temperature reactors operating at 430 °C and 230 °C. Furthermore, the use of reformed hydrogen has been linked

with high polarisation losses as well as carbon monoxide poisoning of the platinum catalyst (Brandon *et al.* 2003, Haile 2003, Inal & Deniz 2020).

Hydrogen can also be produced via water electrolysis (Inal & Deniz 2020). In this study, water electrolysis was used to produce hydrogen due to its advantage of zero emission of green-house gases compared to the other complex technologies of obtaining hydrogen. Hydrogen and oxygen were produced from water electrolysis according to the reactions presented below:

Reduction reaction: Cathode half reaction

$$2H_2O + 2e^- \rightarrow H_2 + 2HO^- \quad (2.24)$$

Oxidation reaction: Anode half reaction

$$2H_2O \rightarrow O_2 + 4e^- + 4H^+ \quad (2.25)$$

Combined half reactions:

$$2H_2O \rightarrow 2H_2 + O_2 \quad (2.26)$$

2.6 POLARISATION CURVES

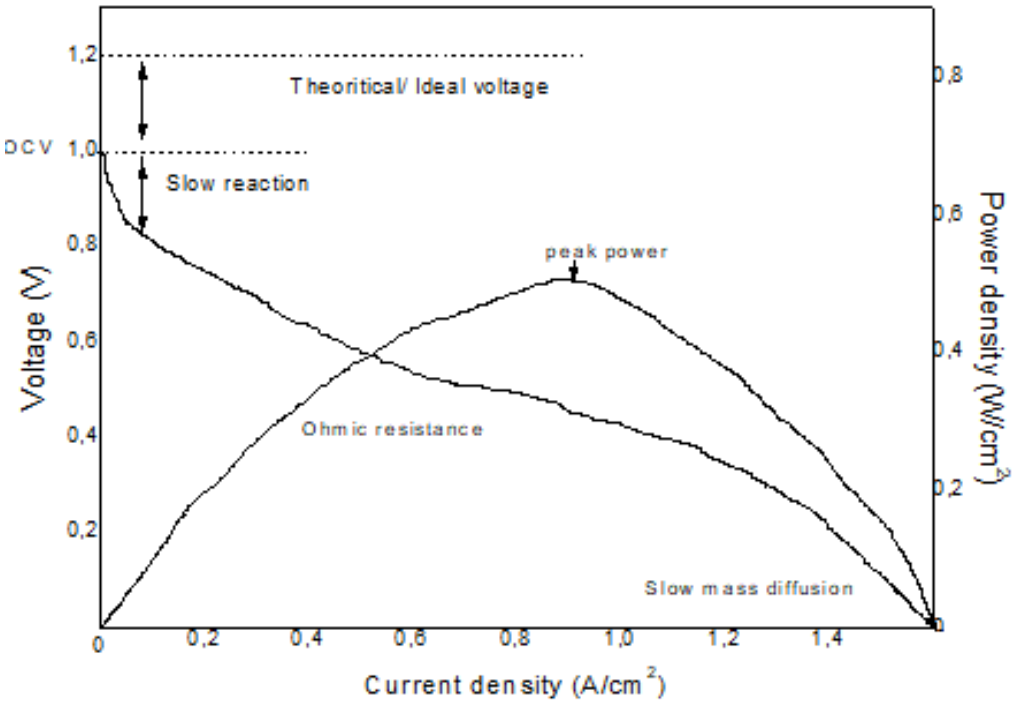

Figure 2. 8: Polarisation curves for fuel cell performance

Figure 2.8 shows the polarisation curves used in the investigation of fuel cell performances when the current generated is used to power the load. The polarisation curves represent a plot of measured voltage output with a corresponding current density. The power density is obtained as a product of the voltage output and current density output. The MEA used in the investigations of fuel cell performances consists of a polymer electrolyte membrane inserted between the anode electrode and cathode electrodes. The voltage output can be optimised through the arrangement of fuel cells in series using bipolar plates. Ideally, a high performing fuel cell would yield an optimum voltage of about 1.2 V at room temperature, but practically this is hard to accomplish because of activation losses due to slow kinetics, ohmic losses and concentration losses associated with slow mass diffusion (Alias *et al.* 2020, Brandon *et al.* 2003, Haile 2003, Ogungbemi *et al.* 2019).

In this study, MEAs investigated for fuel cell performance were prepared using different types of sulfonated chitosan membranes developed in this work and also using the Nafion 117 membrane. The polymer electrolyte membranes were inserted between two gas diffusion electrodes with platinum as a catalyst to form the MEA.

2.7 CONCLUSION

Fuel cell technology is an emerging technology in the endeavour to find renewable sources of energy with reduced or no emission of greenhouse gases such as carbon dioxide. The hydrogen fuel cell (PEMFC) has attained favourable attention as a power source for electric vehicles due to zero emission of green-house gases. Nowadays, the use of fossil fuels in internal combustion engines and in electricity generating plants is a major contributor of pollution and thus both PEMFCs and DMFCs have gained interest as potential power sources for high power density and low power density applications.

This chapter highlighted several challenges hindering the wider application of both PEMFC and DMFC fuel cells. Primarily, the high cost of the Nafion 117 membrane and its susceptibility to methanol permeation in DMFCs was identified as the challenge hindering the wider application of fuel cell technology.

CHAPTER 3: MATERIALS AND METHODS

3.1 INTRODUCTION

This section gives a description of chemicals and analytical equipment that were used to conduct the research presented in this report. This section presents experimental procedures that were implemented in the modification of chitosan into proton exchange membranes that were later tested for fuel cell performances. The mathematical equations that were adopted in the processing of the experimental data are also presented in this section.

3.2 MATERIALS

Chitosan (85% degree of de-acetylation) was obtained from Xian Lukee Bio-Tech Co., Ltd. Silica dioxide nanopowder (10-20nm particle size, 99,5% trace metal basis) was obtained from Sigma-Aldrich Chemistry (USA). Acetic acid (glacial, 100%), sodium hydroxide pellets and sulphuric acid 98% (AR) were purchased from the LABCHEM. N, N- dimethylformamide was purchased from Merck KGaA, Germany. Taurine- 99% (2-aminoethanesulfonic acid) was purchased from Acros Organics (New Jersey, USA). Nafion 117 membrane and GDE Pt-4mg/cm^2 were purchase from the FuelCellStore (USA)

3.3 MEMBRANE PREPARATION PROCEDURES

Different chitosan membranes were fabricated in this study and can be classified as sulfonated chitosan polymer electrolyte membrane modified with:

- 2-aminoethanesulfonic acid (2AESA) and dimethylformamide (DMF)
- 2 –aminoethanesulfonic acid (2AESA)
- Silica nanoparticles

The membranes were developed through the solution casting method and casted using the device in Figure 3.1. The thickness measurement of the developed membranes was performed using the Mitutoyo device shown in Figure 3.2.

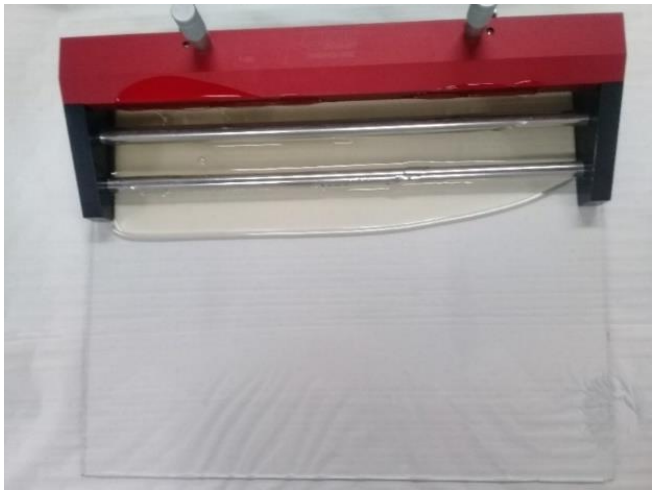

Figure 3. 1: SH0342-002 TQC sheen device for solution casting

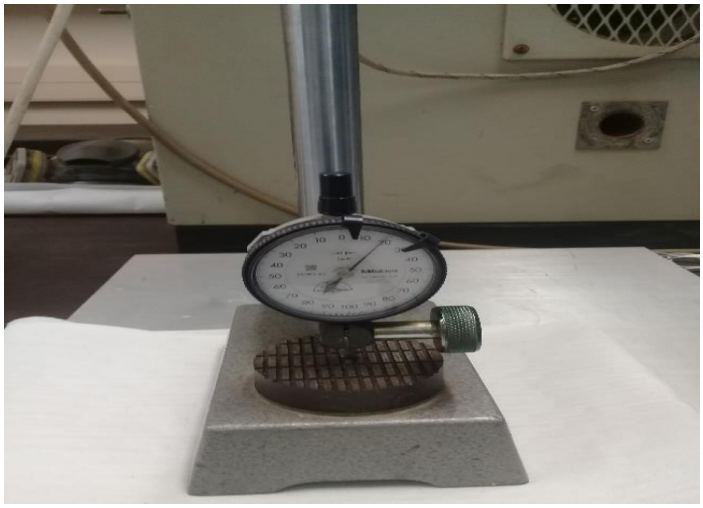

Figure 3. 2: Mitutoyo No.21095-10 [p] device for membrane thickness measurement

3.3.1 Sulfonated chitosan membrane modified with 2AESA and DMF

Objective of the experiment:

- To modify chitosan by plasticisation with DMF to improve flexibility and to incorporate 2AESA to increase proton exchange channels of the resulting membrane
- To vary the concentration of DMF while keeping the concentration of 2AESA constant in the modification to weigh the effect of the plasticiser on the membrane.

a) **Experiment 1**

A chitosan blend (5 wt.% 2AESA) was prepared and solubilised in acetic acid solution (3 v/v%). The mixture was stirred at 1000 rpm for 60 minutes under atmospheric conditions before adding dimethylformamide (15 mL) and de-ionised water (15 mL). The plasticised solution was stirred at a speed of 1000 rpm for 60 minutes at room temperature before casting onto a glass tray. The casted solution was dried for 5 hours at 50 °C before cross-linking in 1000 mL sulphuric acid solution (5 v/v%) for 4 hours. The cross-linked membrane was neutralised for 60 seconds in 1000 mL sodium hydroxide solution (0.025 M) and was rinsed with distilled water before drying at room temperature.

b) Experiment 2:

The second experiment was performed under similar conditions as Experiment 1, but with the exception of the volume of dimethylformamide and deionised water doubled to 30 mL of each.

3.3.2 Sulfonated chitosan membrane modified with 2AESA

Objective of the experiment:

- To develop sulfonated chitosan polymer electrolyte membrane modified with 2-aminoethanesulfonic acid (2AESA) without DMF.
- To conduct the modification of chitosan at different concentration of 2AESA (5 wt.%, 10 wt.%, 13.6 wt.% and 0 wt.%) and investigate different properties of the developed membranes

a) Experiment 1

A chitosan blend (5 wt.% 2AESA) was solubilised in acetic acid solution (3 v/v%) by stirring at 1500 rpm under atmospheric conditions until forming a uniform solution. The homogeneous solution was casted onto a glass tray and dried for 5 hours at 50 °C. The dried film was cross-linked in 1000 mL sulphuric acid solution (5 v/v%) for 1 hour. The membrane was immersed in 1000 mL sodium hydroxide solution (0.1 M) for 60 seconds before rinsing with distilled and drying the film under atmospheric condition.

Note: A similar procedure was followed with the exception of increasing the concentration of 2-aminoethanesulfonic acid to 10 wt.% in the chitosan blend.

b) Experiment 2

A chitosan blend (13.6 wt.% 2AESA) was solubilised in acetic acid solution (3 v/v%) by stirring at 1500 rpm until a uniform solution was formed. The homogeneous solution was casted onto a glass tray and dried for 5 hours at 50 °C. The dried film was cross-linked in 1000 mL sulphuric acid solution (5 v/v%) for 1 hour.

The membrane was immersed in 1000 mL sodium hydroxide solution (0.1 M) for 60 seconds before rinsing with distilled water and drying under atmospheric condition.

c) Experiment 3 (Control membrane)

Chitosan was solubilised in acetic acid solution (3 v/v%) by stirring at 1500 rpm until a homogenous solution was obtained. The homogeneous solution was casted onto a glass tray and dried for 5 hours at 50 ° C. The membrane was cross-linked in 1000 mL sulphuric acid solution (5 v/v%) for 1 hour before immersing in 1000 mL sodium hydroxide solution (0.1 M) for 60 seconds. The resulting membrane was rinsed in distilled and was left to dry under atmospheric condition.

Note: The control membrane was prepared without 2AESA, namely 0 wt.% 2AESA

3.3.3 Sulfonated chitosan membrane modified with silica nanoparticles

Objective of the experiment:

The objective of this experimental procedure was to develop sulfonated chitosan membrane modified with inorganic silica nanoparticles and investigate the membrane properties as well as the fuel cell performance of the MEA.

a) Experiment 1

A chitosan blend consisting of silica nanoparticles (5 wt.%) was prepared and solubilised in acetic acid solution (3 v/v%) by stirring at 1000 rpm to form a uniform solution. The homogenous solution was casted onto a glass tray and was dried at 50 ℃ for 5 hours. The dry film was cross-linked in 1000 mL of sulphuric acid solution (5 v/v%) for 1 hour, this was followed by immersing the film in sodium hydroxide solution (0.1M) for 60 seconds.

Lastly, the membrane was rinsed with distilled water and was left to dry at room temperature before conducting analytical studies.

b) Experiment 2

A chitosan blend consisting of silica nanoparticles (2 wt.%) was prepared and solubilised in acetic acid solution (3 v/v%) by stirring at 1000 rpm to form a uniform solution. The homogenous solution was casted onto a glass tray and was dried at 50 ℃ for 5 hours. The dry film was cross-linked in 1000 mL of sulphuric acid solution (5 v/v%) for 1 hour, this was followed by immersing the film in sodium hydroxide solution (0.1M) for 60 seconds. Lastly, the membrane was rinsed with distilled water and was left to dry at room temperature before conducting analytical studies.

3.4 EXPERIMENTAL DESIGN

The experimental work conducted in this study is summarised in Figure 3.3. The characterisation of chitosan polymer was performed at the initial stage of this study. The study progressed to the modification of chitosan into polymer electrolyte membranes through the tailored chemical agents presented in Figure 3.3. The characterisation techniques employed in this study were explained further in the body of this report. Lastly, the fuel cell performance studies were conducted on the developed chitosan membranes to determine voltage outputs, current densities and power densities. These results were compared to the results obtained for the standard polymer electrolyte membrane, Nafion 117.

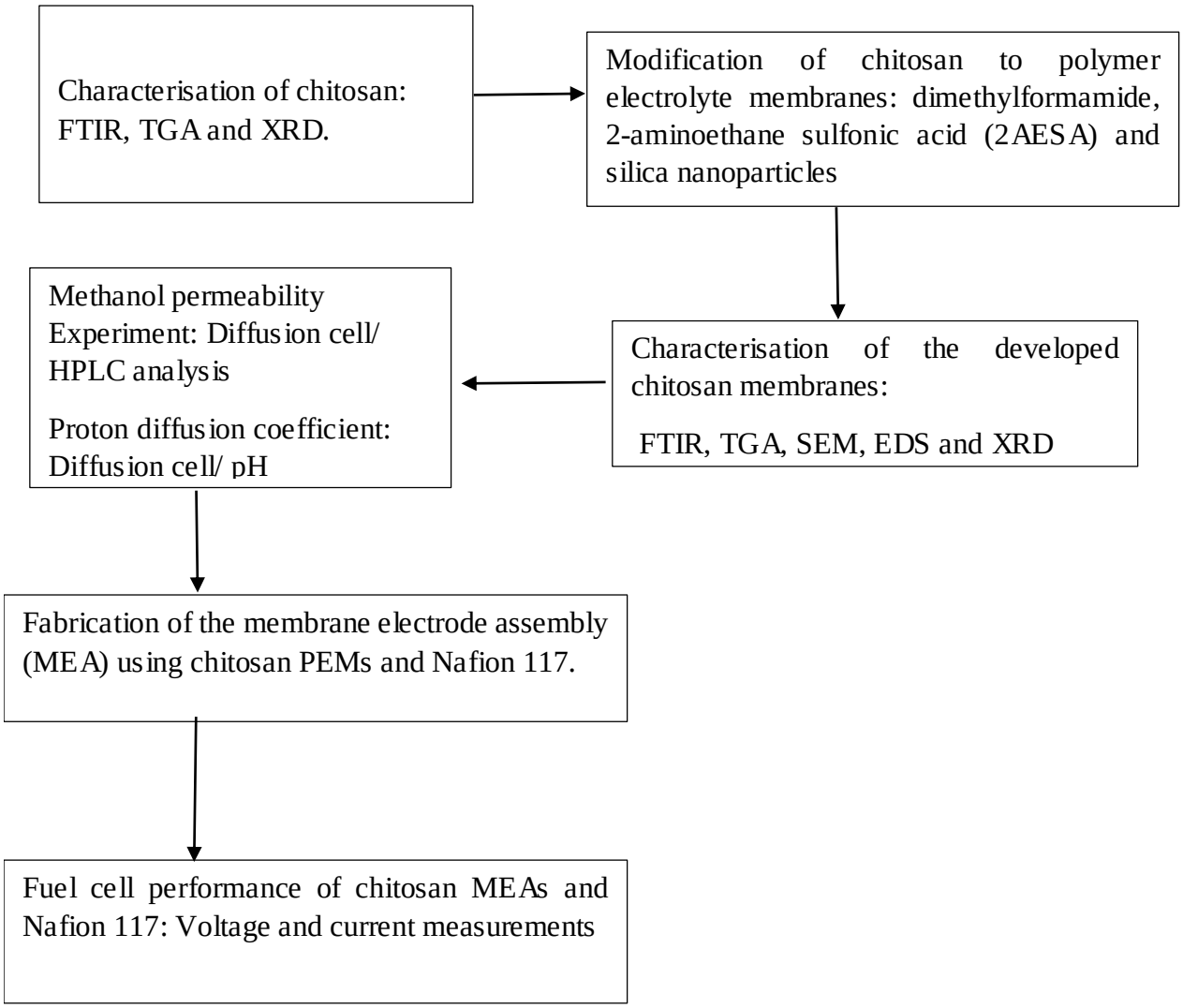

Figure 3. 3: Experimental design for the modification of chitosan

3.5 CHARACTERISATION

3.5.1 Fourier transform infrared (FTIR) spectroscopy

The Fourier transform infrared spectroscopy (FTIR) is the analysis used to determine functional groups present in a chemical structure of a given compound. In this study, the FTIR analysis was performed to investigate the functional groups present in chitosan, the resulting chitosan membranes and in the Nafion 117 membrane.

The FTIR spectra presented in this study were recorded using the PerkinElmer spectrophotometer in the range of 500-4500 cm^{-1} (10 scans) at a resolution of 8 cm^{-1}.

3.5.2 Thermogravimetric analysis (TGA)

The TGA was used to investigated the thermal stability of chitosan, the developed chitosan membranes and Nafion 117 membrane. The chitosan membrane samples and Nafion 117 sample were cut into small pieces of ~6 mg and were placed in an Al_2O_3 DSC/TG pan and were analysed using thermogravimetric analyser NETZSCH STA449F3 at a heating rate of 10 ºC/min over the range of 30 °C to 800 °C under a nitrogen atmosphere. Also, the derivative thermogravimetry (DTG), which is the first change with respect to time, was recorded as a function of temperature and the derivative weight loss was determined as $\frac{dT}{dt} = f(T)$.

3.5.3 X-ray diffraction (X-RD)

The X-ray diffraction (XRD) was used to investigate the XRD patterns of chitosan, the developed sulfonated chitosan membranes and the Nafion 117 membrane. The X-ray diffraction patterns presented in this study were obtained using XPERT-PRO-11018023 X-ray diffractometer with Cobalt (Co) radiation at a voltage of 45 kV and current of 40 mA. The scanning was conducted at a rate of 2° min^{-1} over a 2Θ range of 4º – 100º.

3.5.4 Scanning electron microscopy (SEM)

The surface morphology of the developed chitosan membranes was investigated using SEM (FEI Quanta 250 FEGSEM) coupled to the energy-dispersive X-ray spectroscopy for the elementary analysis. The membrane samples were coated with carbon and thereafter with gold/lead. The SEM imaging was done at 5 kV and 10 mm working distance.

3.5.5 High-performance liquid chromatography (HPLC)

High performance liquid chromatography (HPLC) is an analytical instrument used to separate, identify and quantify different chemical components in a mixture. The HPLC with a UV detector used in this study was supplied by PerkinElmer. The HPLC analysis was conducted to determine the permeation of methanol across the membranes.

The wavelength was set at 197 nm and the reference wavelength was set at 395 nm. Water and acetonitrile at the ratio of 20% and 80% were used as mobile phase, respectively. The C18 column was used as a stationary phase. The concentration of methanol was calculated from the peak area using the equations 3.1 and 3.2:

Calculating the response factor (N_{rf}):

$$\mathrm{Nrf} = \frac{\text{Methanol peak area (standard)}}{\text{Methanol concentration of standard}} \tag{3.1}$$

$$\text{Methanol concentration} = \frac{\text{Methanol peak area at time } t}{\mathrm{Nrf}} \tag{3.2}$$

3.6 METHANOL AND PROTON TRANSPORT ACROSS THE MEMBRANE

Figure 3.4 gives the image of the diffusion cell that was constructed in the laboratory at Technology Station, VUT Science Park, Sebokeng. The diffusion cell was used to measure methanol and proton mass transfer across the membrane. The compartments are fitted with a stirrer to ensure uniform solutions were attained for the duration of the experiment.

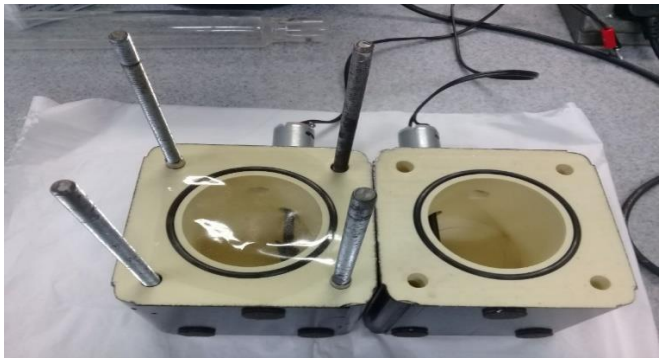

Figure 3. 4: An image of the two-compartment diffusion cell constructed at VUT Science Park, Sebokeng Campus

The schematic representation of the diffusion cell is given in Figure 3.5 with two compartments for investigations of proton diffusion studies across the synthesised polymer electrolyte membranes, which is similar to the work of (Das & Berry 2007).

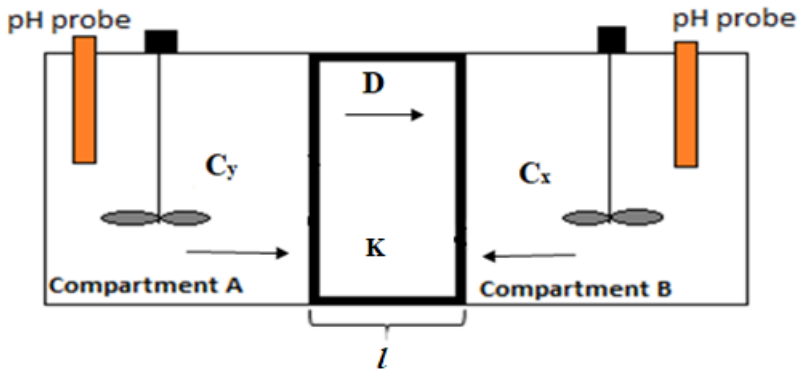

Figure 3. 5: Schematic diagram of a diffusion cell indicating compartments A and B with the polymer electrolyte membrane.

3.6.1 Model for mass transfer

The solute transport across the membrane was studied in a diaphragm diffusion cell similar to the one described by Cussler & Cussler (2009), Mukoma *et al.* (2004), Pivovar *et al.* (1999).

The total mass flux across a thin film as shown in Figure 3.5 is:

$$N = J + C_1V_1 \tag{3.3}$$

where N is total mass flux, J is the diffusive flux and C_1V_1 is the convective flux. For a dilute solution the convective flux can be neglected in which Equation 3.3 yields:

$$N = J \tag{3.4}$$

The mass transfer is in the form of diffusion and by Fick's law of diffusion:

$$J = -D\frac{dc}{d\ell} \tag{3.5}$$

where D (cm^2/s) is the diffusion coefficient and $\frac{dc}{d\ell}$ is the concentration gradient. For Fick's law model to hold, the following assumptions are made:

Assumption 1: The flux is established across the membrane owing to the concentration gradients between the two adjacent solutions.

Assumption 2: The volume of the adjacent compartments is larger than the volume of the membrane and a pseudo-steady state will prevail before the concentration changes significantly. For this case, the flux across the membranes quickly reaches a pseudo steady state.

Assumption 3: The solutions are mixed well enough to prevent concentration gradients in each compartment. Rearranging Equation (3.5) and integrating gives:

$$J\int_0^{\ell} d\ell = -D\int_{C_1}^{C_2} dC \qquad (3.6)$$

$$J = \frac{D}{\ell}(C_1 - C_2) \qquad (3.7)$$

Where C_1 (mol/L) is the concentration of solute in the bulk solution on the feed side of the membrane, as shown in Figure 3.6, C_2 (mol/L) is the concentration of the solute in the bulk solution on the permeate side of the membrane, ℓ (cm) is the membrane thickness, D (cm^2/s) is the diffusion coefficient and is considered constant.

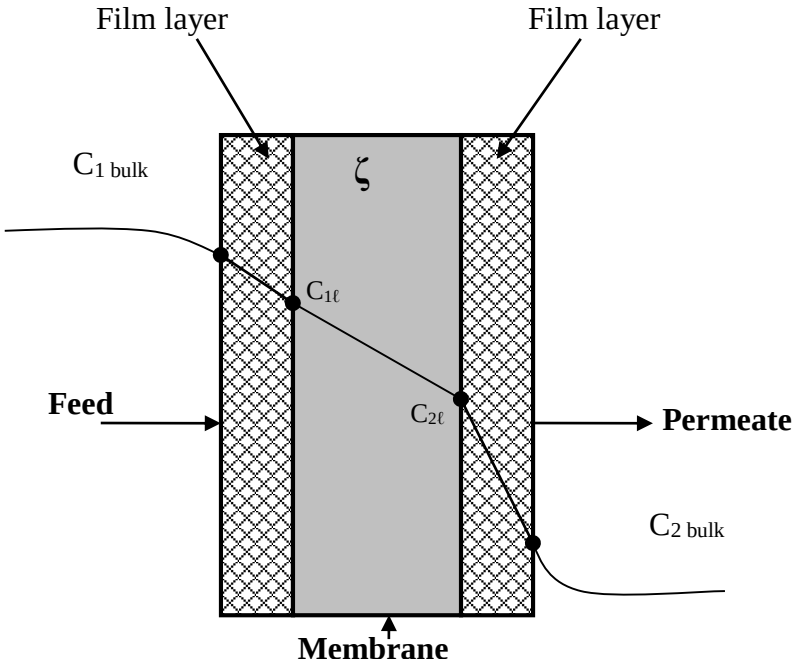

Figure 3. 6: Solute concentration gradient across membrane

For the methanol permeability study, both the compartments were stirred for the duration of the experiment. Compartment (A) consisted of the methanol solution (12M) and compartment (B) consisted of de-ionised water. Samples were taken at a time interval and analysed using the HPLC for the methanol concentration permeated to compartment B.

The data obtained from the methanol diffusion study were used to calculate the methanol permeability coefficient (P) using Equation 3.14.

The partition coefficient (*H*) is introduced in order to relate the flux to the solute concentration in the membrane.

Therefore, the concentration of methanol at the membrane surface on the feed side is:

$$C_{1\ell} = HC_A \tag{3.8}$$

and the concentration of methanol at the membrane surface on the permeate side is:

$$C_{2\ell} = HC_B \tag{3.9}$$

Substituting equations (3.8) and (3.9) into Equation (3.5) gives:

$$J = \frac{DH}{\ell}(C_A - C_B) \tag{3.10}$$

where C_A is the bulk solute concentration in compartment A (feed side) and C_B is the bulk solute concentration in compartment B (permeate side).

For compartment A, the molar flux is:

$$V_A \frac{dC_A}{dt} = -AJ = -A\left[\frac{D \cdot H}{\ell}\right](C_A - C_B) \tag{3.11}$$

For compartment B, the molar flux is:

$$V_B \frac{dC_B}{dt} = AJ = A\left[\frac{D \cdot H}{\ell}\right](C_A - C_B) \tag{3.12}$$

Where V_A and V_B are the volumes of the adjacent solutions in compartment A and B respectively, A is the membrane area exposed to the solutions in either side of the compartments.

K_B is the slope of concentration profile in compartment B and is given by Equation 3.13.

$$K_B = \frac{dC_B}{dt} = -\frac{A}{V_B}\left[\frac{D \cdot H}{\ell}\right](C_A - C_B) \tag{3.13}$$

The product of D and H is defined as the permeability coefficient (P) and was calculated from the experimental data using Equation 3.14:

$$P = (D \cdot H) = \frac{K_B V_B l}{A(C_A - C_B)} \tag{3.14}$$

Where, P is the methanol permeability coefficient (cm^2/s), K_B is the slope obtained from the concentration versus time graph in compartment B, V_B is the solution volume in compartment B, A is the area in cm^2, l is the thickness of the membrane (cm), C_A and C_B are the bulk concentration in compartment A and compartment B, respectively.

The mass transfer co-efficient (K) and proton diffusion co-efficient (D) were calculated from equations 3.15 and 3.16 (Neethu *et al.* 2019).

$$K = \frac{-v}{2at \ln \frac{(C_{x1} + C_{y1} - 2C_{y2})}{(C_{x1} - C_{y1})}} \tag{3.15}$$

The diffusion co-efficient is calculated as:

$$D = Kl \tag{3.16}$$

where D is the diffusion coefficient, C_y is the concentration of the solution on the acid compartment solute and C_x is the concentration of the solute in the water compartment across the membrane, l in cm is the membrane thickness, $-v$ is the equivalent volume of the two compartments in cm^3 separated with a polymer electrolyte membrane, with a fixed surface area of a, cm^2. The initial concentration was denoted as C_{y1} for the acid compartment filled with HCL solution and C_{y2} denoted the concentration at the end of the experiment. Two pH probes were inserted inside the two individual compartments as schematically shown in Figure 3.2.

The pH readings were recorded and converted into concentration profiles for compartment A and compartment B using Equation 3.17 (Das & Berry 2007).

$$pH = -\log\left[H^{+}\right] \tag{3.17}$$

Compartment A was filled with an acidic solution, which served as a proton donor and compartment B consisted of de-ionised water at an equivalent volume (200 mL). Each compartment of the diffusion cell had an area of 36 cm^2 and a height of 6.8 cm.

3.7 WATER UPTAKE PERCENTAGE

The membranes were cut into square pieces of ~2 cm x 2cm and were immersed in de-ionised water under atmospheric conditions for the duration set for the experiment (24h and 4h).

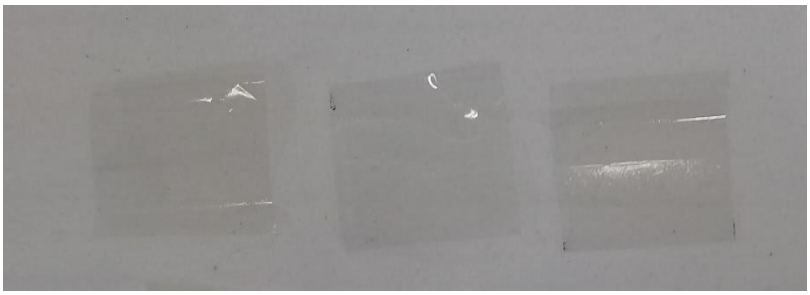

Figure 3. 7: Cut pieces ~2cm x 2cm of the membrane samples

The membranes were wiped with tissue paper to remove surface water before the weight of the wet sample was measured. The water uptake percentages of the membranes were determined from the weight difference between the dry membrane sample and the weight of the wet sample using Equation 3.18.

$$Water Uptake\,(\%) = \frac{M_{wet} - M_{dry}}{M_{dry}} \times 100 \tag{3.18}$$

Where: M_{wet} is the weight of the wet membrane after the experiment and M_{dry} is the weight of the dry sample of the membrane before the experiment.

3.8 PROTON EXCHANGE MEMBRANE FUEL CELL

The fuel cell that was used in this study is shown in Figure 3.8. The fuel cell was manufactured by Pert Industrials (Pty) Ltd and the training and experiments were conducted at Pert Industrial (Pty) premises in Centurion, South Africa. The unit consisted of a direct supply of H_2/O_2 from the water electrolysis. The voltage and current measurements were recorded directly from the electronic display in the fuel cell (Haile 2003).

The sulfonated chitosan membranes that were developed in this study through modification with different chemical agents were constructed into MEAs by inserting the membrane to the two gas diffusion electrodes with Pt-4 mg /cm^2 for the oxidation reaction of hydrogen at the anode and the reduction reaction of oxygen at the cathode.

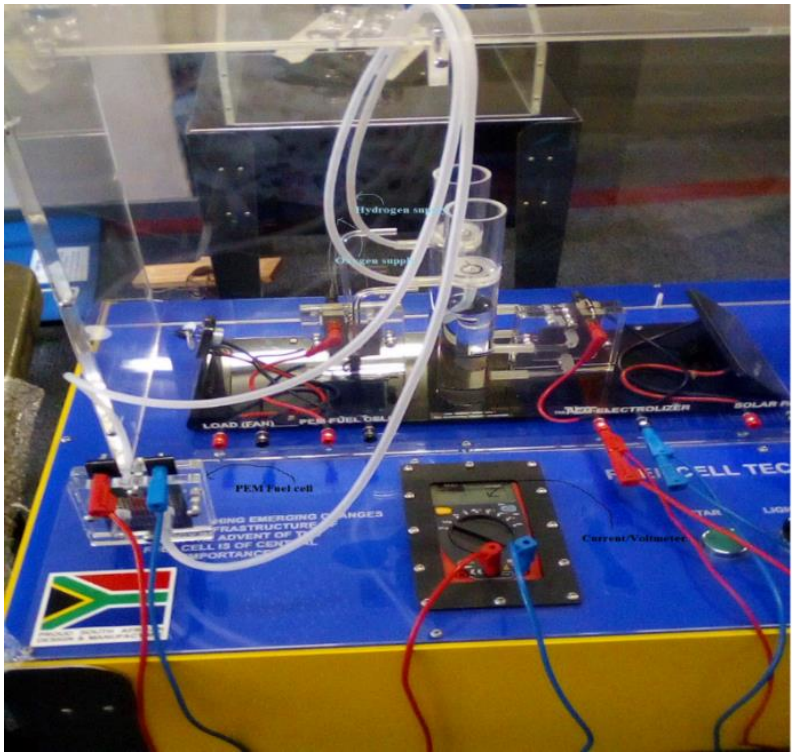

Figure 3. 8: PEM Fuel cell with a fitted electrolyser for H_2/O_2 supply

3.9 CONCLUSION

This section highlighted the experimental work conducted in this study of the development of sulfonated chitosan membranes modified with inorganic nanofillers and organic materials for fuel cell applications. Detailed descriptions were provided for the chemicals and experimental procedures implemented in the development of the chitosan membranes, as well as the characterisation methods used in the analysis of different properties of the membranes. Furthermore, the fuel cell used to investigate the performance of the chitosan MEAs was presented in this section.

CHAPTER 4: RESULTS AND DISCUSSION

4.1 INTRODUCTION

This section expands with a comprehensive discussion on the characterisation results for the different types of sulfonated chitosan membranes developed in this study and Nafion 117. The membranes were characterised using FTIR, TGA, SEM-EDS and XRD.

The water uptake percentage results of membranes are presented and discussed in this section. Furthermore, the mass transfer coefficient and proton diffusion coefficient of the chitosan membrane were calculated from the experimental data and compared with results obtained for the Nafion 117 membrane. Lastly, this chapter provides the experimental results of the fuel cell performances of the MEAs of the developed sulfonated chitosan membranes and Nafion 117 membrane.

4.2 CHARACTERISATION OF CHITOSAN

4.2.1 FTIR results of chitosan

Figure 4.1 shows the FTIR spectrum of the chitosan used in this study. The broad band between ~3600 - 3000 cm^{-1} is attributed to the intermolecular hydrogen bonding of the O-H groups in chitosan polymer chain. The two peaks at 3347 cm^{-1} and 3299 cm^{-1} are associated with the symmetric and asymmetric stretching vibrations of the N-H bonds of the primary amine groups ($-NH_2$) of chitosan. The absorption peaks at 2877 cm^{-1} and 1379 cm^{-1} were corresponded to the C-H stretching vibrations of the sp^3 hybridised alkane groups and C-H bending vibrations of chitosan (Feng *et al.* 2012). The peaks at the wavenumbers of 1655 cm^{-1} and 714 cm^{-1} were attributed to the stretching vibrations and bending vibrations of the carbonyl (C=O) groups of chitosan. The peak at the wavenumber of 1581 cm^{-1} was associated with the bending vibrations of the N-H bonds of the amine groups of chitosan (Li *et al.* 2016, Ma *et al.* 2019, Mauricio-Sánchez *et al.* 2018, Osman & Arof 2003).

The absorption band at 1153 cm^{-1} was associated with the C-O-C stretching vibrations of the ether groups in the chitosan chain. The broad band in the region of 1000 cm^{-1} was associated with the C-O bending vibrations (del Carmen Borja-Urzola *et al.* 2020). The peak at a the

wavenumber of 897 cm^{-1} was attributed to the C-O-C stretching vibrations of the glyosidic bonds linking β-1,4-linked-d-glucosamine monomers and N-acetyl-d-glucosamine monomers in the chitosan chain (Feng *et al.* 2012, Osman & Arof 2003).

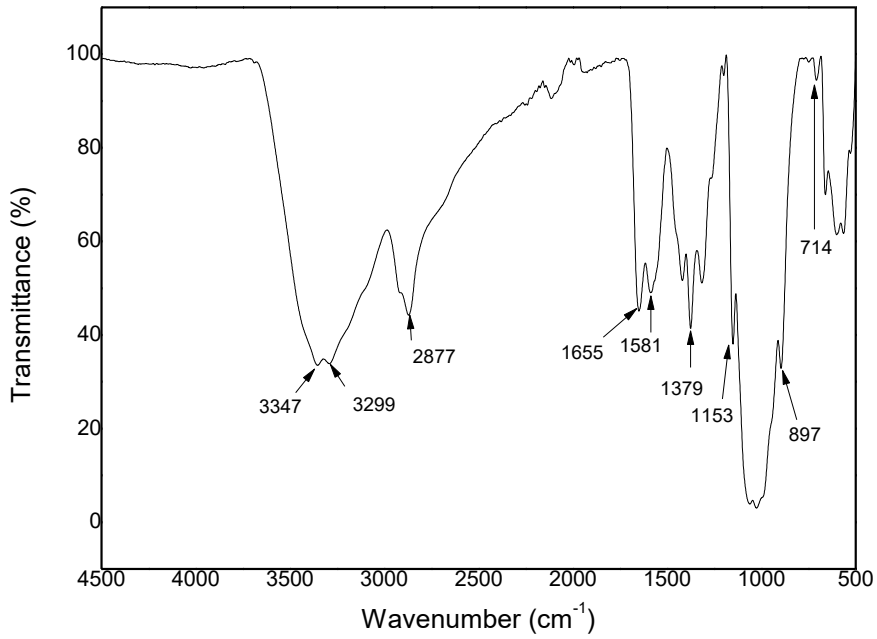

Figure 4.1: FTIR spectrum of chitosan with 85% degree of de-acetylation

4.2.2 XRD results of chitosan

Figure 4.2 shows the X-RD patterns of chitosan powder that were used in this study. The XRD patterns of chitosan showed two peaks at 2theta of ~10º and 20º associated with the two crystalline structures of chitosan. The results were in agreement with other reports from the literature (del Carmen Borja-Urzola *et al.* 2020, Feng *et al.* 2012).

The semi-crystalline character of chitosan results from the occurrence of strong intermolecular hydrogen bonding mainly between the hydroxyl groups of chitosan and the carbonyl groups of the acetyl-glucosamine regions of chitosan (Mallakpour & Ezhieh 2017).

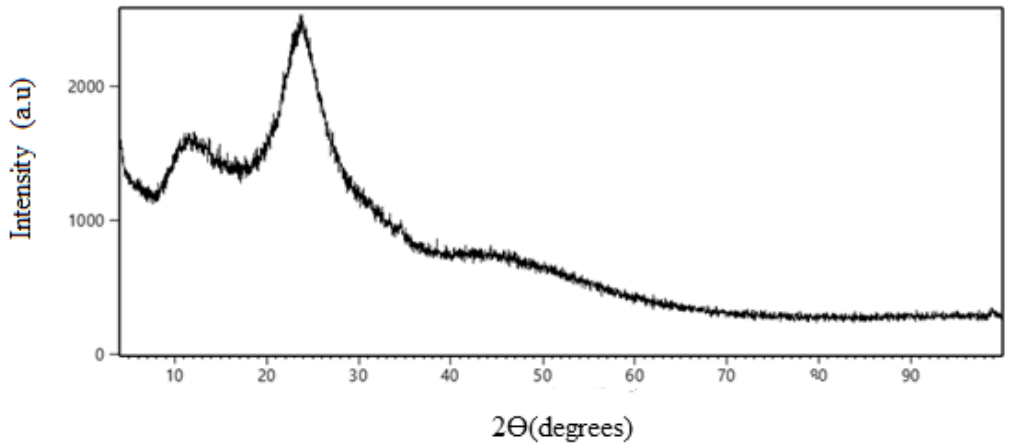

Figure 4.2: X-RD pattern of chitosan material with 85% degree of de-acetylation

4.2.3 TGA and DTG results of chitosan

Figure 4.3 shows the TGA and DTG curves of chitosan. the two degradation stages of chitosan in Figure 4.3 were agreeable with the thermal degradation stages reported for chitosan powder in the literature (del Carmen Borja-Urzola *et al.* 2020).

The first stage occurred between 76 °C – 100 °C with a weight percentage loss of <10% and was associated with the loss of water molecules from the polar regions of chitosan polymer chains. The second degradation occurred at 296 ℃ and was attributed to the degradation of the main polymer backbone of chitosan (del Carmen Borja-Urzola *et al.* 2020, Neto *et al.* 2005).

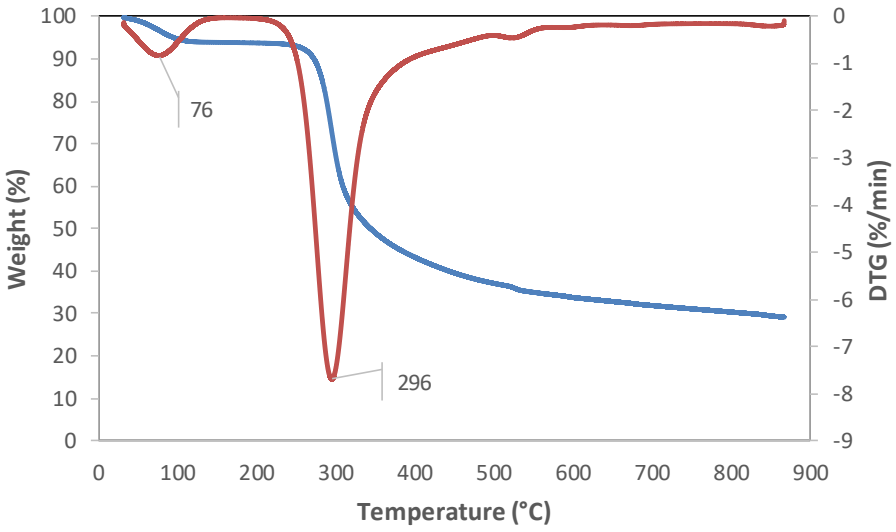

Figure 4.3: TGA/DTA graph of chitosan

4.3 SULFONATED CHITOSAN MEMBRANES MODIFIED WITH 2AESA&DMF

4.3.1 FTIR results and images of the developed membranes

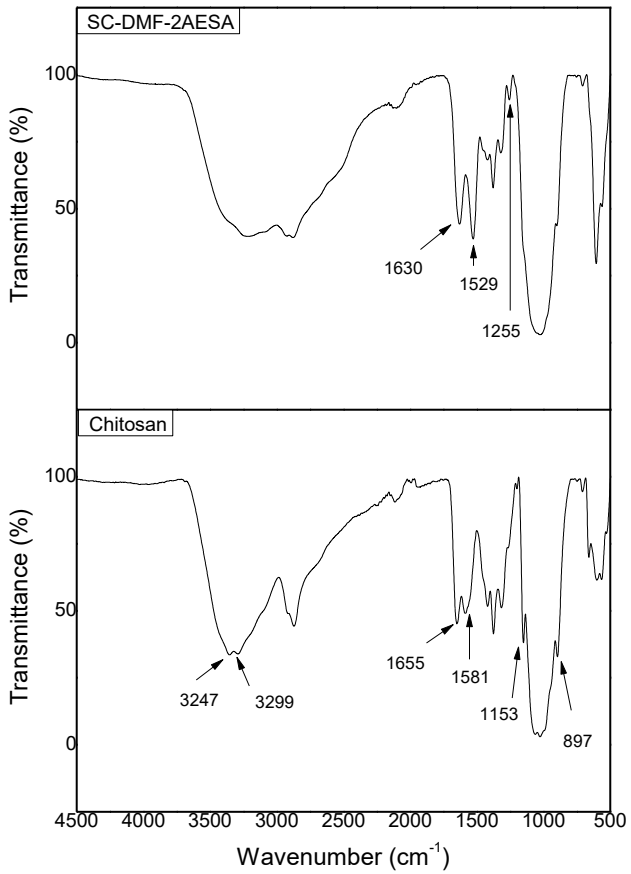

Figure 4.4: FTIR spectrum of sulfonated chitosan membrane with 2AESA and DMF

Figure 4.4 shows the FTIR spectrum of the developed sulfonated chitosan membrane modified with 2AESA and DMF (SC-DMF-2AESA). The image of the developed membrane is shown in Figure 4.5.

Notably, compared to the FTIR spectrum of chitosan, the absence of the stretching vibration peaks at the wavenumbers of 3247 cm^{-1} and 3299 cm^{-1} for the primary amine ($-NH_2$) groups on the developed chitosan membrane, as well as the absence of the stretching vibrations at 1153 cm^{-1} and 876 cm^{-1} attributed to the ether groups (C-O-C) confirmed the occurrence of the modification via the polar functional groups of the chitosan chain (Zhang *et al.* 2016).

Figure 4.4 shows a shift in the wavenumber of the carbonyl group (C=O) from 1655 cm^{-1} in chitosan to 1630 cm^{-1} in the developed chitosan membrane; this was attributed to the

weakening of the bond energy during the modification. The shift in the N-H bonds from 1581 cm^{-1} on the chitosan chain to a lower wavenumber of 1529 cm^{-1} in the developed membrane was attributed to the protonation of amino groups into the $-NH_3^+$ cations by the sulfonic acid groups and sulphate groups from 2AESA and sulphuric acid used in cross-linking, respectively (Shirdast *et al.* 2016, Xiang *et al.* 2009, Ma *et al.* 2019).

The new band observed on the membrane structure at the wavenumber of 1255 cm^{-1} was attributed to the asymmetric stretching vibrations of O=S=O from the incorporated sulfonic acid groups of 2-aminoethanesulfonic acid (2AESA) and sulphate from the sulphuric acid solution (Osman & Arof 2003, Xiang *et al.* 2009).

Figure 4.5: Developed sulfonated chitosan membrane with 2AESA and DMF

Theoretically, the plasticiser improves the flexibility of the film via dipole moment and retains its original chemical structure. Ideally, DMF integrates the chitosan polymer through hydrogen bonding without altering the functional groups of chitosan. However, a further investigation was conducted by doubling the ratio of DMF during the modification of chitosan. The results of the modification are presented in figures 4.6 and 4.7.

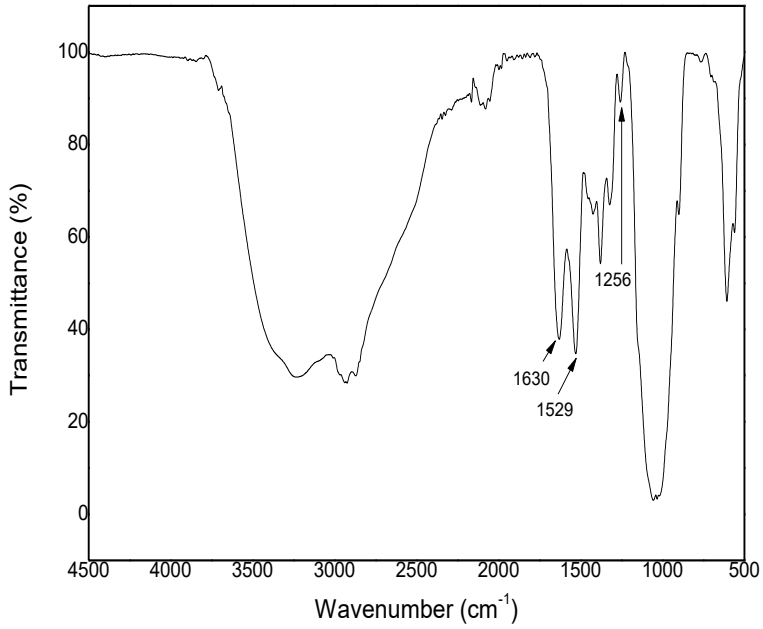

Figure 4.6: FTIR spectrum of CS with 2AESA at a higher ratio of DMF

Figure 4.6 shows the FTIR spectrum of the sulfonated chitosan membrane modified with 2-aminoethanesulfonc acid at a higher ratio of dimethylformamide. The FTIR results of the developed membrane presented in Figure 4.6 show similar patterns to the FTIR spectrum already discussed for Figure 4.4, with the exception, however, of new peaks in the region of 2000 cm^{-1} – 2500 cm^{-1} attributed to C-N associated products likely formed from the unwanted hydrolysis of dimethylformamide to formic acid and dimethylamine.

Figure 4.7: Image of CS with 2AESA at a higher ratio of DMF

The image of the developed membrane is presented in Figure 4.7. Notably, the membrane presented an uneven surface. This property is deemed undesirable in fuel cell applications due to the requirement of a uniform distribution of the anode catalyst and cathode catalyst in the surface of the membrane (Brandon *et al.* 2003).

The findings presented in figures 4.6 and 4.7 elucidate the incompatibility of DMF as a plasticiser in the current modification of chitosan to polymer electrolyte membranes. The next section explores the modification of chitosan into polymer electrolyte membrane with 2-aminoethanesulfonic acid, without incorporating dimethylformamide.

4.4 SULFONATED CHITOSAN MEMBRANES MODIFIED WITH 2AESA

4.4.1 FTIR results of the sulfonated chitosan membranes modified with 2AESA

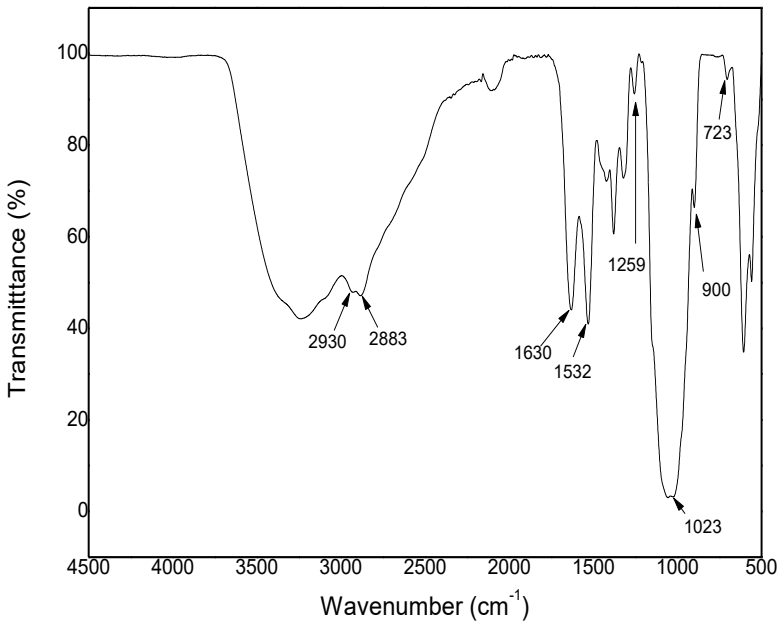

Figure 4.8 :FTIR spectrum of sulfonated chitosan modified with 5 wt.% 2AESA

Figure 4.8 shows the FTIR spectrum of sulfonated chitosan membrane modified with 2-aminosulfonic acid (5 wt.%). The broad band around 3600 – 3000 cm^{-1} was attributed to the intermolecular hydrogen bonding of hydroxyl groups (-OH) present in the membrane. The

peaks at 2930 cm^{-1} and 2883 cm^{-1} were assigned to asymmetric and symmetric stretching vibrations of sp^3 hybridised C-H groups in the membrane.

The peaks at the wavenumbers of 1630 cm^{-1} and 1532 cm^{-1} were attributed to the stretching vibrations of C=O groups and the protonation of amino groups to $-NH_3^+$ cations, respectively. The shift in stretching vibrations of N-H bonds and C=O from 1581 cm^{-1} and 1655 cm^{-1} on the chitosan polymer to lower wavenumbers on the developed membrane was associated to the weakening of the bond energy as a result of the modification with 2AESA. Furthermore, the new peak at the wavenumber at 1259 cm^{-1} was attributed to the asymmetric stretching vibrations of O=S=O groups from the sulfonic acid groups of 2-aminoethanesulfonic acid and sulphate groups from the sulphuric acid solution tailored into the chitosan matrix during cross-linking (Li *et al.* 2016, Osman & Arof 2003, Shirdast *et al.* 2016, Xiang *et al.* 2009).

The broad absorption band observed at ~1000 cm^{-1} region was associated with the overlapping of the sulfonic acid groups ($-SO_3H$) with the C-O bending vibrations of the alcohol groups and ether groups present in the membrane (Osman & Arof 2003, Shirdast *et al.* 2016).

The peak at the wavenumber of 900 cm^{-1} was attributed to the C-H wagging vibrations of the glyosidic (C-O-C) bonds. The peak at the wavenumber of 723 cm^{-1} was attributed to bending vibrations of the carbonyl (C=O) groups in the developed membrane. Notably, the shift of the carbonyl groups to a higher wavenumber compared to 714 cm^{-1} observed on the FTIR spectrum of chitosan elucidated the formation of stronger bonds between the carbonyl groups and the modifying agents (Feng *et al.* 2012, Osman & Arof 2003).

Another experiments were performed varying the concentration of 2-aminoethanesufonic acid to 13.6 wt.% 2AESA on the chitosan matrix and the other membrane was developed without 2-aminothanesulfonic acid and was denoted as the control membrane.

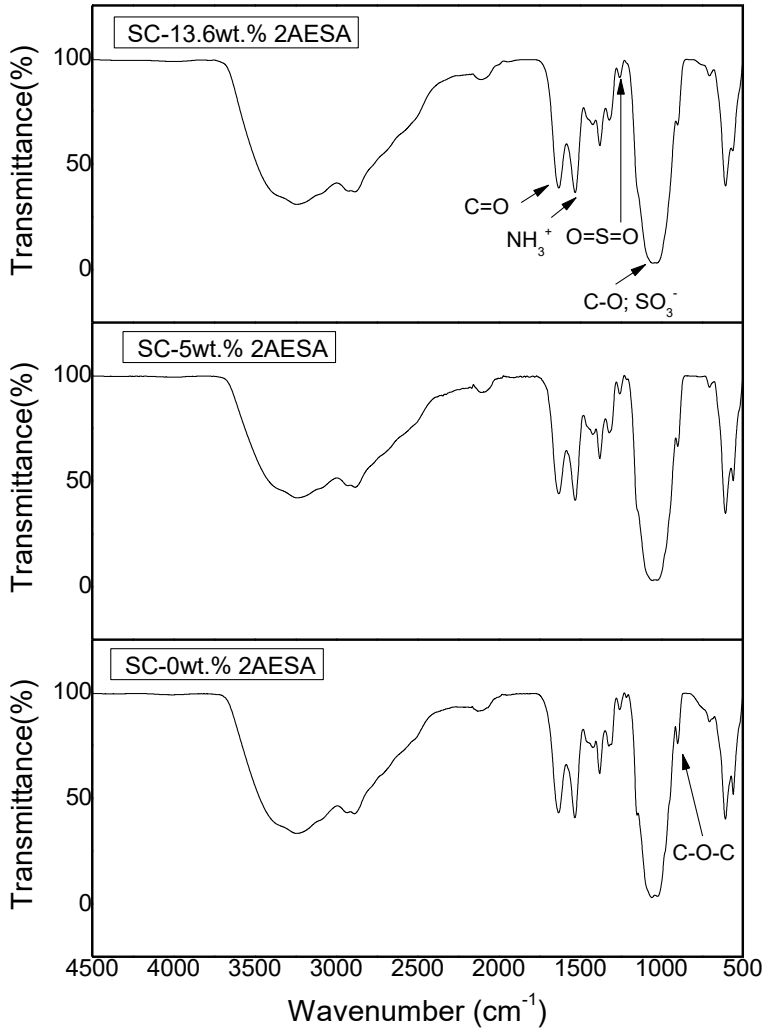

Figure 4.9 : FTIR spectra of sulfonated chitosan membranes at varied wt.% of 2AESA

Figure 4.9 shows the FTIR spectra of the sulfonated chitosan membrane modified at varied concentrations of 2-aminoethanesulfonic acid (2AESA) on the chitosan matrix.

The sulfonated chitosan membrane modified with 13.6 wt.% 2AESA exhibited a similar pattern of functional groups already discussed in Figure 4.8 for the sulfonated chitosan membrane with 2-aminoethanesulfonic acid (5 wt.% 2AESA).

Notably, the FTIR spectra of the three membranes in Figure 4.9 showed absence of the stretching vibration at 1153 cm^{-1} compared to the FTIR spectrum of chitosan in Figure 4.1. This elucidated the alteration of the asymmetric C-O-C ether groups of chitosan during the modification with 2-aminoethanesulfonic acid and the cross-linking step with sulphuric acid

solution. Furthermore, a decline of the peak at the wavenumber of 897 cm^{-1} for the C-O-C skeletal backbone separating the pyranose rings was observed in Figure 4.9 with an increase in the concentration of 2-aminoethanesulfonic acid, which was attributed to an increase in the formation of cross-linking networks in the chitosan matrix.

Figures 4.10 to 4.12 show the proposed reaction mechanism for the modification of chitosan into sulfonated chitosan membrane modified with 2-aminoethanesulfonic acid.

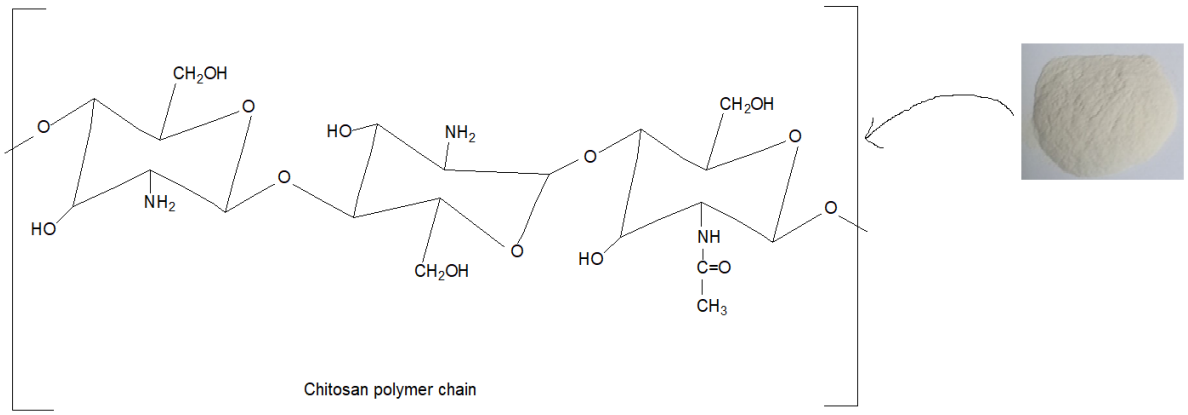

Figure 4.10: Chemical structure of chitosan polymer

Notably, the FTIR results of the developed chitosan membranes in Figure 4.9 show absence of the C-O-C stretching vibrations at the wavenumber of 1153 cm^{-1} associated with polysaccharide ring of chitosan. Figure 4.11 shows the conversion proposed in this study of the pyranose ring of chitosan into a poly (cyclohexene oxide) thermoplastic ring.

In this study, it is proposed that the reaction begins with the protonation of the primary alcohol groups in the pyranose ring of chitosan with sulphuric acid solution during cross-linking. The alcohol groups are dehydrated after accepting a proton, which results in the loss of a water molecule and the formation of a carbocation, as shown in Figure 4.11.

The primary carbocation is unstable, instead a secondary carbocation is formed, which results in the breakage of the pyranose ring. The adjacent hydrogen atom to the carbocation is slightly acidic and gets removed by water or the dilute sodium hydroxide, which acts as a base. It is proposed that the protonation of the primary alcohol groups attached to the pyranose ring of chitosan results in the formation of a poly (cyclohexene oxide) thermoplastic backbone with a carbocation. The carbocation in the thermoplastic backbone acts as an electrophile and forms a bond with sulphate group in the presence of the cross-linking sulphuric acid solution.

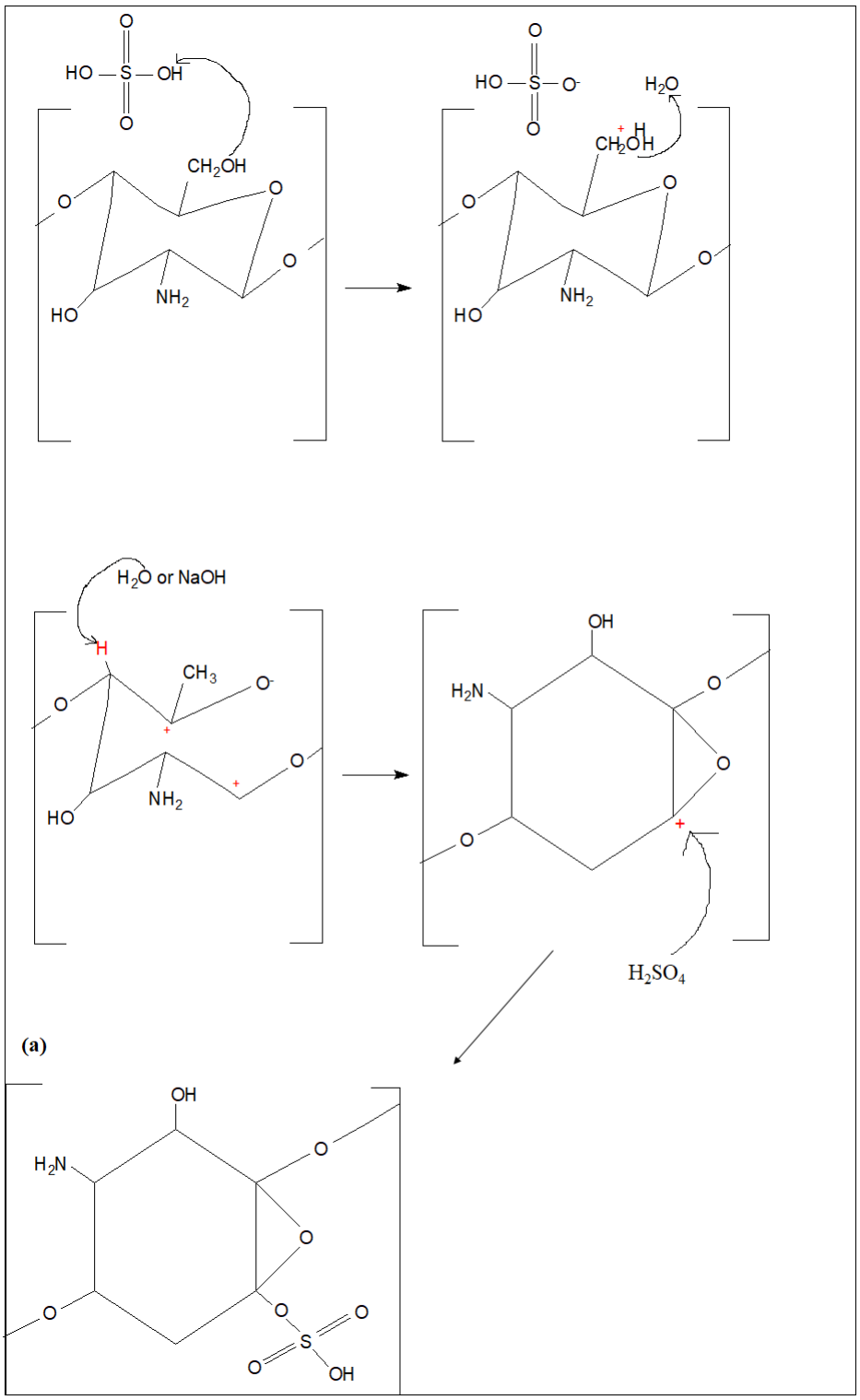

Figure 4.11: Proposed conversion of chitosan pyranose ring into thermoplastic backbone

The proposed reaction mechanism in Figure 4.11 is in agreement with the FTIR results of the developed chitosan membranes, which show absence of the polysaccharide ring C-O-C peak at 1153 cm^{-1}; moreover, a new peak at 1259 cm^{-1} attributed to the O=S=O stretching vibrations of the sulphate groups was observed on the developed membranes as the result of sulphate

anion incorporated from the sulphuric acid solution during cross-linking. Furthermore, it was proposed that chitosan interacts with 2-aminoethesulfonic acid (2AESA) and sulphate groups from sulphuric acid through the proposed chemical structure in Figure 4.12.

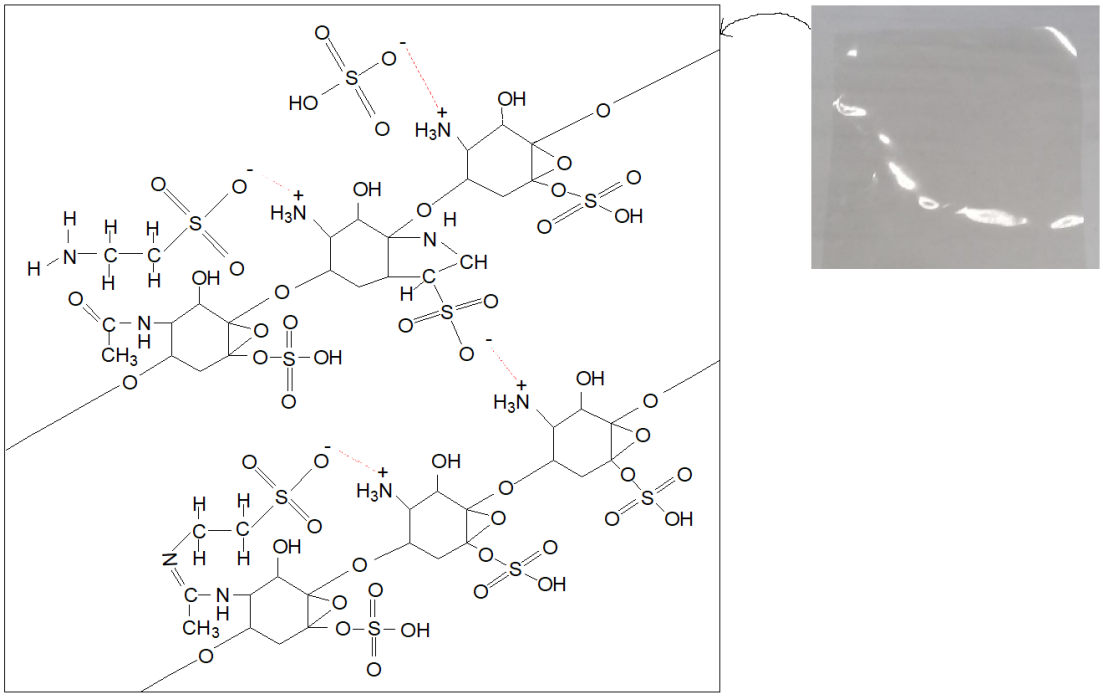

Figure 4.12: Proposed chemical structure of sulfonated chitosan membrane with 2AESA

The proposed chemical structure of the sulfonated chitosan membrane modified with 2-aminoethanesulfonic acid in Figure 4.12 was formulated through the reaction mechanism proposed to occur via:

- Electrostatic interactions formed between sulfonic acid groups of 2-aminoethanesulfonic acid and the amino groups of chitosan.
- Electrostatic interactions formed between sulfate groups of the sulfuric acid solution and the amino groups of chitosan.
- Hydrogen bonds formed between the oxygen atoms of hydroxyl groups of chitosan and hydrogen atom of amino groups of 2-aminoethanesulfonic acid.
- Hydrogen bonds formed between the carbonyl groups of chitosan and hydrogen atom of the amino groups of 2-aminoethanesulfonic acid. Alternatively, via an imine linkage formed between the carbonyl group of chitosan and the amino group of 2-aminothanesulfonic acid.

4.4.2 Images of the developed sulfonated chitosan membranes with 2AESA

Figures 4.13 to 4.15 show the images of the three membranes discussed in Figures 4.8 and 4.9. Notably, the sulfonated chitosan membranes modified with 2-aminoethanesulfonic acid as well as the control membrane exhibited smooth even surfaces, a property desirable in the fabrication of the MEAs.

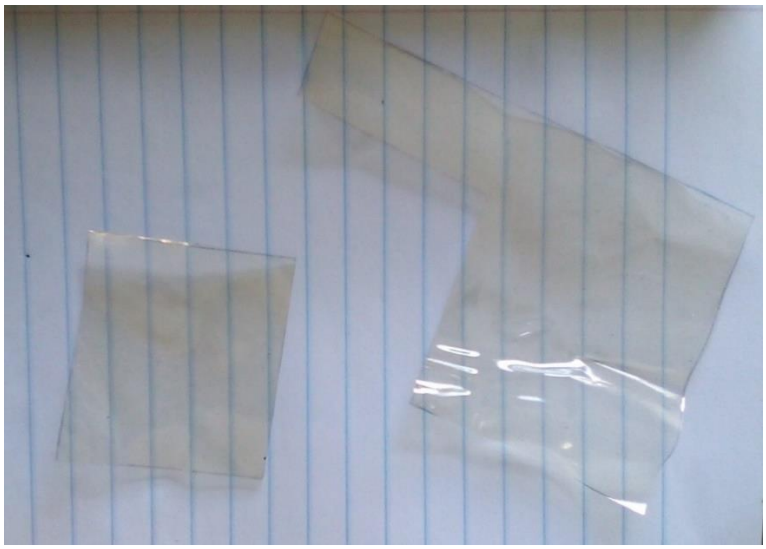

Figure 4.13: Image of sulfonated chitosan membrane modified with 2AESA (13.6 wt.%)

Figure 4.14: Image of sulfonated chitosan membrane modified with 2AESA (5 wt.%)

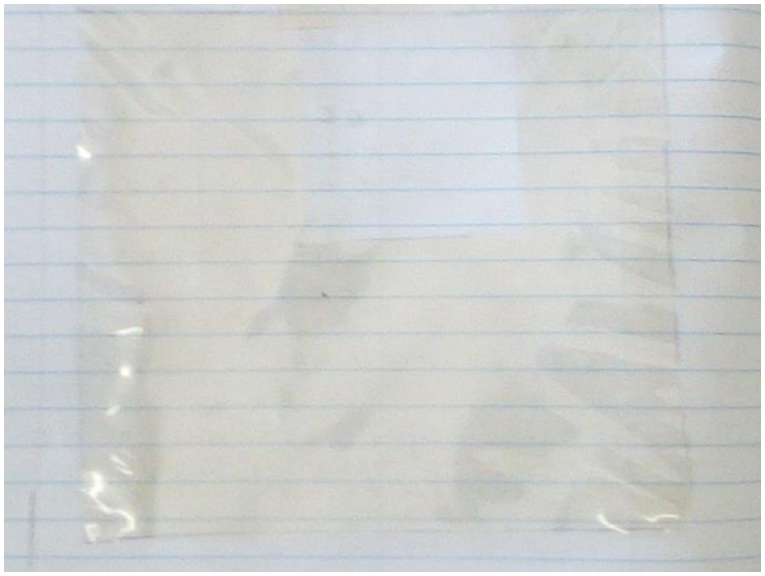

Figure 4.15: Image of sulfonated chitosan membrane (0 wt.% 2AESA)

4.4.3 TGA and DTG curves of the developed sulfonated chitosan membranes

Figure 4.16 shows the TGA/DTA thermal profile of the developed sulfonated chitosan membranes modified with 2-aminoethanesulfonic acid and the control membrane. Three stages of degradation were observed for the three membranes, as shown in Figure 4.16.

The first degradation stage occurred at a temperature <100 °C and extended until ~205 °C. This stage was associated with a weight reduction of about 15% linked to the evaporation of water molecules and solvent molecules in the membrane.

The second degradation stage occurred at 208 °C and was associated with a loss in weight of >30% linked to the decomposition of the cross-linked networks formed within the membrane as the results of the modification. Notably, the second degradation occurred earlier at 206 °C for the sulfonated chitosan membrane modified without 2AESA, which elucidated the incorporation of 2-aminoethanesulfoning acid on the chitosan matrix to yield enhanced thermal properties on the developed membranes.

The third degradation stage occurred at 263 °C and was associated with the decomposition of the main polymer chain in the developed membranes.

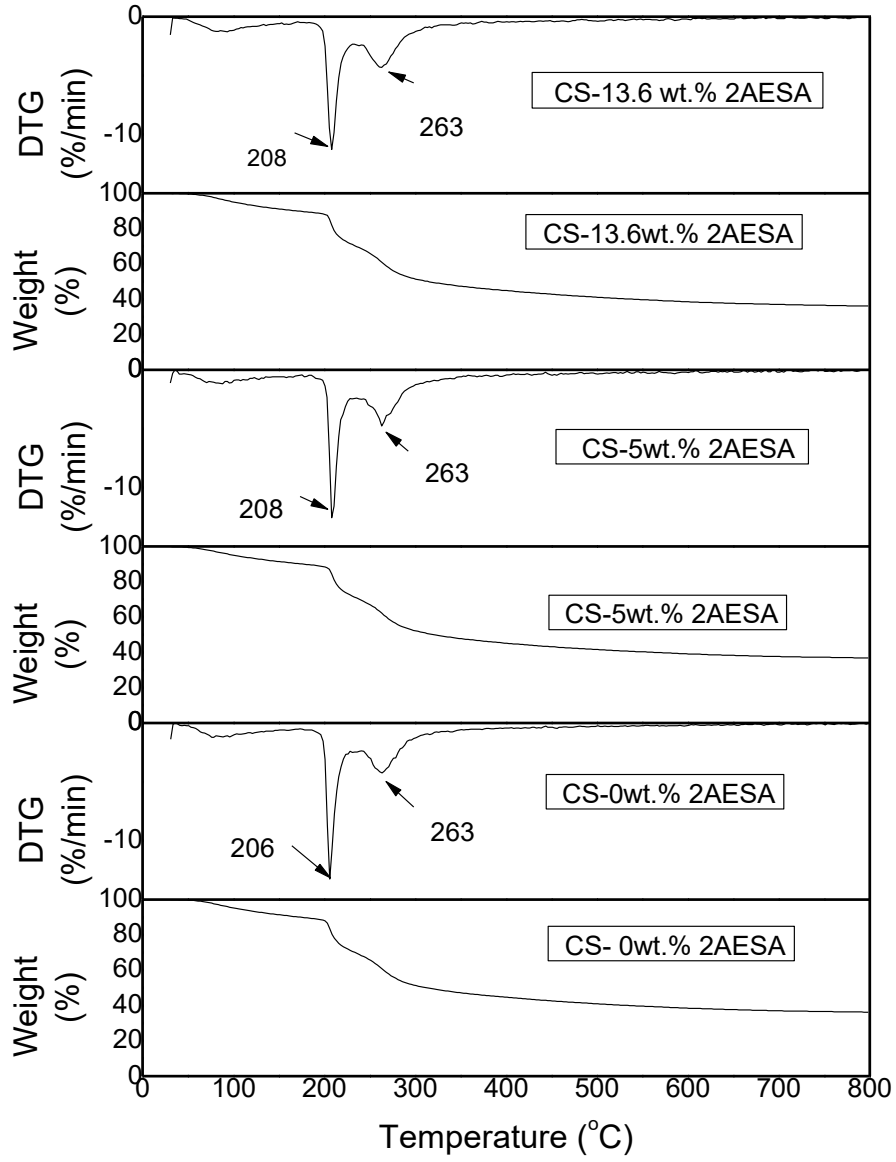

Figure 4.16: TGA/DTG thermographs of sulfonated chitosan membranes with 2AESA

4.4.4 SEM results of the sulfonated chitosan membranes modified with 2AESA

Figures 4.17 – 4.19 show the SEM micrographs of three sulfonated chitosan membranes consisting of different weight percentages of 2-aminoethanesulfonic acid (2AESA). Notably, the sulfonated chitosan membrane modified with 13.6 wt.% 2AESA showed a uniform surface compared to the high agglomeration observed on the membrane modified with 5 wt.% 2AESA and the control membrane prepared without 2AESA.

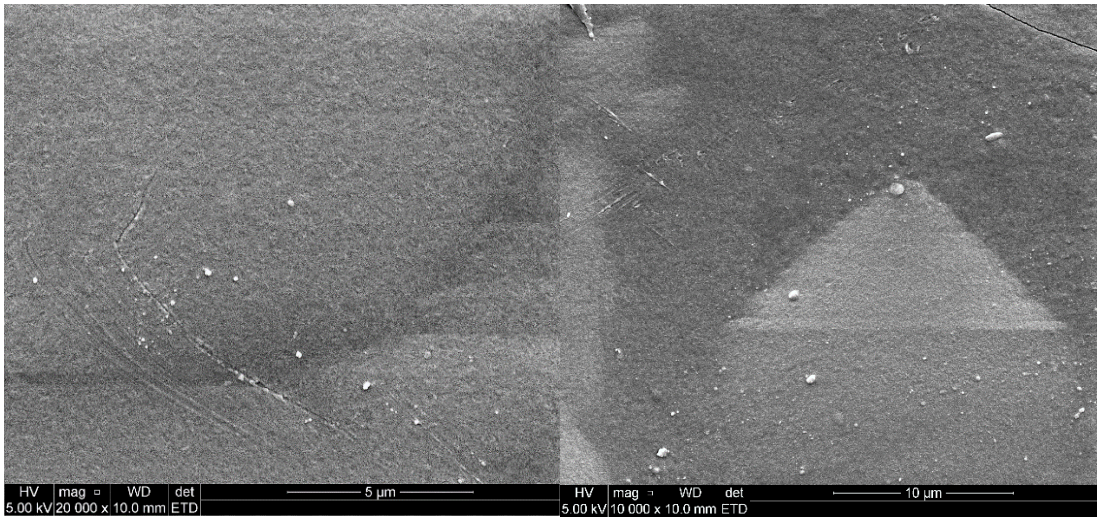

Figure 4.17: SEM analysis of the surface of the CS-13.6 wt.% 2AESA membrane

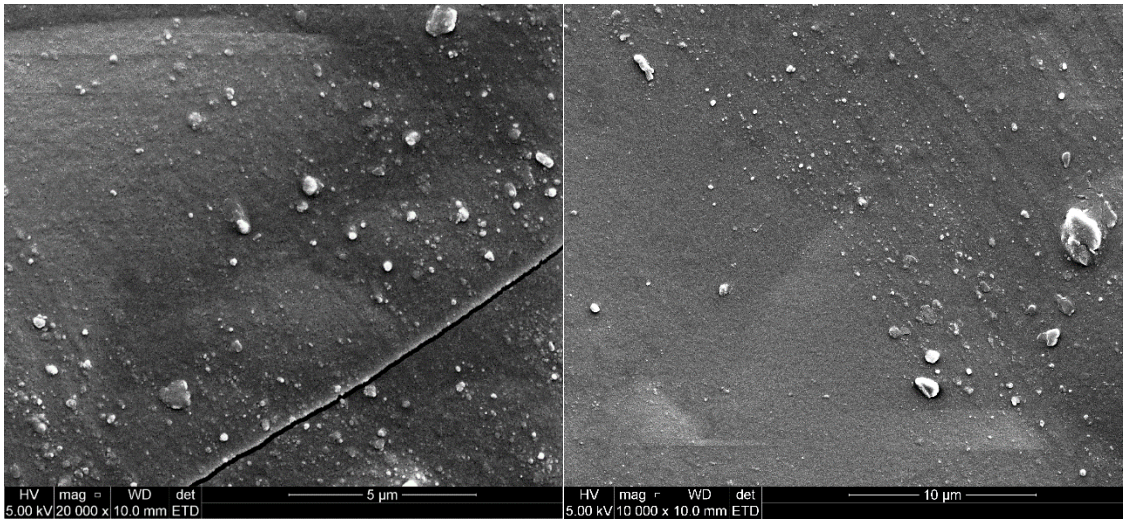

Figure 4.18: SEM analysis of the surface of the CS-5 wt.% 2AESA membrane

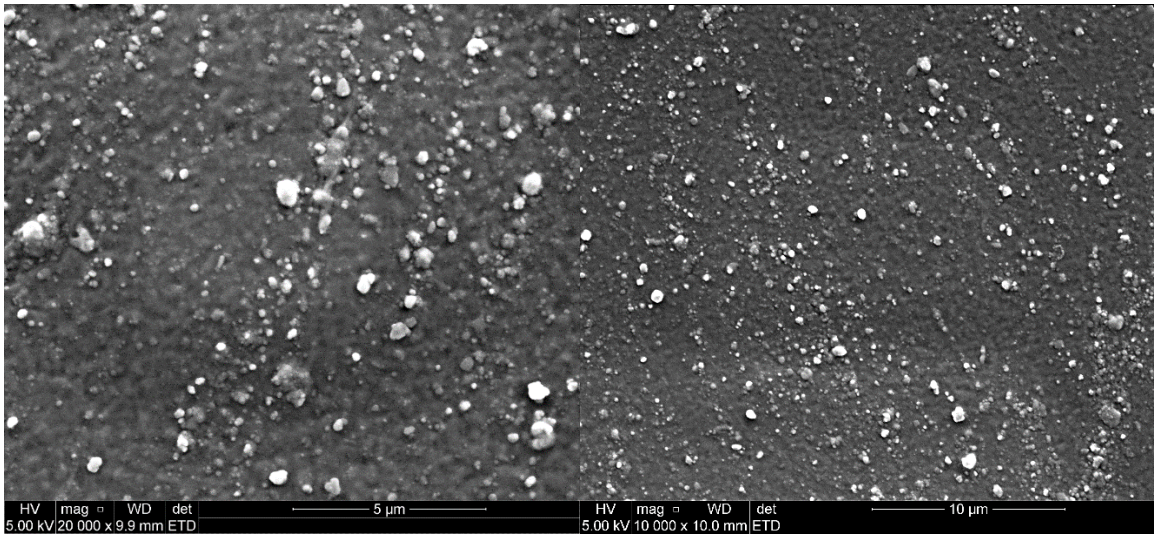

Figure 4.19: SEM analysis of the surface of the CS-0 wt.% 2AESA membrane

4.4.5 Energy- dispersive X-ray spectroscopy (EDS) results of the membranes

Table 4.1 shows the elementary composition obtained from the EDS analysis of the surface morphology of the three membranes. The EDS analysis of the surface of the membranes showed presence of ~44 wt.% carbon (C), ~50 wt.% oxygen atom (O) for all the membranes, these elements are present on the polymer chain of chitosan.

Table 4.1: EDS results of the sulfonated chitosan membranes modified with 2AESA

Membrane code	C (wt.%)	O (wt.%)	S (wt.%)	Total
CS-13.6wt%2AESA	43,84	50,32	5,85	100
CS-5wt.%2AESA	44,1	50,2	5,7	100
CS-0wt.%2AESA	44,05	49,91	6,04	100

Notably, the composition of elementary sulphur (S) appeared lower for the membranes modified with 2-aminoethanesulfonic acid compared to the sulphur content of 6.04 wt.% seen on the surface of the control membrane resulting from the incorporation of the sulphate groups on the chitosan chain during the cross-linking. The EDS results suggested that the sulfonic acid groups ($-SO_3H$) from 2AESA are integrated within the developed membrane structure via the formation of electrostatic interaction with the amino groups of chitosan.

4.4.6 XRD results of the sulfonated chitosan membranes modified with 2AESA

Figure 4.20 shows the XRD patterns of chitosan, Nafion 117 and the developed chitosan membranes. Chitosan showed two crystalline characteristics peaks at 2thetha of ~10° and 20°. The flattening of the two crystal peaks of chitosan at 2thetha of ~10° and 20° in the developed chitosan membranes indicated a disruption of the crystalline structures during the modification of chitosan with 2-aminoethanesulfonic acid. The XRD patterns of the developed sulfonated chitosan membranes consisted of amorphous phases, a property affiliated to promote proton conductivity in membranes used in fuel cell applications.

The Nafion 117 membrane showed two crystalline peaks at 2Θ of ~17° and 40°. The former has been associated to the hydrophobic backbone of Nafion 117 (Nørgaard *et al.* 2012, del Carmen Borja-Urzola *et al.* 2020).

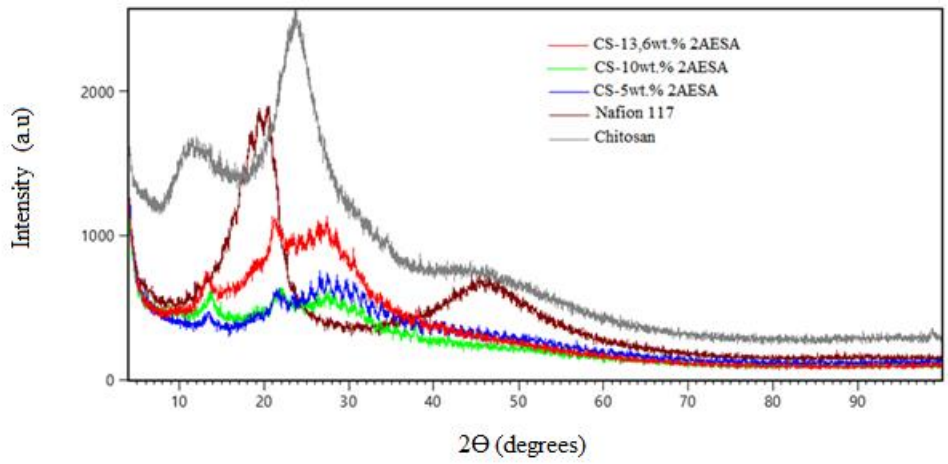

Figure 4.20: XRD patterns of sulfonated chitosan membranes modified with 2AESA

4.5 SULFONATED CHITOSAN MEMBRANE MODIFIED WITH NANOSILICA

4.5.1 FTIR results of sulfonated chitosan membrane modified with nanosilica

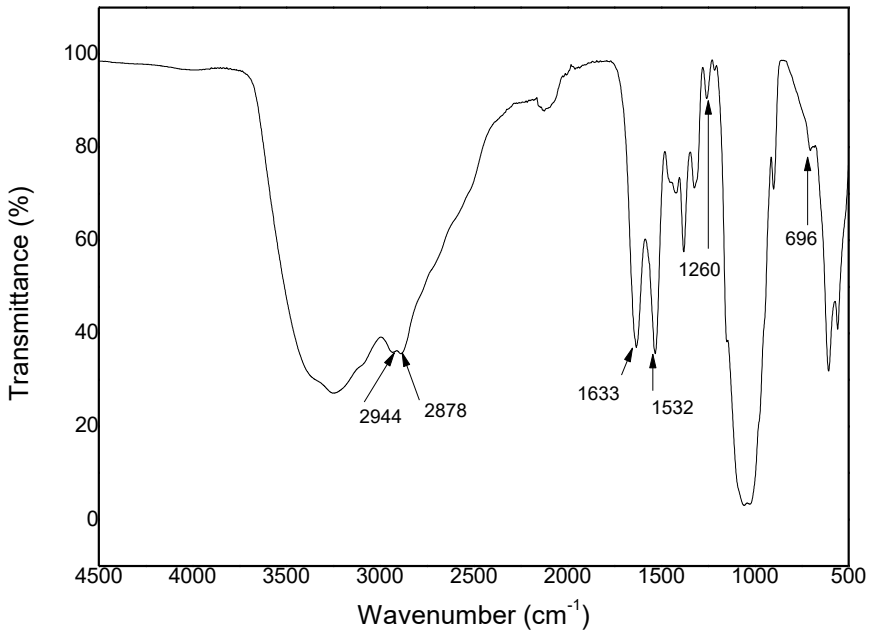

Figure 4.21: FTIR spectrum of chitosan membrane with silica nanoparticles

Figure 4.21 shows FTIR spectra of the sulfonated chitosan membrane modified with silica nanoparticles. The broad band at around 3700 cm^{-1} and 3000 cm^{-1} was attributed to the intermolecular hydrogen bonding of the hydroxyl groups (-OH) of chitosan and silica. The wavelengths at 2944 cm^{-1} and 2886 cm^{-1} were associated with asymmetric and symmetric stretching vibrations of sp^3 hybridised C-H of the chitosan chain. The broad band at the wavelength of ~1000 cm^{-1} was attributed to the overlapping of the C-O bending vibration and the Si-O-Si groups in the synthesised membrane (Vijayalekshmi & Khastgir 2018).

The wavenumber at 1633 cm^{-1} was associated with the stretching vibration of the C=O in the membrane matrix. The peak at the wavenumber of 1532 cm^{-1} was attributed to the formation of $–NH_3^+$ cations in the developed membrane as a results of amino groups accepting a proton from sulphuric acid during cross-linking. The wavenumbers at 1260 cm^{-1} and 696 cm^{-1} were attributed to the asymmetric stretching vibrations of the O=S=O groups and the S-O stretching vibrations in the membrane as the result of cross-linking the chitosan matrix with sulphuric acid (Vijayalekshmi & Khastgir 2017).

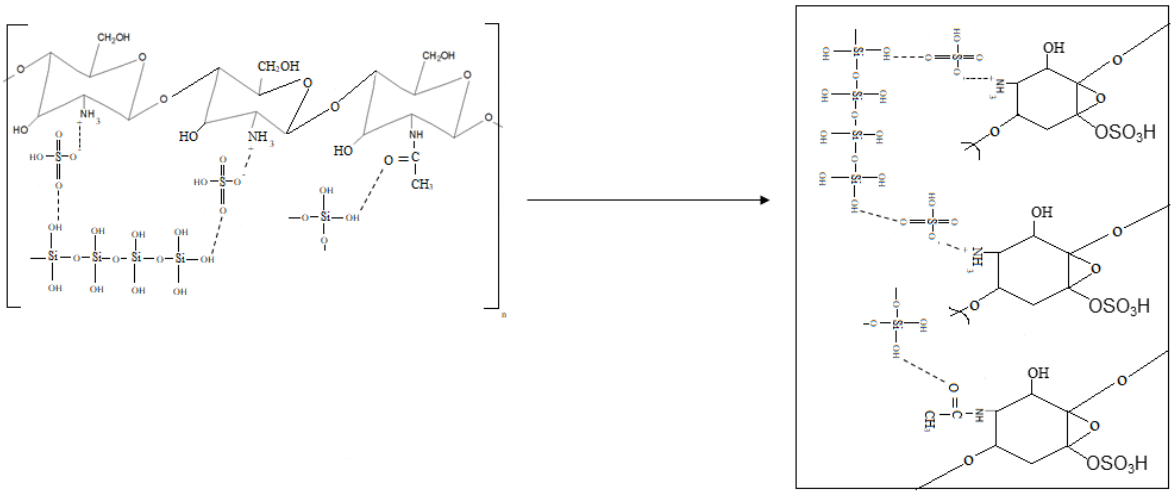

Figure 4.22: Proposed chemical structure of chitosan membrane modified with nanosilica

Figure 4.22 shows the proposed interaction between chitosan and the incorporated silica nanoparticles. It is proposed that the chemical interactions occur through the hydrogen bonds between carbonyl groups of chitosan and silanol groups of silica nanoparticles; hydrogen bonds between silanol groups and the sulphate groups. The sulphate groups in the proposed chemical structure in Figure 4.22 results from the sulphuric acid solution used during cross-linking in the membrane development process.

Interestingly, when the chitosan membrane was modified with 5 wt.% silica nanoparticles, the developed membrane was brittle and cracked, which was associated to the optimum loading of nanosilica exceeded at 5 wt.% (refer to Appendix A for the FTIR results of the membrane).

4.5.2 TGA/ DTG curves of sulfonated chitosan membrane modified with nanosilica

Figure 4.23 shows the TGA/DTG results of a sulfonated chitosan membrane modified with silica nanoparticles (2 wt.%). The thermographs of the membrane showed three stages.

The first degradation stage occurred at a temperature <100 °C and extended until ~203 °C; this stage was associated with a weight reduction of 12% attributed to the loss of water molecules and light solvents. The second and third degradation stages occurred at 208 °C and 266 °C. The two stages were associated with the decomposition of cross-linked networks and the main polymer chain of the membrane, respectively.

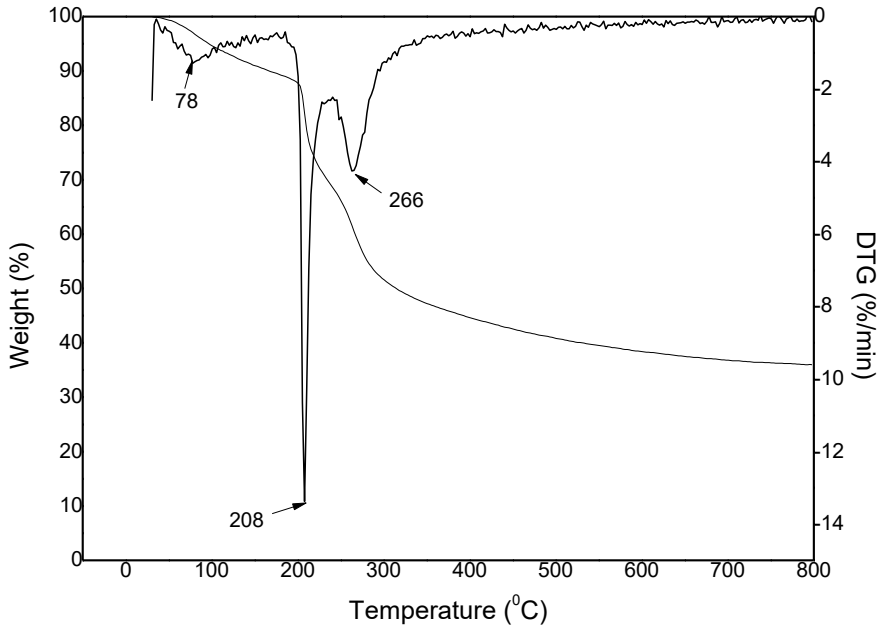

Figure 4.23:TGA/DTG thermographs of sulfonated chitosan membrane with nanosilica

4.5.3 SEM results of the sulfonated chitosan membranes modified with nanosilica

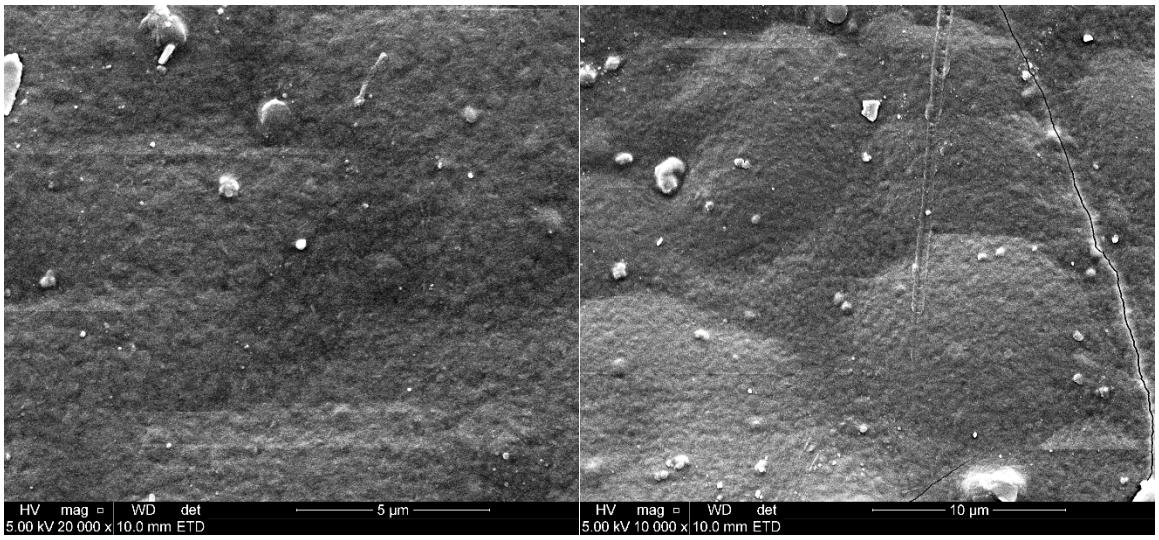

Figure 4. 24: SEM analysis of the sulfonated chitosan membrane with nanosilica

The SEM image of the sulfonated chitosan membrane modified with silica nanoparticles is shown in Figure 4.24. The surface of the membrane showed agglomeration, which was attributed to the reported tendency of silica to migrate to the surface of the membrane and also its ability to form hydrogen bonding with sulphate groups (Su *et al.* 2007).

4.5.4 EDS results of the sulfonated chitosan membrane modified with nanosilica

Table 4. 2: Elementary analysis of the CS membrane modified with silica nanoparticles

Membrane code	C (wt.%)	O (wt.%)	S (wt.%)	Si (wt.%)	Total
CS-2 wt.% nanoSiO_2	43,64	50,37	5,45	0,54	100

Table 4.2 shows the elementary composition from the EDS analysis of the surface of the sulfonated chitosan membrane modified with silica nanoparticle. The elementary composition on the surface of the membrane consisted of 43.64 wt.% carbon (C), 50.37 wt.% oxygen atom (O), 5.45 wt.% sulphur (S) and 0.45 wt.% silica (Si).

4.6 CHARACTERISATION OF NAFION 117 MEMBRANE

4.6.1 FTIR results of Nafion 117 membrane

Figure 4.25 shows the FTIR spectrum of the commercial Nafion 117 membrane. The stretching vibration at 1208 cm^{-1} was associated with the overlapping of the asymmetric stretching vibration of O=S=O from the sulfonic acid groups, as well as the asymmetric stretching vibrations of the $–CF_2$ groups. The wavenumber of 1146 cm^{-1} was attributed to the overlapping symmetric stretching vibrations of the C-O-C groups and $–CF_2$ groups. The stretching vibrations at 1056 cm^{-1} and 974 cm^{-1} were associated with the $–SO_3^-$ and C-O groups, respectively. The peaks at 3436 cm^{-1} and 1687 cm^{-1} were attributed to the asymmetric stretching vibrations and the bending vibrations of the water molecules in the Nafion 117 membrane (Mališ *et al.* 2018, Sahu *et al.* 2009, Zakil *et al.* 2016a).

The chemical structure of Nafion 117 is shown in Figure 4.26.

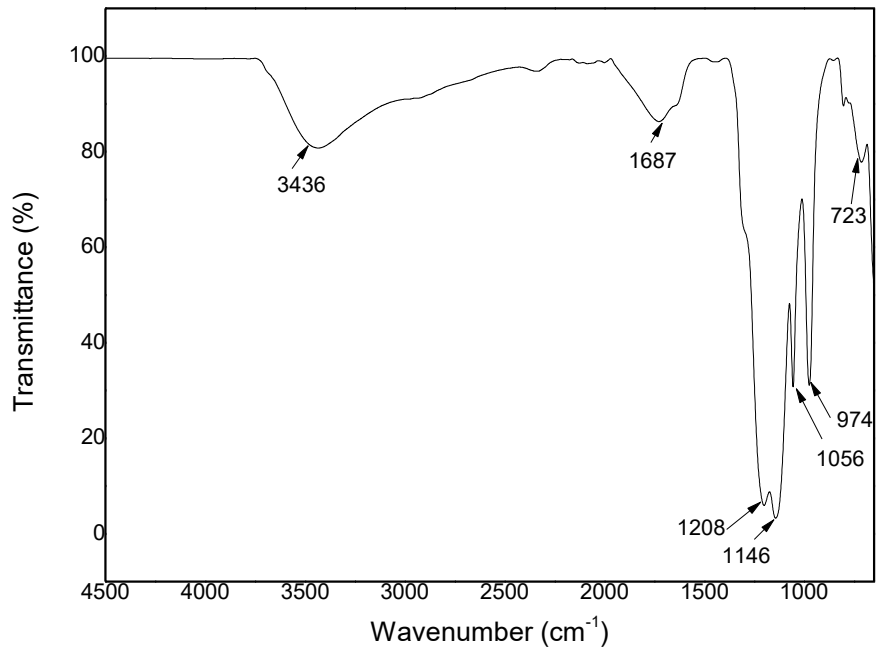

Figure 4.25: FTIR spectrum of Nafion 117 membrane

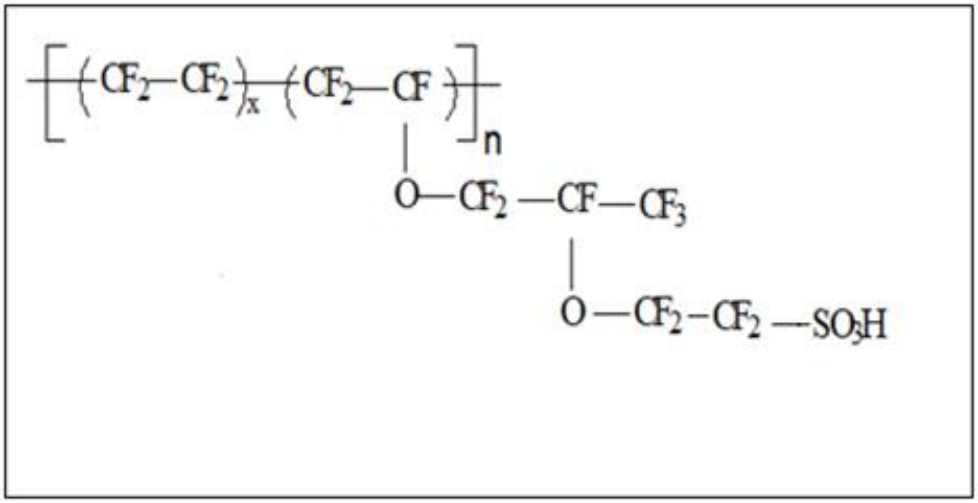

Figure 4.26: Nafion 117 polymer chain unit

4.6.2 TGA and DTG curves of Nafion 117 membrane

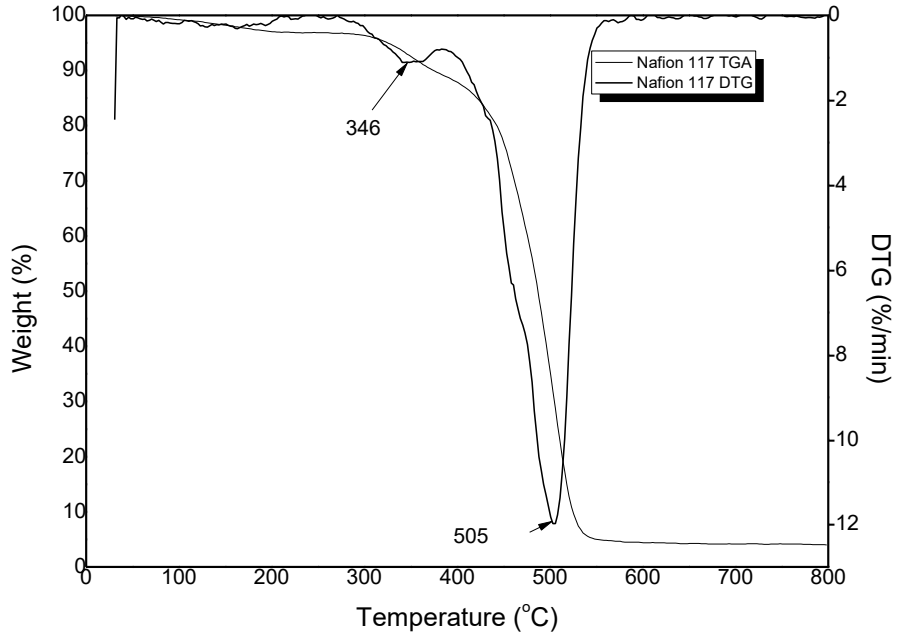

Figure 4.27: TGA/DTG thermographs of Nafion 117 membrane

Figure 4.27 shows the TGA and DTG curves of the Nafion 117 membrane; the membrane maintained more than 95 % of its original weight up to a temperature of ~310 °C. However, a rapid thermal degradation of the Nafion 117 membrane was observed between a temperature range of ~346 °C – 505 °C (Zakil *et al.* 2016a).

4.6.3 SEM results of Nafion 117 membrane

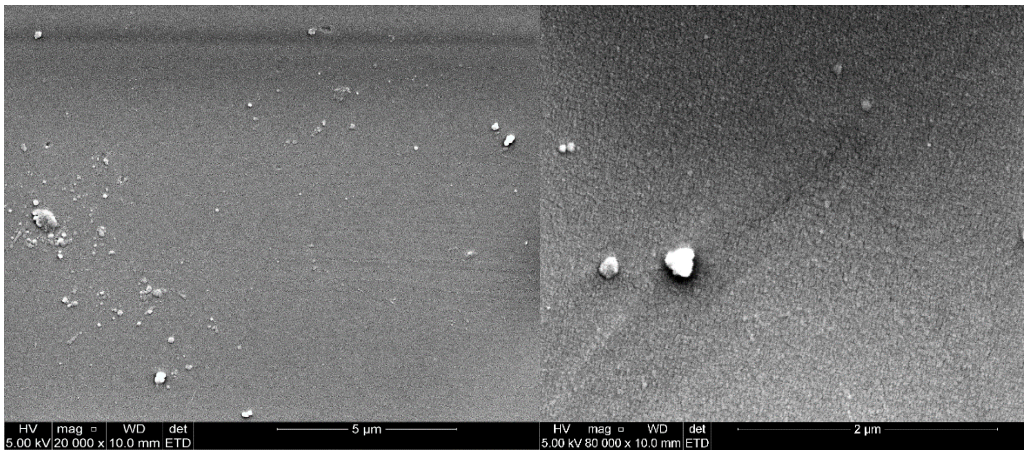

Figure 4.28: SEM analysis of the Nafion 117 membrane

Figure 4.28 shows the SEM image of Nafion 117. The SEM analysis of the membrane indicated a homogenous surface morphology with minor aggregation. The Nafion 117 membrane used in this study was used in its raw form without pre-treating the membrane with hydrogen peroxide and sulphuric acid solution.

4.6.4 EDS results of Nafion 117 membrane

Table 4. 3: Elementary analysis of the Nafion 117 membrane

Membrane code	C (wt.%)	O (wt.%)	S (wt.%)	F (wt.%)	Total
Nafion 117	20,62	8,11	2,43	68,84	100

Table 4.3 shows the results from the EDS analysis performed on the surface of the commercial Nafion 117 membrane. The elementary analysis of the surface of the membrane indicated presence of 20.62 wt.% of carbon, 8.11 wt.% oxygen, 2.43 wt.% of sulphur and 68.84 wt.% of fluorine atom.

4.7 WATER UPTAKE PERCENTAGE RESULTS OF THE MEMBRANES

Figure 4.29 shows the water uptake results of Nafion 117 and the three types of sulfonated chitosan membranes developed in this study after immersing the membranes for 24 hours in de-ionised water at room temperature.

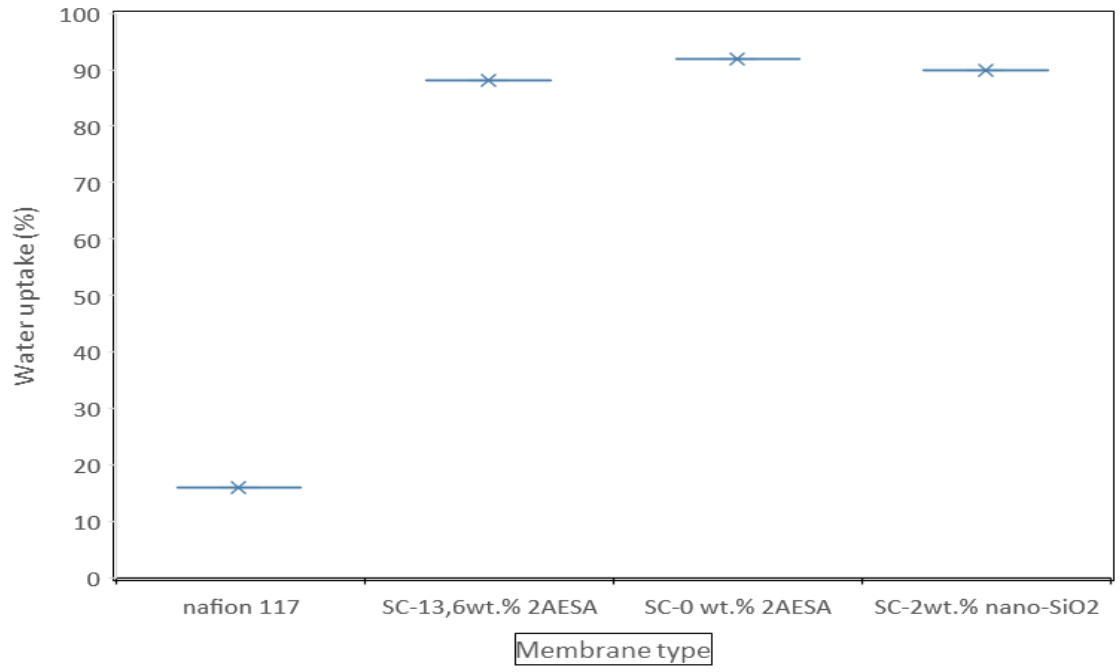

Figure 4.29: Water uptake results of Nafion 117 and chitosan membranes

The experimental data were converted to the water uptake percentages in Figure 4.29 using Equation 3.18 (refer to Appendix B for calculations). Figure 4.29 shows the water uptake percentages of the developed chitosan membranes to decrease with the incorporation of cross-linking agents on the chitosan matrix.

The control membrane (SC- 0 wt.% 2AESA) had the highest water uptake percentage of 92% compared to the water uptake percentage of 88% obtained using the CS-13.6 wt.% 2AESA membrane and the water uptake percentage of 90% using the sulfonated chitosan membrane modified with silica nanoparticle (2 wt.%). Notably, the developed chitosan membranes showed higher water absorption capacities compared to Nafion 117, which attained a water uptake percentage of 16% under similar conditions.

A good water uptake percentage is a prerequisite in the formation of proton hopping channels inside the membrane and also assists during high temperature operation of the MEA under low humidity inside the fuel cell. However, excessive water uptake induces swelling of the membrane, which in turn reduces fuel cell performance.

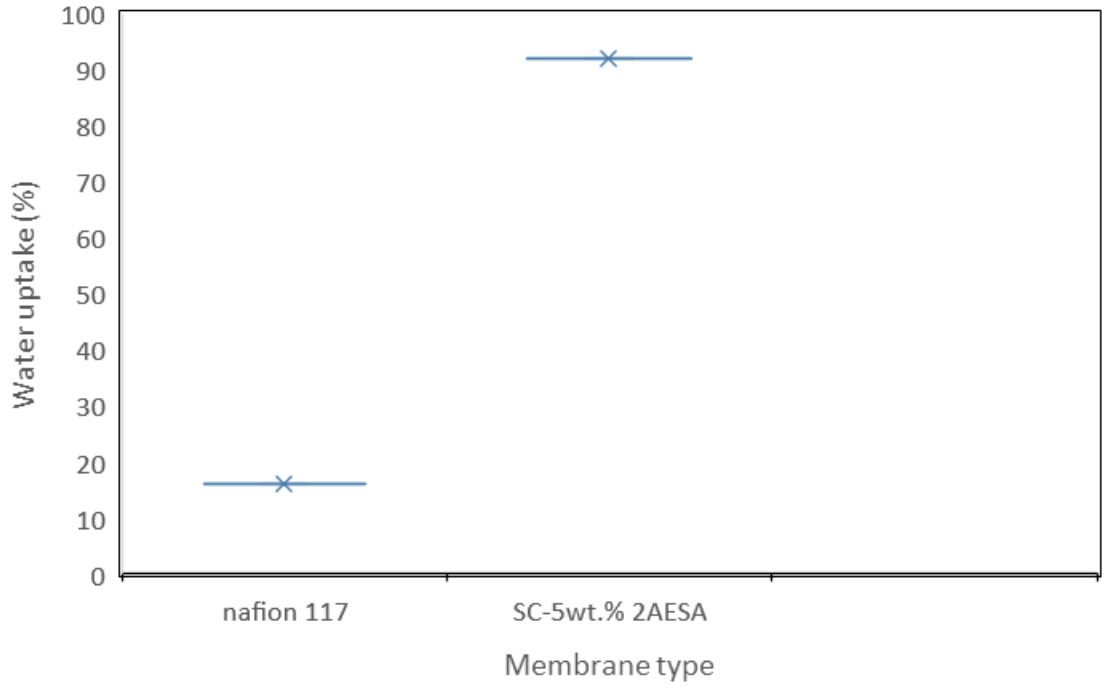

Figure 4.30: Water uptake results of Nafion 117 and chitosan membranes

Figure 4.30 shows the water uptake results of Nafion 117 and the sulfonated chitosan membrane modified with 5 wt.% 2AESA after the two membranes were immersed in de-ionised water for four hours at room temperature. The water uptake percentages obtained were 16% for Nafion 117 and 92% for the sulfonated chitosan membrane modified with 2-aminoethanesulfonic acid (5 wt.% 2AESA).

The water uptake results were in agreement with the FTIR analysis of these two membranes in Figure 4.8 and Figure 4.25. The broad band in the region of 3700 cm^{-1} – 3000 cm^{-1} attributed to strong intermolecular hydrogen bonding of the hydroxyl groups was strongly absorbed in the chitosan membrane compared to Nafion 117 suggesting a higher affinity to water molecules in the chitosan membrane compared to Nafion 117.

4.8 PROTON DIFFUSION COEFFICIENT OF CHITOSAN MEMBRANE

The aim of this section was to determine the proton diffusion coefficient of the developed sulfonated chitosan membrane modified with 2-aminoethanesulfonic acid. The findings from the study elucidate the ability of the developed membrane to permeate protons from one compartment to the next compartment. A good proton exchange membrane in fuel cell application permeate protons from the anode electrode towards the cathode electrode where the reduction of oxygen occurs.

The mass transfer coefficient and the proton diffusion coefficient of the sulfonated chitosan membrane modified with 2-aminoethanesulfonic acid were investigated in a two-compartment diffusion, the thickness of the membrane used in the study was measured to be 41 µm and was inserted between the two compartments as shown in Figure 3.4.

Table 4.4 shows the measured pH over time in compartment A and B. The pH measurements were converted using Equation 3.17 into the concentration graph shown in Figure 4.31.

Table 4.4: Results for pH measurement in compartment A and compartment B

Time (min)	A compartment pH	A compartment Conc.(mol/L)	B compartment pH	B compartment Conc.(mol/L)
0	3.12	7.59E-4	7.40	3.9E-8
5	3.14	7.24E-4	6.57	2.69E-7
10	3.05	8.91E-4	5.04	9.12E-6
15	3.07	8.51E-4	4.64	2.29E-5
20	3.09	8.13E-4	4.56	2.75E-5
25	3.09	8.13E-4	4.50	3.16E-5
30	3.12	7.59E-4	4.45	3.55E-5
35	3.14	7.24E-4	4.42	3.80E-5
40	3.14	7.24E-4	4.39	4.07E-5
45	3.14	7.24E-4	4.36	4.36E-5
50	3.16	6.92E-4	4.34	4.57E-5
55	3.15	7.08E-4	4.34	4.57E-5
60	3.17	6.76E-4	4.32	4.79E-5
65	3.19	6.46E-4	4.31	4.90E-5
70	3.17	6.76E-4	4.31	4.90E-5
75	3.19	6.46E-4	4.31	4.90E-5
80	3.19	6.46E-4	4.31	4.90E-5

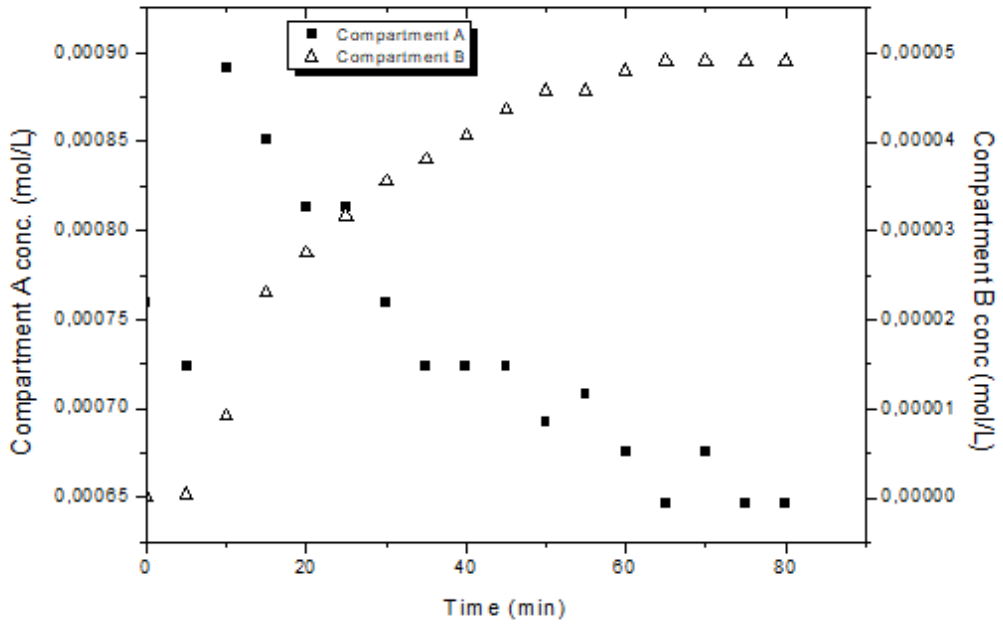

Figure 4.31: Change in concentration over time in compartment A and B

Figure 4.31 shows an increasing concentration of hydronium ions in compartment B initially consisting of de-ionised water. This pattern elucidated the ability of the developed chitosan membrane to transfer protons from the acid compartment A to the water compartment B.

The concentration profile in Figure 4.31 was used to calculate the mass transfer coefficient and proton diffusion coefficient of the membrane using equations 3.15 and 3.16. The mass transfer coefficient and proton diffusion coefficient of the membrane were calculated to be 1.6×10^{-3} cm/s and 6.56×10^{-6} cm^2/s, respectively (refer to Appendix C for calculations)

4.9 PROTON DIFFUSION COEFFICIENT OF NAFION 117 MEMBRANE

The objective of this experiment was to investigate the mass transfer coefficient and proton diffusion coefficient of the commercial polymer electrolyte membrane Nafion 117 and to compare the results obtained for Nafion 117 with that obtained using the sulfonated chitosan membrane modified with 2AEA presented in the previous section.

The experiment was performed using the two-compartment diffusion cell shown in Figure 3.4. The Nafion 117 membrane used in this study had a thickness of 168 µm.

Table 4.5: Results for pH measurement in compartment A and B with Nafion 117

Time (min)	A compartment pH	A. compartment Conc. (mol/L)	B compartment pH	B Compartment Conc.(mol/L)
0	3.99	1.02E-4	6.10	7.70E-7
10	4.00	1.00E-4	5.52	3.02E-6
20	4.03	9.30E-5	5.5	3.16E-6
30	4.06	8.70E-5	5.48	3.30E-6
40	4.08	1.58E-5	5.42	3.80E-6
50	4.10	7.94E-5	5.38	4.17E-6
60	4.09	8.13E-5	5.35	4.47E-6
70	4.10	7.94E-5	5.30	5.01E-6
80	4.10	7.94E-5	5.30	5.01E-6

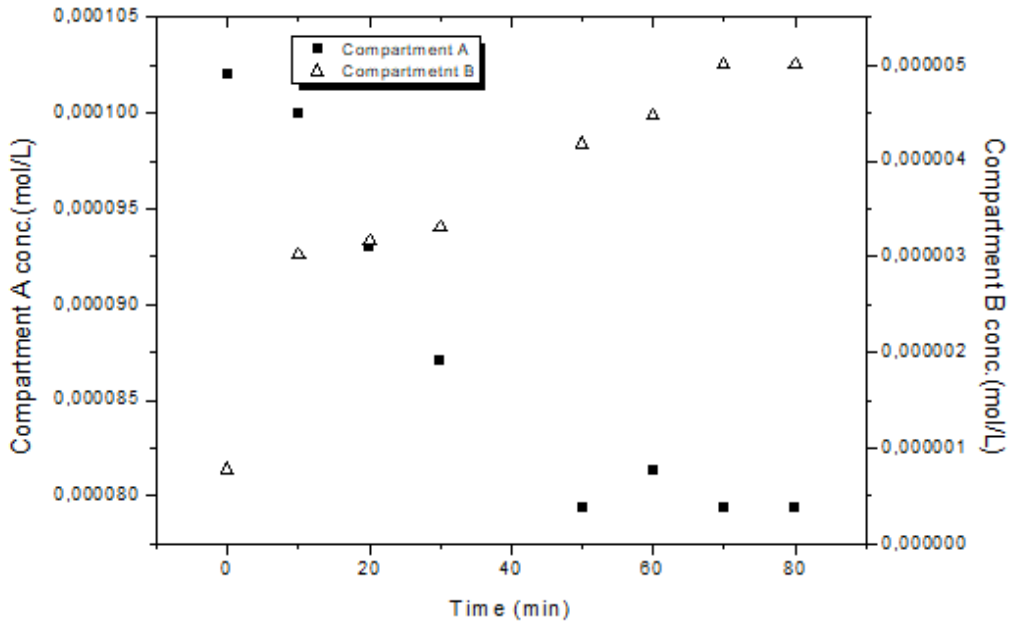

Figure 4.32: Change in concentration across Nafion 117 in compartment A and B

Table 4.5 shows the measured pH over time in compartment A and B. The pH results were converted into the concentration graphs presented in Figure 4.32 using Equation 3.17. The concentration profile observed in Figure 4.32 was associated with the high proton conducting ability of the Nafion 117 membrane to transfer protons from the acid compartment A to the water compartment B.

The experimental data in Figure 4.32 were used to calculate the mass transfer coefficient and proton diffusion coefficient of the Nafion 117 membrane using equations 3.10 and 3.11. The mass transfer coefficient and the proton diffusion coefficient of Nafion 117 were calculated to be 9.78×10^{-4} cm/s and 1.64×10^{-5} cm^2/s, respectively.

The proton diffusion coefficient of 1.64×10^{-5} cm^2/s obtained in the study for the Nafion 117 membrane was about twice the value of 5.3×10^{-6} cm^2/s reported in the literature but was close to the water diffusion coefficient of 2.00×10^{-5} cm^2/s reported for Nafion 117 in its fully hydrated form (Hickner & Pivovar 2005, Stenina *et al.* 2004)

4.10 METHANOL PERMEABILITY COEFFICIENT OF CHITOSAN PEM

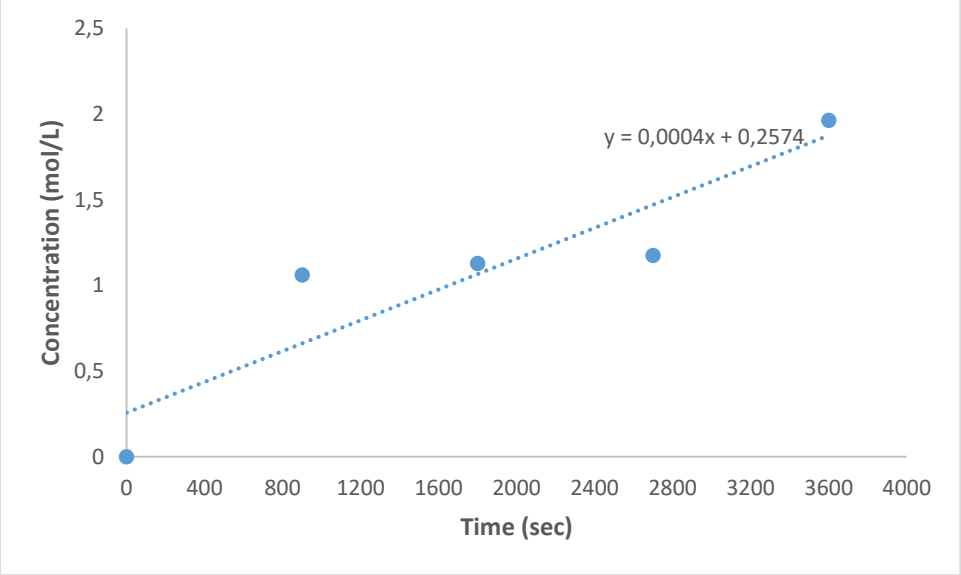

Figure 4. 33: Change in methanol concentration with time in compartment B

Figure 4.33 shows the change in methanol concentration in a water compartment B of the diffusion cell as a result of methanol permeation from compartment A to compartment B across the developed sulfonated chitosan membrane modified with 2AESA (5 wt.%). The change in the concentration of methanol was calculated using equations 3.1 and 3.2 from the peak areas obtained from the HPLC analysis (refer to Appendix D for calculations). The methanol permeability coefficient of the chitosan membrane was calculated using equation 3.14 and was found to be 2.29×10^{-6} cm^2/s. This value was considered high and too close to the methanol permeability coefficient of Nafion 117 reported to be 2.33×10^{-6} cm^2/s when using 12M methanol (Hickner & Pivovar 2005, Mukoma *et al.* 2004). Hence, the remaining work was directed at using the modified membranes in PEMFC.

4.11 FUEL CELL PERFORMANCES OF CHITOSAN AND NAFION 117 MEAs

Figures 4.34 to 4.37 show the MEA components of the four types of membranes investigated in this study. The MEAs were constructed by inserting the membrane between two gas diffusion electrodes (GDE) with Pt-4 mg/cm^2 for the anode electrode and cathode electrode, respectively.

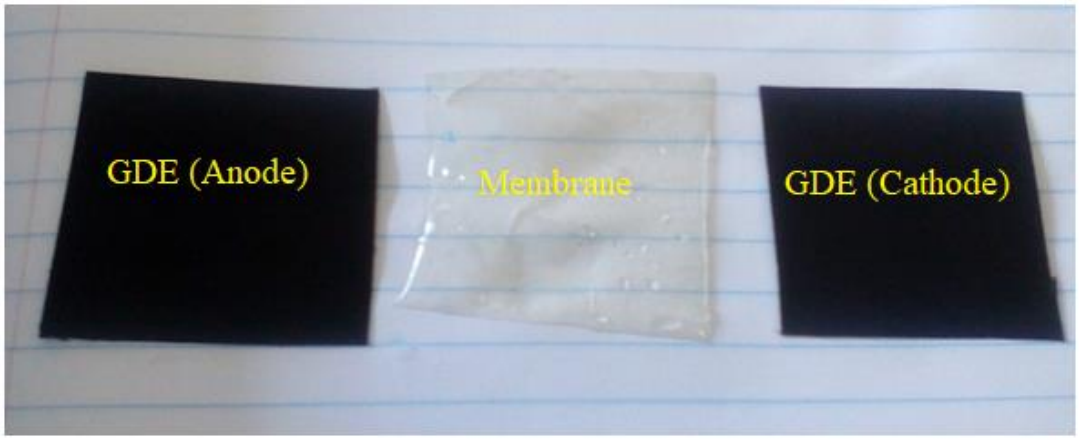

Figure 4.34: MEA components of sulfonated chitosan membrane (13.6 wt.% 2AESA)

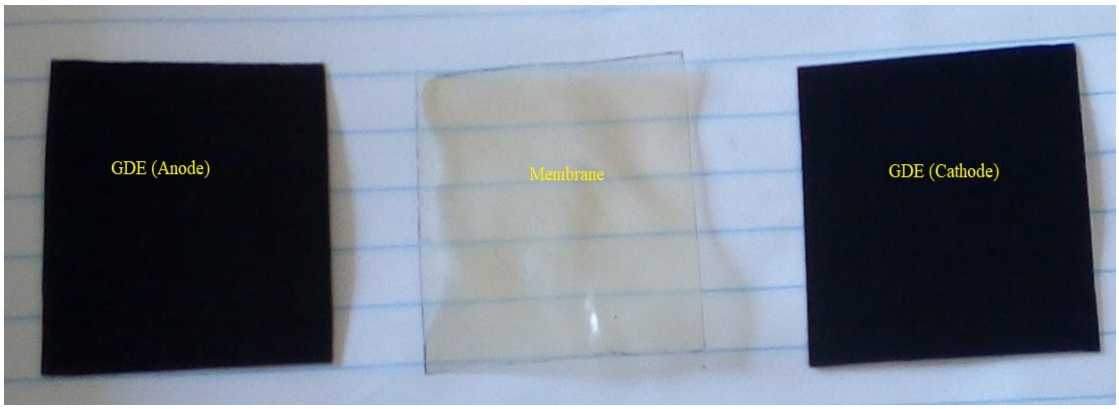

Figure 4.35: MEA components of sulfonated chitosan membrane with nanosilica

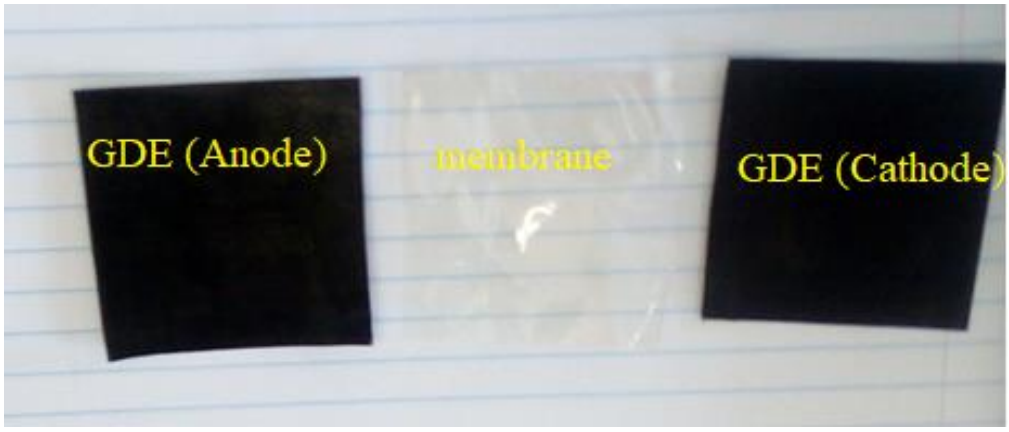

Figure 4.36: MEA components of the sulfonated chitosan membrane (control)

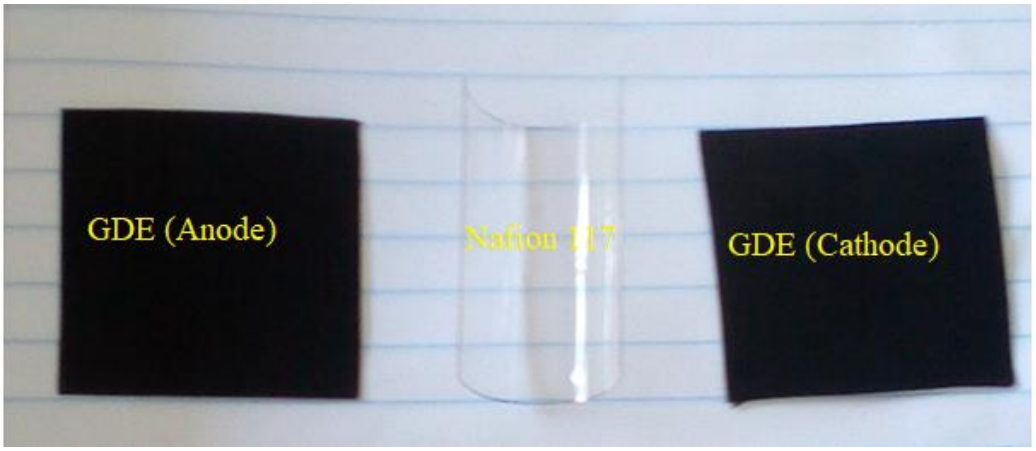

Figure 4.37: MEA components using Nafion 117 membrane

Four types of polymer electrolyte membranes were investigated for fuel cell performance in a single PEM fuel cell with H_2/O_2 supply from the electrolyser. The fuel cell performances of the MEAs were recorded over a period of time and the output results are presented in figures 4.38 to 4.44.

4.11.1 Fuel cell performance of sulfonated chitosan membrane with 2AESA

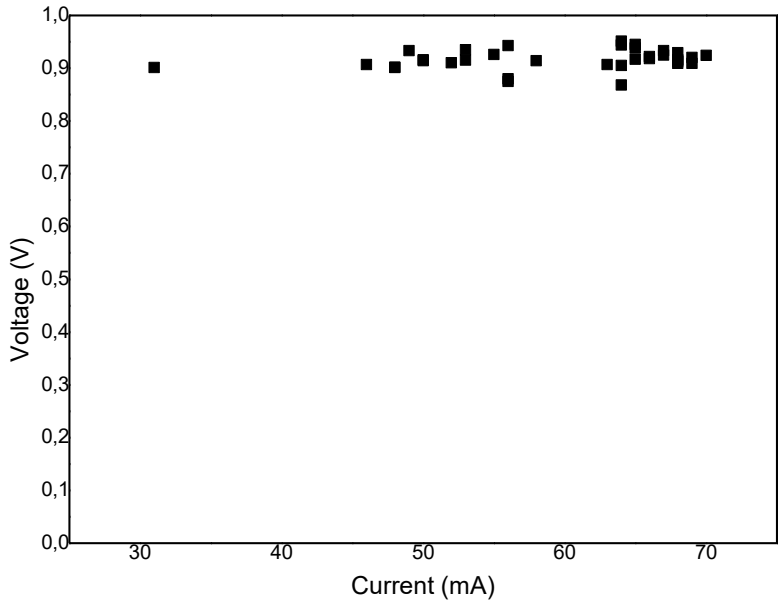

Figure 4.38: Voltage and Current output using the CS-13.6 wt.% 2AESA MEA

Figure 4.38 shows the fuel cell performance graph of the (CS-13.6 wt.% 2AESA) MEA. The (CS-13.6 wt.% 2AESA) MEA yielded an open-circuit voltage of ~0.9 V and a maximum power output of 64,7 mW/cm^2 at a maximum current output of 70 mA.

The current generated was applied onto a load and was able to turn the small electric fan shown in Figure 4.39 (refer to Appendix E).

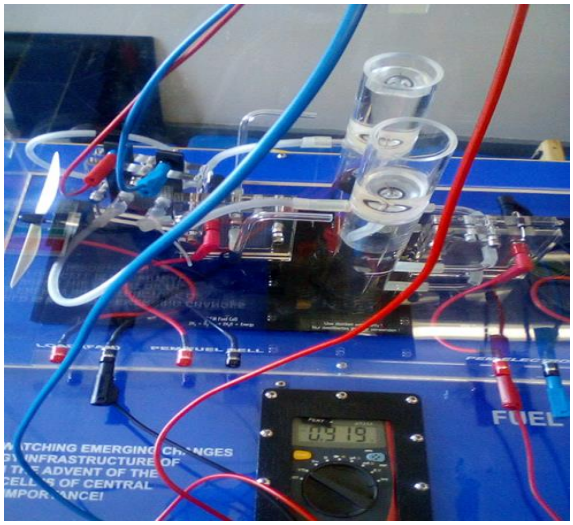

Figure 4.39: Voltage output using the sulfonated chitosan MEA (CS-13,6 wt.% 2AESA).

4.11.2 Fuel cell performance of sulfonated chitosan PEM with silica nanoparticles

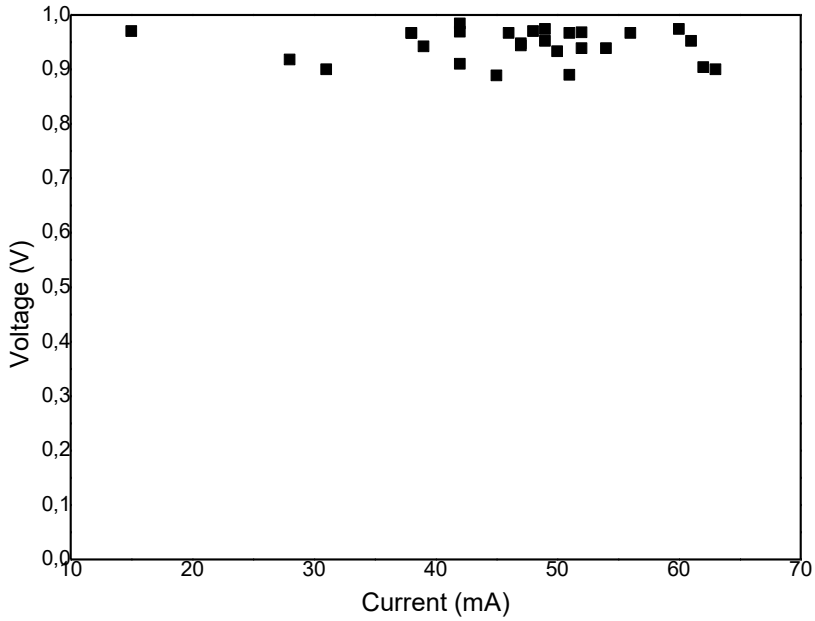

Figure 4.40: Voltage and Current output using the MEA consisting of nanosilica

Figure 4.40 shows the fuel cell performance graph of the MEA constructed using the sulfonated chitosan membrane consisting of silica nanoparticles. The MEA delivered an open-circuit voltage of ~0.9 V and maximum power output of 58.4 mW/cm^2 at the maximum current output of 60 mA. The current generated was applied onto a load shown in Figure 4.41 and was able to power the small electric fan (refer to Appendix E).

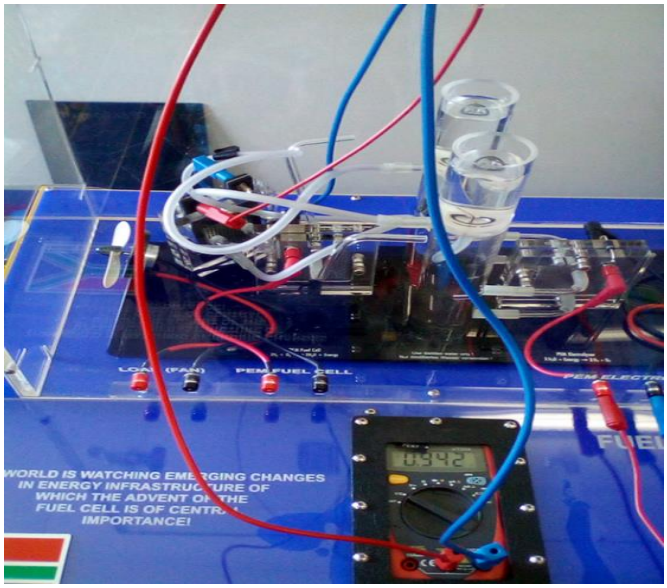

Figure 4.41: Voltage output using the sulfonated chitosan MEA with nanosilica

4.11.3 Fuel cell performance of sulfonated chitosan membrane (control)

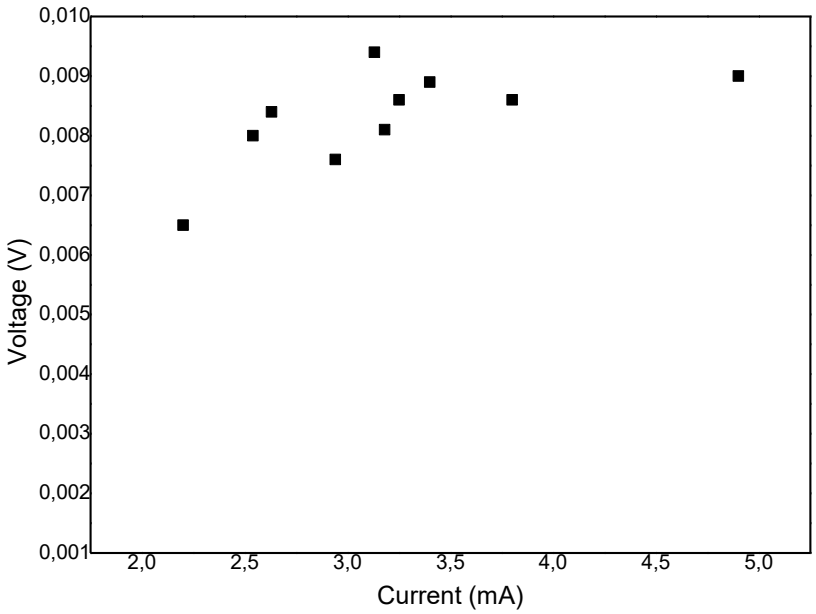

Figure 4.42: Voltage and current output using the control MEA

Figure 4.42 shows the fuel cell performance of the control MEA fabricated using a chitosan membrane modified without the incorporation of either 2-aminoethanesulfonic acid or the silica nanoparticles. The results in Figure 4.42 elucidate the poor performance of the control MEA and its inability to generate electricity.

Note: All MEA presented in this section were not hot-pressed due to the poor fuel cell performance obtained for the hot-pressed MEA fabricated with the CS-5 wt.% 2AESA membrane, which was linked to heat damage on the membrane structure (refer to Appendix E).

4.11.4 Fuel cell performance of Nafion 117 membrane

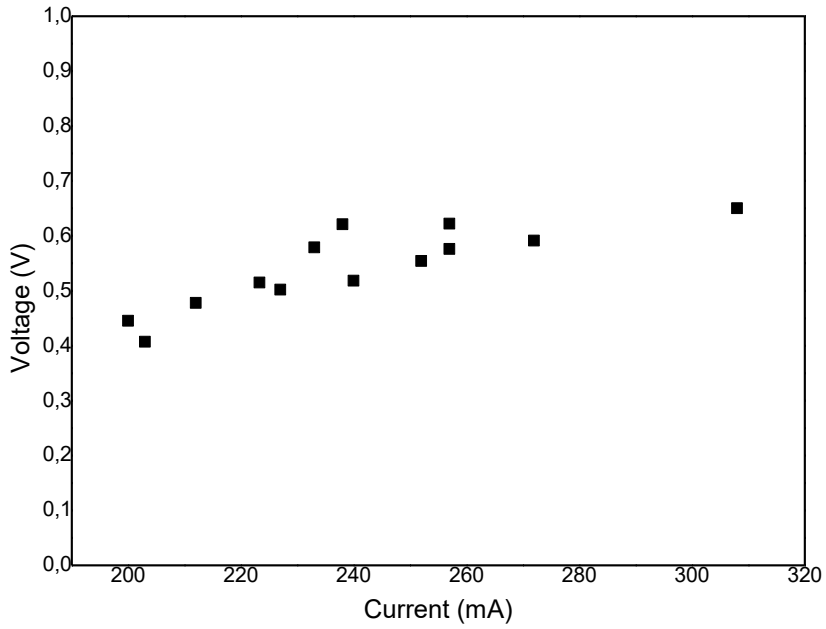

Figure 4. 43: Voltage and current output using the Nafion 117 MEA

Figure 4.43 shows the fuel cell performance using the MEA constructed using the Nafion 117 membrane. The MEA using Nafion 117 yielded an open-circuit voltage of ~0.6 V and a maximum power output of 130 mW/cm^2 at the maximum current output of 308 mA (refer to Appendix E).

The current generated was able to power the small electric fan shown in Figure 4.44.

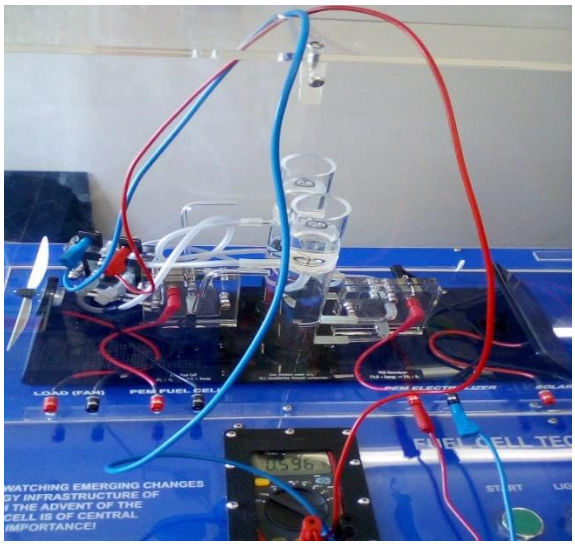

Figure 4. 44: Voltage output using Nafion 117 MEA

4.12 CONCLUSION

In this work, chitosan was successfully modified into flexible sulfonated chitosan membranes modified with 2-aminoethanesulfonic acid and silica nanoparticles. The developed membranes were characterised using FTIR, SEM-EDS, TGA and XRD and the results were discussed. Furthermore, the results of water uptake percentages, methanol permeability coefficient, mass transfer coefficients and proton diffusion coefficients of the membranes were discussed.

The FTIR spectra of the developed chitosan membranes consisted of a new peak at the wavenumber of ~1260 cm^{-1} originally absent in the FTIR spectrum of chitosan, which was attributed to the O=S=O stretching vibrations of the sulphate groups and confirmed the sulfonation of chitosan membranes. Notably, the absence of the C-O-C peak in the developed sulfonated chitosan membranes yielded the proposed reaction mechanism that the polysaccharide rings of chitosan are converted to a sulfonated poly (cyclohexene-oxide) thermoplastic backbone, as explained in Figure 4.11.

The proposed sulfonated poly (cyclohexene-oxide) backbone for the developed chitosan membranes was in agreement with the SEM-EDS results, which show the presence of elementary sulphur (S) in the range of 5.45 – 6.04 wt.% on the surface of the membranes. Notably, the control membrane had a higher water uptake percentage but poor fuel cell performance compared to the two membranes consisting of 2-aminoethanesulfonic acid and silica nanoparticles, which elucidated that the incorporation of the sulphate groups during cross-linking with sulphuric acid aided the water absorption, not the formation of electrostatic interactions. In contrast, the sulfonated chitosan membranes modified with 2-aminoethanesulfonic acid and those modified with silica nanoparticles achieved good fuel cell performances, achieving maximum power outputs of 64.7 mW/cm^2 and 58.4 mW/cm^2, respectively; the current generated was able to turn the small electric fan. The Nafion 117 membrane delivered a maximum power output of 130 mW/cm^2 when investigated under similar conditions to the chitosan MEAs in the PEMFC.

CHAPTER 5: CONCLUSIONS AND RECOMMENDATIONS

5.1 CONCLUSIONS

In this study, the successful modification of chitosan into sulfonated chitosan membranes was achieved via the solution casting method. The sulfonation of the developed chitosan membranes was confirmed by the FTIR results of the membranes, which exhibited a new peak at the wavenumber of ~1260 cm^{-1} attributed to the O=S=O stretching vibration peaks from the incorporated cross-linking agents. The developed chitosan MEAs were tested for fuel cell performances in a PEMFC and the results were compared to that obtained using the Nafion 117 MEA under similar conditions.

The sulfonated chitosan membrane modified with 2-aminoethanesulfonic acid, Nafion 117 and the sulfonated chitosan membrane modified with silica nanoparticles achieved maximum power output of 64.7 mW/cm^2 at the maximum current output of 70 mA, 130 mW/cm^2 at the maximum current output of 308 mA and 58.4 mW/cm^2 at the maximum current output of 60 mA, respectively.

The current generated by the chitosan membranes was able to turn (power) the small electric fan (load). It was concluded from the experimental findings that the chitosan membranes developed in this study were able to generate electricity in a single fuel cell unit.

The results obtained from the proton diffusion study elucidated the Nafion 117 membrane to consist of a proton diffusion coefficient of $1.64x10^{-5}$ cm^2/s, which was approximately three times higher than obtained for the chitosan membrane investigated. The results obtained from the proton diffusion study suggested that Nafion 117 membrane exhibited faster reaction kinetics for proton conduction compared to the developed chitosan membranes.

The XRD patterns of the developed chitosan membranes elucidated amorphous phases. The amorphous characteristics of the developed chitosan membranes were linked to the ability of the membranes to generate electricity.

The developed chitosan membranes elucidated high water uptake percentages of ~90% with a slight decrease seen with the incorporation of 2-aminoethanesulfonic acid (13.6 wt.%) in the modification. The high water absorption characteristic of the developed chitosan membranes corresponded to the high methanol permeability coefficient of $2.29x10^{-6}$ cm^2/s obtained in this

study. It was concluded that the developed sulfonated chitosan membranes will not be suitable for application in DMFC due to the high affinity of the membrane to both water and methanol and the risk of depolarisation at the cathode and reduced fuel cell performance as a result of methanol cross-over.

The absence of C-O-C stretching vibrations at the wavenumber of ~1153 cm^{-1} on the FTIR spectra of the developed sulfonated chitosan membranes suggested the pyranose rings of chitosan were altered during the modification; it was proposed that the polysaccharide ring of chitosan was converted to a poly (cyclohexene oxide) thermoplastic backbone. The TGA and DTG curves of the sulfonated chitosan membrane modified with 2-aminoethanesulfonic acid and that of the sulfonated chitosan membrane modified with silica nanofillers showed the degradation of the main polymer backbone to occur at 263 °C and 266 °C, respectively, contrary to the degradation of the main polymer backbone of chitosan, which occurred at 296 °C.

The SEM images of the sulfonated chitosan membrane modified with 2-aminoethanesulfonic acid (13,6 wt.%) showed a homogenous surface morphology, however, agglomeration was observed on the surface of the membrane modified with silica nanoparticles and was affiliated with the undesirable property of un-bonded silica to migrate to the surface of the membrane.

5.2 RECOMMENDATIONS

The fuel cell performance of chitosan membranes developed in this study was investigated in a single fuel cell unit. It is recommended to investigate fuel cell performance of chitosan membranes in a PEMFC fuel cell stack in future studies.

It is recommended that future studies be carried out to investigate how to reduce water uptake percentages of chitosan membranes for application in DMFCs.

REFERENCES

ALIAS, M., KAMARUDIN, S., ZAINOODIN, A. & MASDAR, M. 2020. Active direct methanol fuel cell: An overview. *International Journal of Hydrogen Energy*.

BAI, H., LI, Y., ZHANG, H., CHEN, H., WU, W., WANG, J. & LIU, J. 2015. Anhydrous proton exchange membranes comprising of chitosan and phosphorylated graphene oxide for elevated temperature fuel cells. *Journal of Membrane Science,* 495**,** 48-60.

BOCCHETTA, P. 2020. Ionotropic Gelation of Chitosan for Next-Generation Composite Proton Conducting Flat Structures. *Molecules,* 25**,** 1632.

BRANDON, N. P., SKINNER, S. & STEELE, B. C. 2003. Recent advances in materials for fuel cells. *Annual Review of Materials Research,* 33**,** 183-213.

CHAKRABARTY, T., KUMAR, M. & SHAHI, V. K. 2010. Chitosan based membranes for separation, pervaporation and fuel cell applications: Recent developments. *biopolymers,* 10**,** 201-226.

CHEN, M., RUNGE, T., WANG, L., LI, R., FENG, J., SHU, X.-L. & SHI, Q.-S. 2018. Hydrogen bonding impact on chitosan plasticization. *Carbohydrate polymers,* 200**,** 115-121.

CUSSLER, E. L. & CUSSLER, E. L. 2009. *Diffusion: mass transfer in fluid systems*, Cambridge university press.

DAS, S. K. & BERRY, K. J. 2007. Two-cell theory to measure membrane resistance based on proton flow: Theory development and experimental validation. *Journal of power sources,* 173**,** 909-916.

DEL CARMEN BORJA-URZOLA, A., GARCÍA-GÓMEZ, R. S., FLORES, R. & DEL CARMEN DURÁN-DOMÍNGUEZ-DE, M. 2020. Chitosan from shrimp residues with a saturated solution of calcium chloride in metanol and water. *Carbohydrate Research,* 497**,** 108116.

FENG, F., LIU, Y., ZHAO, B. & HU, K. 2012. Characterization of half N-acetylated chitosan powders and films. *Procedia Engineering,* 27**,** 718-732.

GABRIELE, F., DONNADIO, A., CASCIOLA, M., GERMANI, R. & SPRETI, N. 2021. Ionic and covalent crosslinking in chitosan-succinic acid membranes: Effect on physicochemical properties. *Carbohydrate Polymers,* 251**,** 117106.

GENG, P., TAN, Q., ZHANG, C., WEI, L., HE, X., CAO, E. & JIANG, K. 2016. Experimental investigation on NOx and green house gas emissions from a marine auxiliary diesel engine using ultralow sulfur light fuel. *Science of the Total Environment,* 572**,** 467-475.

HAILE, S. M. 2003. Fuel cell materials and components. *Acta Materialia,* 51**,** 5981-6000.

HICKNER, M. A. & PIVOVAR, B. 2005. The chemical and structural nature of proton exchange membrane fuel cell properties. *Fuel cells,* 5**,** 213-229.

HUANG, Q., ZHANG, Q., HUANG, H., LI, W., HUANG, Y. & LUO, J. 2008. Methanol permeability and proton conductivity of Nafion membranes modified electrochemically with polyaniline. *Journal of Power Sources,* 184**,** 338-343.

INAL, O. B. & DENIZ, C. 2020. Assessment of fuel cell types for ships: Based on multi-criteria decision analysis. *Journal of Cleaner Production,* 265**,** 121734.

KAMARUDIN, M., KAMARUDIN, S., MASDAR, M. & DAUD, W. 2013. Direct ethanol fuel cells. *International Journal of Hydrogen Energy,* 38**,** 9438-9453.

KHAN, U., YAMAMOTO, T. & SATO, H. 2021. An insight into potential early adopters of hydrogen fuel-cell vehicles in Japan. *International Journal of Hydrogen Energy*.

KHUHRO, A. A., ALI, Y., NAJAM-UDDIN, M. & KHAN, S. A technological, economical and efficiency review of direct methanol fuel cell. 2018 International Conference on Computing, Mathematics and Engineering Technologies (iCoMET), 2018. IEEE, 1-4.
KUMAR, R., SHARMA, S., PATHAK, D., DHIMAN, N. & ARORA, N. 2017. Ionic conductivity, FTIR and thermal studies of nano-composite plasticized proton conducting polymer electrolytes. *Solid State Ionics,* 305**,** 57-62.
LI, P.-C., LIAO, G. M., KUMAR, S. R., SHIH, C.-M., YANG, C.-C., WANG, D.-M. & LUE, S. J. 2016. Fabrication and characterization of chitosan nanoparticle-incorporated quaternized poly (vinyl alcohol) composite membranes as solid electrolytes for direct methanol alkaline fuel cells. *Electrochimica Acta,* 187**,** 616-628.
LIN, J., WU, P.-H., WYCISK, R., TRIVISONNO, A. & PINTAURO, P. N. 2008. Direct methanol fuel cell operation with pre-stretched recast Nafion®. *Journal of Power Sources,* 183**,** 491-497.
LIU, Y., WANG, J., ZHANG, H., MA, C., LIU, J., CAO, S. & ZHANG, X. 2014. Enhancement of proton conductivity of chitosan membrane enabled by sulfonated graphene oxide under both hydrated and anhydrous conditions. *Journal of Power Sources,* 269**,** 898-911.
MA, J. & SAHAI, Y. 2013. Chitosan biopolymer for fuel cell applications. *Carbohydrate Polymers,* 92**,** 955-975.
MA, X., QIAO, C., WANG, X., YAO, J. & XU, J. 2019. Structural characterization and properties of polyols plasticized chitosan films. *International journal of biological macromolecules,* 135**,** 240-245.
MALIŠ, J., PAIDAR, M., BYSTRON, T., BROŽOVÁ, L., ZHIGUNOV, A. & BOUZEK, K. 2018. Changes in Nafion® 117 internal structure and related properties during exposure to elevated temperature and pressure in an aqueous environment. *Electrochimica Acta,* 262**,** 264-275.
MALLAKPOUR, S. & EZHIEH, A. N. 2017. Preparation and characterization of chitosan-poly (vinyl alcohol) nanocomposite films embedded with functionalized multi-walled carbon nanotube. *Carbohydrate polymers,* 166**,** 377-386.
MAURICIO-SÁNCHEZ, R. A., SALAZAR, R., LUNA-BÁRCENAS, J. G. & MENDOZA-GALVÁN, A. 2018. FTIR spectroscopy studies on the spontaneous neutralization of chitosan acetate films by moisture conditioning. *Vibrational Spectroscopy,* 94**,** 1-6.
MOURYA, V. & INAMDAR, N. N. 2008. Chitosan-modifications and applications: opportunities galore. *Reactive and Functional polymers,* 68**,** 1013-1051.
MUKOMA, P., JOOSTE, B. & VOSLOO, H. 2004. A comparison of methanol permeability in Chitosan and Nafion 117 membranes at high to medium methanol concentrations. *Journal of Membrane Science,* 243**,** 293-299.
NEETHU, B., BHOWMICK, G. & GHANGREKAR, M. 2019. A novel proton exchange membrane developed from clay and activated carbon derived from coconut shell for application in microbial fuel cell. *Biochemical Engineering Journal,* 148**,** 170-177.
NETO, C. D. T., GIACOMETTI, J. A., JOB, A. E., FERREIRA, F. C., FONSECA, J. L. C. & PEREIRA, M. R. 2005. Thermal analysis of chitosan based networks. *Carbohydrate Polymers,* 62**,** 97-103.
NITHYA, H., SELVASEKARAPANDIAN, S., SELVIN, P. C., KUMAR, D. A. & KAWAMURA, J. 2012. Effect of propylene carbonate and dimethylformamide on ionic conductivity of P (ECH-EO) based polymer electrolyte. *Electrochimica acta,* 66**,** 110-120.
NØRGAARD, C. F., NIELSEN, U. G. & SKOU, E. M. 2012. Preparation of Nafion 117™-SnO_2 composite membranes using an ion-exchange method. *Solid State Ionics,* 213**,** 76-82.

OGUNGBEMI, E., IJAODOLA, O., KHATIB, F., WILBERFORCE, T., EL HASSAN, Z., THOMPSON, J., RAMADAN, M. & OLABI, A. 2019. Fuel cell membranes–Pros and cons. *Energy,* 172**,** 155-172.

OSMAN, Z. & AROF, A. K. 2003. FTIR studies of chitosan acetate based polymer electrolytes. *Electrochimica Acta,* 48**,** 993-999.

PIVOVAR, B. S., WANG, Y. & CUSSLER, E. 1999. Pervaporation membranes in direct methanol fuel cells. *Journal of Membrane Science,* 154**,** 155-162.

SAHU, A., PITCHUMANI, S., SRIDHAR, P. & SHUKLA, A. 2009. Nafion and modified-Nafion membranes for polymer electrolyte fuel cells: An overview. *Bulletin of Materials Science,* 32**,** 285-294.

SHIRDAST, A., SHARIF, A. & ABDOLLAHI, M. 2016. Effect of the incorporation of sulfonated chitosan/sulfonated graphene oxide on the proton conductivity of chitosan membranes. *Journal of Power Sources,* 306**,** 541-551.

SMITHA, B., SRIDHAR, S. & KHAN, A. 2005. Solid polymer electrolyte membranes for fuel cell applications—a review. *Journal of membrane science,* 259**,** 10-26.

STENINA, I., SISTAT, P., REBROV, A., POURCELLY, G. & YAROSLAVTSEV, A. 2004. Ion mobility in Nafion-117 membranes. *Desalination,* 170**,** 49-57.

SU, Y.-H., LIU, Y.-L., SUN, Y.-M., LAI, J.-Y., WANG, D.-M., GAO, Y., LIU, B. & GUIVER, M. D. 2007. Proton exchange membranes modified with sulfonated silica nanoparticles for direct methanol fuel cells. *Journal of Membrane Science,* 296**,** 21-28.

TAKARA, E. A., MARCHESE, J. & OCHOA, N. A. 2015. NaOH treatment of chitosan films: Impact on macromolecular structure and film properties. *Carbohydrate polymers,* 132**,** 25-30.

UMADEVI, M. & POORNIMA, R. R. 2009. Investigations of molecular interactions in propionic acid–N, N-dimethyl formamide binary system—FTIR study. *Spectrochimica Acta Part A: Molecular and Biomolecular Spectroscopy,* 73**,** 815-822.

VIJAYALEKSHMI, V. & KHASTGIR, D. 2017. Eco-friendly methanesulfonic acid and sodium salt of dodecylbenzene sulfonic acid doped cross-linked chitosan based green polymer electrolyte membranes for fuel cell applications. *Journal of Membrane Science,* 523**,** 45-59.

VIJAYALEKSHMI, V. & KHASTGIR, D. 2018. Fabrication and comprehensive investigation of physicochemical and electrochemical properties of chitosan-silica supported silicotungstic acid nanocomposite membranes for fuel cell applications. *Energy,* 142**,** 313-330.

WANG, H., DING, F., MA, L. & ZHANG, Y. 2021. Edible films from chitosan-gelatin: Physical properties and food packaging application. *Food Bioscience,* 40**,** 100871.

WANG, S. & JIANG, S. P. 2017. Prospects of fuel cell technologies. *National Science Review,* 4**,** 163-166.

WANG, Y., YANG, D., ZHENG, X., JIANG, Z. & LI, J. 2008. Zeolite beta-filled chitosan membrane with low methanol permeability for direct methanol fuel cell. *Journal of Power Sources,* 183**,** 454-463.

WU, D., SONG, L., ZHU, C., ZHANG, X., GUO, H. & YANG, C. 2017. Solubility of taurine and its application for the crystallization process improvement. *Journal of Molecular Liquids,* 241**,** 326-333.

XIANG, Y., YANG, M., GUO, Z. & CUI, Z. 2009. Alternatively chitosan sulfate blending membrane as methanol-blocking polymer electrolyte membrane for direct methanol fuel cell. *Journal of Membrane Science,* 337**,** 318-323.

YING, Y., KAMARUDIN, S. & MASDAR, M. 2018. Silica-related membranes in fuel cell applications: An overview. *International Journal of Hydrogen Energy*.

YUAN, S., TANG, Q., HE, B., CHEN, H., LI, Q., MA, C., JIN, S. & LIU, Z. 2014. H_3PO_4 imbibed polyacrylamide-graft-chitosan frameworks for high-temperature proton exchange membranes. *Journal of Power Sources,* 249**,** 277-284.

YUAN, Y., LI, H., LEITE, W., ZHANG, Q., BONNESEN, P. V., LABBÉ, J. L., WEISS, K. L., PINGALI, S. V., HONG, K., URBAN, V. S., SALMON, S. & O'NEILL, H. 2021. Biosynthesis and characterization of deuterated chitosan in filamentous fungus and yeast. *Carbohydrate Polymers,* 257**,** 117637.

ZAKIL, F. A., KAMARUDIN, S. & BASRI, S. 2016a. Modified Nafion membranes for direct alcohol fuel cells: An overview. *Renewable and Sustainable Energy Reviews,* 65**,** 841-852.

ZAKIL, F. A., KAMARUDIN, S. K. & BASRI, S. 2016b. Modified Nafion membranes for direct alcohol fuel cells: An overview. *Renewable and Sustainable Energy Reviews,* 65**,** 841-852.

ZHANG, H.-P., LUO, X.-G., LIN, X.-Y., LU, X. & TANG, Y. 2016. The molecular understanding of interfacial interactions of functionalized graphene and chitosan. *Applied Surface Science,* 360**,** 715-721.

ZHU, K., SHI, S., CAO, Y., LU, A., HU, J. & ZHANG, L. 2019a. Robust chitin films with good biocompatibility and breathable properties. *Carbohydrate polymers,* 212**,** 361-367.

ZHU, L.-F., LI, J.-S., MAI, J. & CHANG, M.-W. 2019b. Ultrasound-assisted synthesis of chitosan from fungal precursors for biomedical applications. *Chemical Engineering Journal,* 357**,** 498-507.

APPENDIX A

A.1 FTIR spectrum of the brittle chitosan membrane with nanosilica

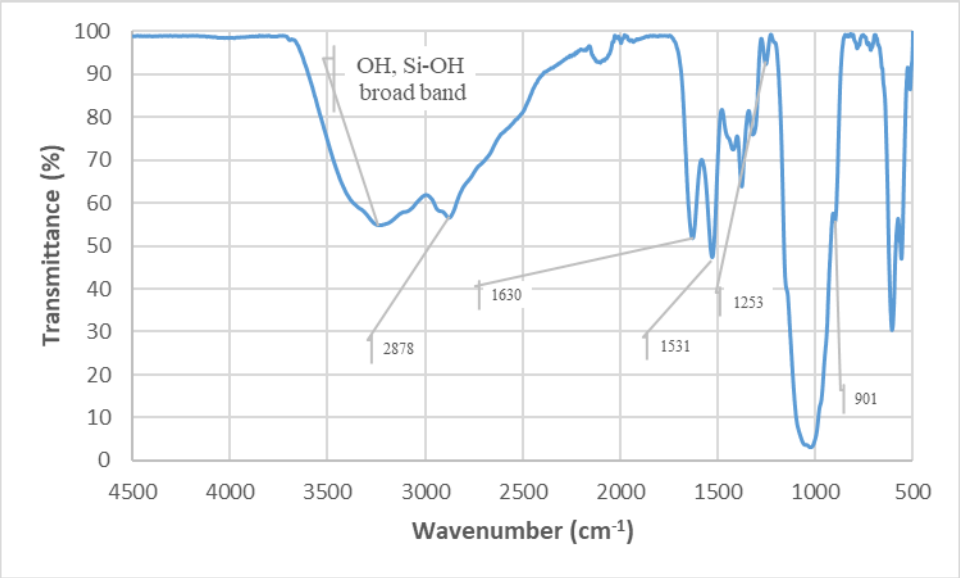

Figure A. 1: FTIR spectra of chitosan membrane with silica nanoparticles (5 wt.%)

Figure A.1 shows the FTIR spectrum of the sulfonated chitosan membrane modified with silica nanoparticles (5 wt.%), the developed membrane was brittle, this was associated to the loading capacity of silica nanoparticles at the chitosan matrix being exceeded at 5 wt.%.

The experiment was repeated by reducing the nanofiller on the chitosan matrix to 2 wt.%.

APPENDIX B

B.1 Membrane Water Uptake Experiments

$$Water Uptake\,(\%) = \frac{M_{wet} - M_{dry}}{M_{dry}} \times 100 \tag{3.18}$$

Table X. 1: Water Uptake percentage results: 24 hours

Membrane Type	Mass dry (g)	Mass wet (g)	Water Uptake %
CS-0 wt.% 2AESA	0.0591	0.113	91
CS-0 wt.% 2AESA	0.0593	0.114	92
CS-13,6 wt.% 2AESA	0.0769	0.1447	88
CS-13,6 wt.% 2AESA	0.0767	0.1434	87
CS-2 wt.% nano-SiO_2	0.0778	0.1484	91
CS-2 wt.% nano-SiO_2	0.0707	0.1339	89
Nafion 117	0.132	0.153	16
Nafion 117	0.122	0.142	16

The water uptake percentage of each membrane type was taken as the average of the two set of data.

Table X. 2: Water Uptake percentage results: 4 hours

Membrane Type	Mass dry (g)	Mass wet (g)	Water uptake %
CS-5wt.% 2AESA	0.031	0.063	103
CS-5wt.% 2AESA	0.030	0.054	80
CS-5wt.% 2AESA	0.043	0.083	93

The water uptake percentage was taken as the average of the three set of data.

APPENDIX C

C.1 Mass transfer and proton diffusion coefficient: CS-5wt.% 2AESA

Mass Transfer coefficient:

$$K = \frac{-v}{2at \ln \frac{(C_{x1} + C_{y1} - 2C_{y2})}{(C_{x1} - C_{y1})}} \tag{3.15}$$

Table X. 3: Results for pH measurement in compartment A and compartment B

Time (min)	A compartment pH	A compartment Conc.(mol/L)	B compartment pH	B compartment Conc.(mol/L)
0	3.12	7.59E-4	7.40	3.9E-8
5	3.14	7.24E-4	6.57	2.69E-7
10	3.05	8.91E-4	5.04	9.12E-6
15	3.07	8.51E-4	4.64	2.29E-5
20	3.09	8.13E-4	4.56	2.75E-5
25	3.09	8.13E-4	4.50	3.16E-5
30	3.12	7.59E-4	4.45	3.55E-5
35	3.14	7.24E-4	4.42	3.80E-5
40	3.14	7.24E-4	4.39	4.07E-5
45	3.14	7.24E-4	4.36	4.36E-5
50	3.16	6.92E-4	4.34	4.57E-5
55	3.15	7.08E-4	4.34	4.57E-5
60	3.17	6.76E-4	4.32	4.79E-5
65	3.19	6.46E-4	4.31	4.90E-5
70	3.17	6.76E-4	4.31	4.90E-5
75	3.19	6.46E-4	4.31	4.90E-5
80	3.19	6.46E-4	4.31	4.90E-5

$$K = \frac{-200}{2x36x4800 \ln \frac{3.98X10^{-8} + 7.59X10^{-4} - 2\left(6.46X10^{-4}\right)}{(3.98X10^{-8} - 7.59X10^{-4})}}$$

$$K = 0.0016\, cm/s$$

Proton diffusion coefficient:

The thickness, *l* of the membrane was measured using the Mitutoyo No.21095-10 [(p)] device to be 41 µm, the value was obtained as the difference between the two readings in the Mitutoyo device before and after insertion of the membrane as shown in Figure C.1.

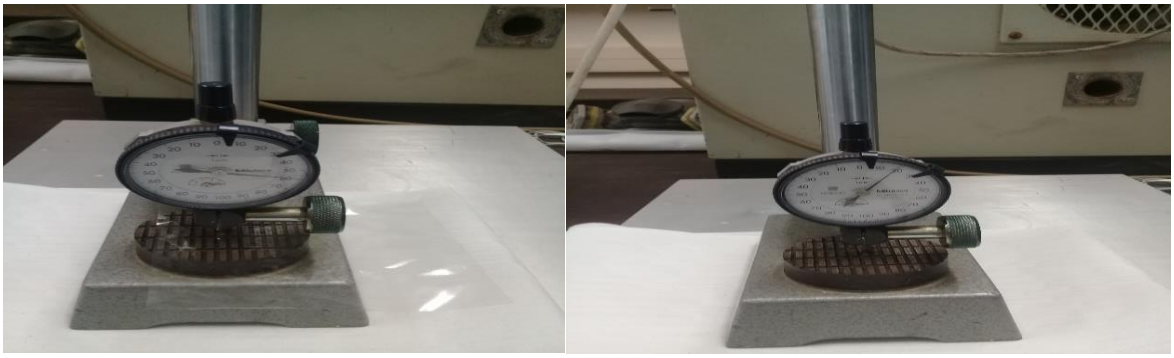

Figure C. 1: Chitosan membrane thickness measurement

$$D = Kl \tag{3.16}$$

$$D = 0.0016\frac{cm}{s} X\, 0.0041cm \qquad D = 6.56X10^{-6} cm^2/s$$

C.2 Mass Transfer and proton diffusion coefficient: Nafion 117

Mass Transfer coefficient:

$$K = \frac{-v}{2at \ln \dfrac{(C_{x1} + C_{y1} - 2C_{y2})}{(C_{x1} - C_{y1})}} \tag{3.15}$$

Table X. 4: Results for pH measurement in compartment A and B with Nafion 117

Time (min)	A compartment pH	A. compartment Conc. (mol/L)	B compartment pH	B Compartment Conc.(mol/L)
0	3.99	1.02E-4	6.1	7.7E-7
10	4	1.00E-4	5.52	3.02E-6
20	4.03	9.30E-5	5.5	3.16E-6
30	4.06	8.70E-5	5.48	3.3E-6
40	4.08	1.58E-5	5.42	3.8E-6
50	4.1	7.94E-5	5.38	4.17E-6
60	4.09	8.13E-5	5.35	4.47E-6
70	4.1	7.94E-5	5.30	5.01E-6
80	4.1	7.94E-5	5.30	5.01E-6

$$K = \frac{-200}{2x36x4800 \ln \frac{7.76X10^{-7} + 1.02X10^{-4} - 2\left(7.94X10^{-5}\right)}{(7.76X10^{-7} - 1.02X10^{-4})}}$$

$$K = 0.000978\, cm/s$$

Proton diffusion coefficient:

The thickness, *d* of the membrane was measured using the MitutoyoNo.21095-10 (p) device. The thickness of the membranes was measured to be 168 µm.

$$D = Kl \tag{3.16}$$

$$D = 0.000978 \frac{cm}{s} x0.0168cm$$

$$D = 1.64X10^{-5} cm^2/s$$

APPENDIX D

D.1 Methanol permeability coefficient

Table X. 5: Methanol peak area over time in compartments A and B

Time (s)	Peak Area, A	Peak Area, B
0	673915,49	0
900	-	59583,6
1800	-	63373,99
2700	-	66075,22
3600	457057	110273,19

Calculating methanol concentration from the HPLC results:

$$\text{Nrf} = \frac{\text{Methanol peak area (standard)}}{\text{Methanol concentration of standard}} \quad (3.1)$$

$$\text{Nrf} = \frac{673915,49}{12}$$

$$\text{Nrf} = 56159,62$$

$$\text{Methanol concentration} = \frac{\text{Methanol peak area at time } t}{\text{Nrf}} \quad (3.2)$$

Table X. 6: Methanol concentration over time in compartments A and B

Time (s)	Concentration (mol/L), A	Concentration (mol/L), B
0	12	0
900	-	1,06
1800	-	1,13
2700	-	1,18
3600	8,14	1,96

The slope K_B was obtained from the concentration versus time graph:

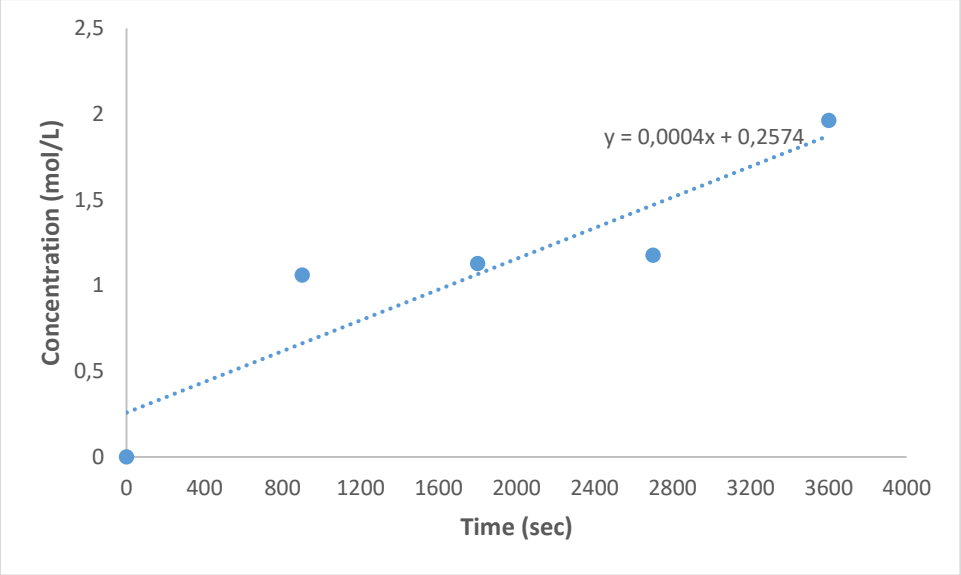

Figure D. 1: Change in methanol concentration with time in compartment B

Calculation the methanol permeability co-efficient:

$$P = (D \cdot H) = \frac{K_B V_B l}{A(C_A - C_B)} \qquad (3.14)$$

$$P = (D \cdot H) = \frac{0.0004 X\ 200 X\ 0.0062}{36(8\ -2)}$$

$$P = (D \cdot H) = 2.29 X 10^{-6} cm^2 / s$$

APPENDIX E

E.1 Fuel cell performance of chitosan membranes and Nafion 117

Table X. 7: Voltage and current results of the (CS-13.6 wt.% 2AESA) MEA

Current(mA)	Voltage (V)	Power (mW)
50	0,916	45,8
46	0,907	41,722
31	0,901	27,931
48	0,901	43,248
48	0,902	43,296
56	0,875	49
56	0,880	49,28
64	0,868	55,552
52	0,910	47,32
68	0,913	62,084
66	0,918	60,588
69	0,920	63,48
67	0,925	61,975
55	0,926	50,93
68	0,929	63,172
70	0,924	64,68
56	0,943	52,808
65	0,945	61,425
53	0,935	49,555
64	0,951	60,864
53	0,915	48,495
65	0,917	59,605
67	0,933	62,511
63	0,907	57,141
64	0,905	57,92
49	0,933	45,717
66	0,922	60,852
65	0,938	60,97
64	0,944	60,416
68	0,909	61,812
68	0,916	62,288
69	0,909	62,721
58	0,914	53,012
50	0,914	45,7

Table X. 8: Voltage and Current results of the MEA consisting of nanosilica

Current (mA)	Voltage (V)	Power (mW)
28	0,918	25,704
42	0,910	38,22
31	0,900	27,9
47	0,948	44,556
45	0,889	40,005
39	0,942	36,738
52	0,968	50,336
38	0,967	36,746
50	0,933	46,65
48	0,970	46,56
15	0,970	14,55
47	0,944	44,368
51	0,890	45,39
54	0,939	50,706
42	0,984	41,328
52	0,939	48,828
49	0,952	46,648
42	0,969	40,698
46	0,967	44,482
38	0,967	36,746
60	0,974	58,44
49	0,974	47,726
56	0,967	54,152
51	0,967	49,317
61	0,952	58,072
63	0,900	56,7
62	0,904	56,048

Table X. 9: Voltage and Current results using the control MEA

Current (mA)	Voltage (V)	Power (mW)
2,2	0,0065	0,0143
2,54	0,0080	0,02032
4,9	0,0090	0,0441
2,94	0,0076	0,022344
3,13	0,0094	0,029422
3,18	0,0081	0,025758
3,4	0,0089	0,03026
3,25	0,0086	0,02795
3,8	0,0086	0,03268
2,63	0,0084	0,022092

Table X. 10: Voltage and Current results using the Nafion 117 MEA

Current (mA)	Voltage (V)	Power (mW)
200	0,445	89
240	0,518	103,6
238	0,621	124,2
308	0,65	130
257	0,622	124,4
272	0,591	118,2
227	0,502	100,4
223,3	0,515	103
212	0,478	95,6
257	0,576	115,2
203	0,407	81,4
252	0,554	110,8
233	0,579	115,8

E.2. Fuel cell performance of hot pressed chitosan membrane

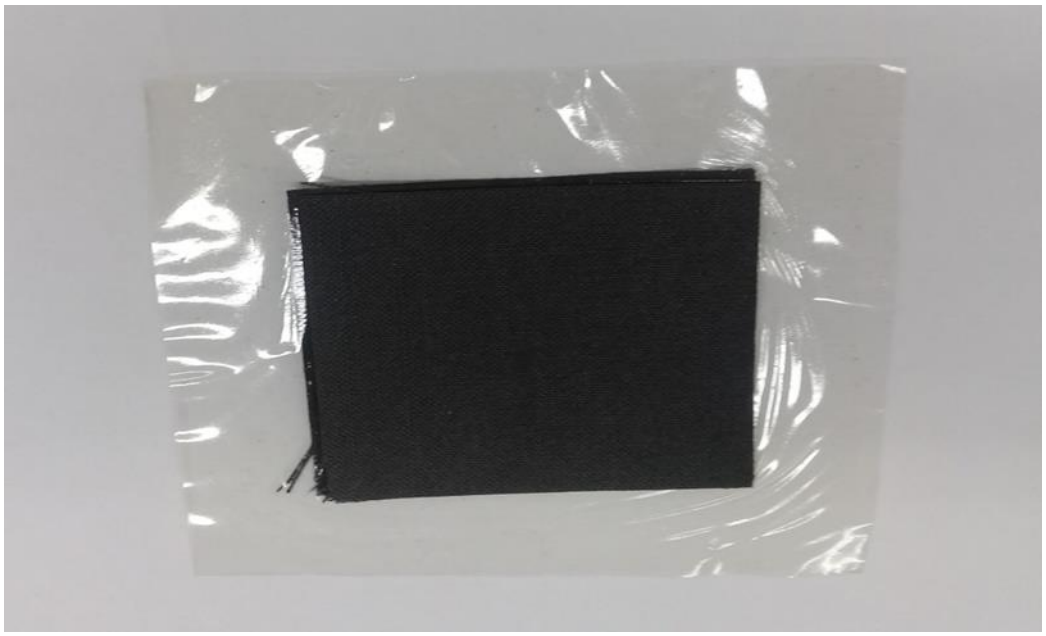

Figure E. 1: Hot-Pressed chitosan MEA (5 wt.% 2AESA)

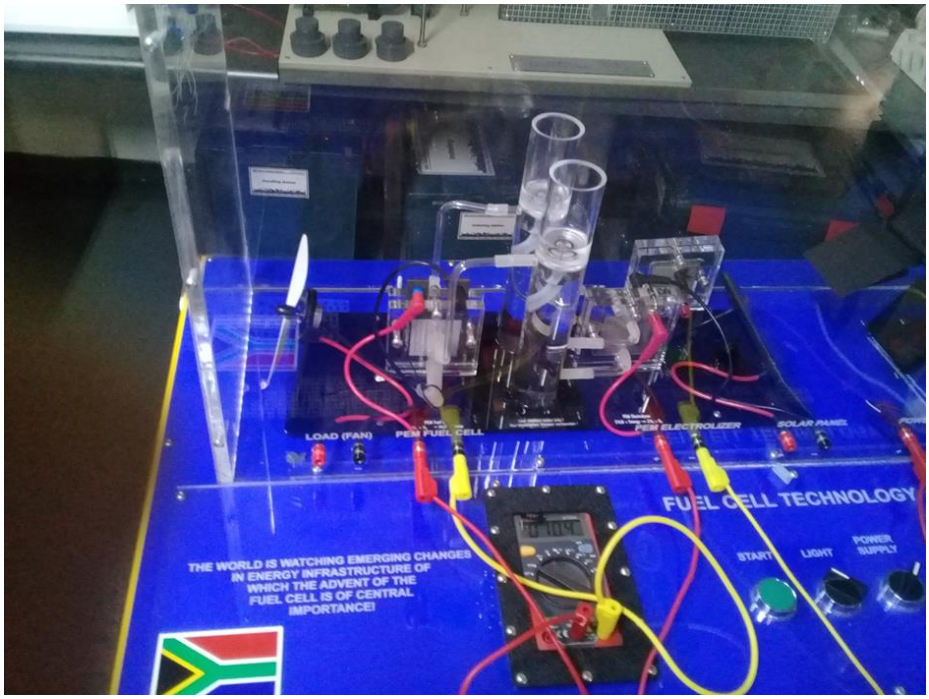

Figure E. 2: Experimental set-up showing performance of the sulfonated-chitosan PEM

Figure E.1 shows the MEA fabricated with the sulfonated chitosan membrane modified with 5 wt.% 2AESA and hot pressed onto two GDE at 88 ℃ and 2000 psi for 5 minutes. The performance of the MEA was investigated in a hydrogen fuel cell shown in Figure E.2.

The hot pressed chitosan MEA performed poorly, yielding low voltage out-put of not more than 25.3 mV. The results obtained from this experiment suggested that hot pressing may not be suitable for the membranes developed in this work due to the risk of heat in impacting the structure of the membrane and its performance.

The hot-press used in this study is shown in Figure E.3:

Figure E. 3: Carver Hydraulics press used to hot-press the chitosan membranes